NATIONAL ADVISORY COMMITTEE FOR AERONAUTICS

REPORT No. 920

THE DEVELOPMENT AND APPLICATION OF HIGH-CRITICAL-SPEED NOSE INLETS

By DONALD D. BAALS, NORMAN F. SMITH, and JOHN B. WRIGHT

1948

AERONAUTIC SYMBOLS

1. FUNDAMENTAL AND DERIVED UNITS

	Symbol	Metric		English	
		Unit	Abbreviation	Unit	Abbreviation
Length	l	meter	m	foot (or mile)	ft (or mi)
Time	t	second	s	second (or hour)	sec (or hr)
Force	F	weight of 1 kilogram	kg	weight of 1 pound	lb
Power	P	horsepower (metric)		horsepower	hp
Speed	V	kilometers per hour	kph	miles per hour	mph
		meters per second	mps	feet per second	fps

2. GENERAL SYMBOLS

W Weight$=mg$

g Standard acceleration of gravity$=9.80665$ m/s^2 or 32.1740 ft/sec^2

m Mass$=\frac{W}{g}$

I Moment of inertia$=mk^2$. (Indicate axis of radius of gyration k by proper subscript.)

μ Coefficient of viscosity

ν Kinematic viscosity

ρ Density (mass per unit volume)

Standard density of dry air, 0.12497 kg-m^{-4}-s^2 at 15° C and 760 mm; or 0.002378 lb-ft^{-4} sec^2

Specific weight of "standard" air, 1.2255 kg/m^3 or 0.07651 lb/cu ft

3. AERODYNAMIC SYMBOLS

S Area

S_w Area of wing

G Gap

b Span

c Chord

A Aspect ratio, $\frac{b^2}{S}$

V True air speed

q Dynamic pressure, $\frac{1}{2}\rho V^2$

L Lift, absolute coefficient $C_L=\frac{L}{qS}$

D Drag, absolute coefficient $C_D=\frac{D}{qS}$

D_0 Profile drag, absolute coefficient $C_{D_0}=\frac{D_0}{qS}$

D_i Induced drag, absolute coefficient $C_{D_i}=\frac{D_i}{qS}$

D_p Parasite drag, absolute coefficient $C_{D_p}=\frac{D_p}{qS}$

C Cross-wind force, absolute coefficient $C_C=\frac{C}{qS}$

i_w Angle of setting of wings (relative to thrust line)

i_t Angle of stabilizer setting (relative to thrust line)

Q Resultant moment

Ω Resultant angular velocity

R Reynolds number, $\rho\frac{Vl}{\mu}$ where l is a linear dimension (e.g., for an airfoil of 1.0 ft chord, 100 mph, standard pressure at 15° C, the corresponding Reynolds number is 935,400; or for an airfoil of 1.0 m chord, 100 mps, the corresponding Reynolds number is 6,865,000)

α Angle of attack

ϵ Angle of downwash

α_0 Angle of attack, infinite aspect ratio

α_i Angle of attack, induced

α_a Angle of attack, absolute (measured from zero-lift position)

γ Flight-path angle

REPORT No. 920

THE DEVELOPMENT AND APPLICATION OF HIGH-CRITICAL-SPEED NOSE INLETS

By DONALD D. BAALS, NORMAN F. SMITH, and JOHN B. WRIGHT

Langley Memorial Aeronautical Laboratory
Langley Field, Va.

National Advisory Committee for Aeronautics

Headquarters, 1724 F Street NW, Washington 25, D. C.

Created by act of Congress approved March 3, 1915, for the supervision and direction of the scientific study of the problems of flight (U. S. Code, title 50, sec. 151). Its membership was increased to 17 by act approved May 25, 1948. (Public Law 549, 80th Congress). The members are appointed by the President, and serve as such without compensation.

REPORT No. 920

THE DEVELOPMENT AND APPLICATION OF HIGH-CRITICAL-SPEED NOSE INLETS

By Donald D. Baals, Norman F. Smith, and John B. Wright

SUMMARY

An analysis of the nose-inlet shapes developed in previous investigations to represent the optimum from the standpoint of critical speed has shown that marked similarity exists between the nondimensional profiles of inlets which have widely different proportions and critical speeds. With the nondimensional similarity of such profiles established, the large differences in the critical speeds of these nose inlets must be a function of their proportions.

An investigation was undertaken in the Langley 8-foot high-speed tunnel to establish the effects of nose-inlet proportions on critical Mach number and to develop a rational method for the design of high-critical-speed nose inlets to meet desired requirements. The nondimensional ordinates of the B nose inlet, which were developed in a previous investigation to be optimum from the standpoint of critical speed, were extended and modified slightly to improve the fairing. These ordinates, now designated the NACA 1-series, were then applied to a group of nose inlets involving a systematic variation of proportions. Wind-tunnel tests of these nose inlets were made through wide ranges of inlet-velocity ratio and angle of attack at Mach numbers of 0.3 and 0.4. Tests of representative nose inlets were carried to high speed (a maximum Mach number of 0.7). Pressure distributions and critical Mach number characteristics are presented for each of the nose inlets tested. The results of these tests show that the length ratio (ratio of length to maximum diameter) of the nose inlet is the primary factor governing the maximum critical speed. The effect of inlet-diameter ratio (ratio of inlet diameter to maximum diameter) on critical speed is, in general, secondary; but this ratio has an important function in governing the extent of the inlet-velocity-ratio range for maximum critical speed. The highest critical Mach number attained for any of the nose inlets tested was 0.89.

The data have been arranged in the form of design charts from which NACA 1–series nose-inlet proportions can be selected for given values of critical Mach number and airflow quantity. Examples of nose-inlet selections are presented for a typical jet-propulsion installation (critical Mach number of 0.83) and for two conventional radial-engine installations (critical Mach number of 0.76).

The selection charts and NACA 1–series ordinates are shown to be applicable to the design of cowlings with spinners and to the design of high-critical-speed fuselage scoops. The possibility of application of the NACA 1–series ordinates to the experimental development of wing inlets is also indicated.

INTRODUCTION

Marked increases in airplane speeds have created a demand for design data on high-critical-speed air inlets suitable for use with jet-propulsion units, gas-turbine propeller units, and conventional engine installations. Previous development programs on air inlets have produced the NACA C cowling having a critical Mach number of 0.63 (reference 1) and the B nose inlet having a critical Mach number of 0.84 (reference 2). These inlets have widely different proportions; the first is short with a large-diameter air inlet; the second is of considerably greater length with a small-diameter air inlet. Each nose inlet was developed to represent the optimum design from the standpoint of critical speed for the particular proportions involved.

Little information has been available on air inlets having proportions in the range between these two specific shapes. The research program reported herein was undertaken at the Langley 8-foot high-speed tunnel to establish the effects of variations of nose-inlet proportions on the critical Mach number and to develop a rational method for the design of nose inlets intermediate to the NACA C cowling and B nose inlets, both in proportions and in design critical Mach numbers. Such data have direct application to the design of high-critical-speed nose inlets and to the development of scoop-type air inlets.

SYMBOLS

a	speed of sound, feet per second
V	velocity, feet per second
M	Mach number (V/a)
V_1/V_0	inlet-velocity ratio
α	model angle of attack, measured from model center line, degrees
ρ	density, slugs per cubic foot
γ	ratio of specific heats (for air, 1.40)
p	static pressure, pounds per square foot
P	pressure coefficient $\left(\frac{p-p_0}{q_0}\right)$
P_{cr}	critical pressure coefficient, corresponding to local Mach number of 1.0
m	mass flow, slugs per second (ρAV)
A	area, square feet
$\frac{m}{\rho_0 F V_0}$	mass-flow coefficient
q	dynamic pressure, pounds per square foot $\left(\frac{1}{2}\rho V^2\right)$

ΔH	total-pressure loss between free stream and measurement station, pounds per square foot
θ	total conical-diffuser angle, degrees
D	maximum diameter of nose inlet
d	inlet diameter
d/D	inlet-diameter ratio
x	distance from entrance, measured along nose-inlet center line
X	nose-inlet length, measured from inlet to maximum-diameter station
X/D	length ratio
F	maximum frontal area of nose inlet, corresponding to D, square feet
y	ordinate measured perpendicular to reference line
Y	maximum ordinate, measured perpendicular to reference line at maximum-diameter station (See table I.)
r	nose-inlet lip radius
K	arbitrary factor (See section entitled "Effects of variations in basic profile" and fig. 7.)

Subscripts:

min	minimum
cr	critical
0	free stream
1	nose-inlet entrance

DESIGN ANALYSIS

DERIVATION OF BASIC NOSE ORDINATES

The A, B, and C nose inlets presented in reference 2 were derived experimentally in a systematic series of wind-tunnel tests to approach the optimum from the standpoint of critical speed. A comparison from reference 2 of the nondimensional profiles for these nose inlets having different proportions (fig. 1) indicates a similarity of profile for all three inlets. Marked similarity of profile is noted for the B and C nose inlets; the A nose inlet, however, varies somewhat from the basic profile of the B and C nose inlets. This variation is believed to be due to the limitations encountered in the tests of reference 2, which involved the fairing of this nose inlet of large diameter into the basic streamline body at a given

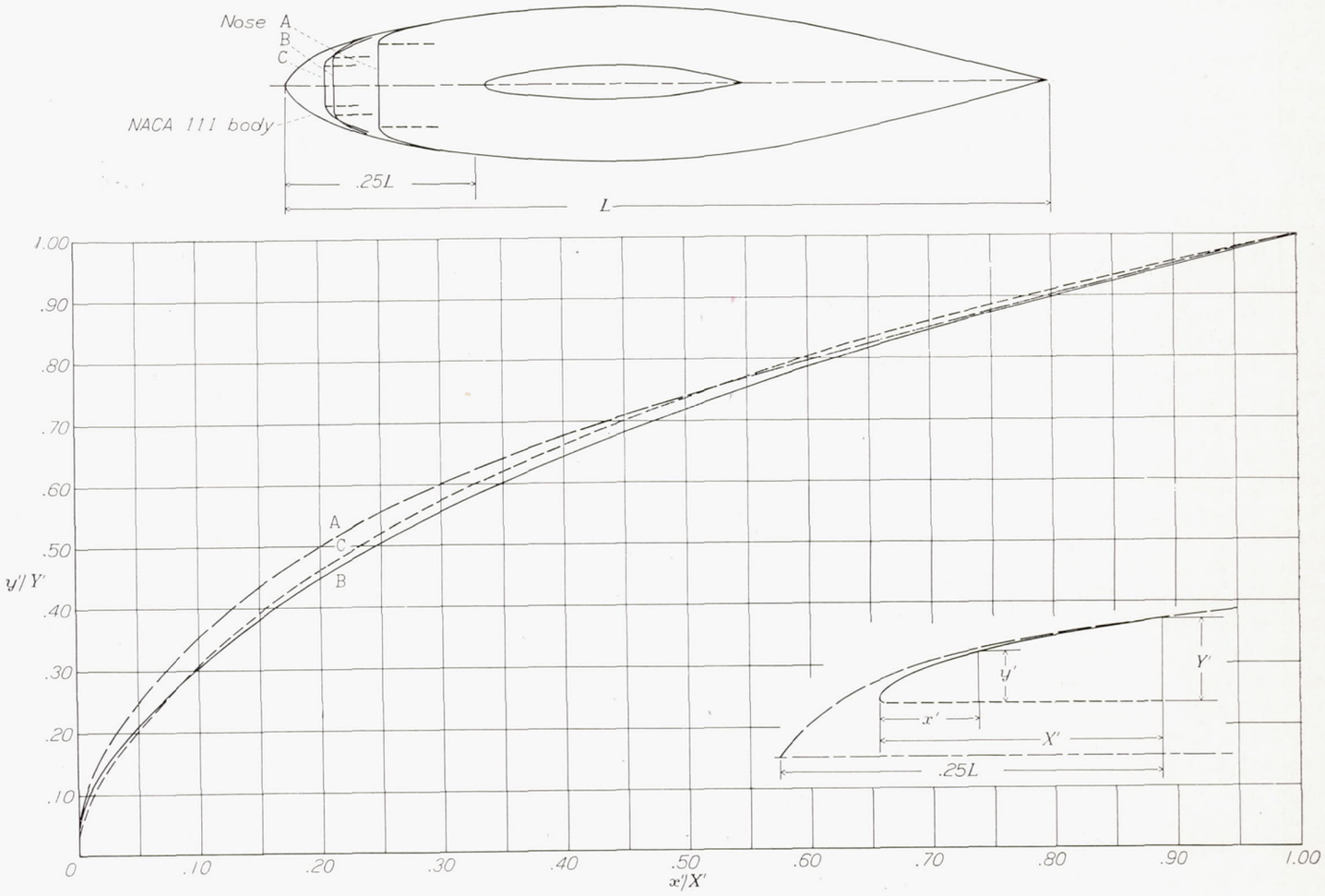

FIGURE 1.—Comparison of nondimensional profiles and proportions of the three high-critical-speed nose inlets developed in tests of reference 2.

point and with a given slope. These limitations were not serious for the B and C nose inlets, which have small inlet diameters, and correspondingly greater lengths were available for fairing than for the A nose inlet. A flat pressure distribution similar to the distributions obtained for the B and C nose inlets was not obtained for the A nose inlet, for which a pressure peak occurred at all inlet-velocity ratios.

Although the difference between the nondimensional B and C nose-inlet ordinates is small, the ordinates of the B nose inlet have been selected for general use because the original proportions were considered to correspond more nearly to current design applications than those of the C nose inlet. The nondimensional B nose-inlet ordinates have been applied to the layout of various nose inlets that differ appreciably from the original nose-inlet proportions in length, inlet diameter, and maximum diameter. In reference 3, in which the variation from the original B nose-inlet proportions was considerable, the pressure distribution over the resulting nose inlets exhibited the characteristic flat contour with low values of the pressure peak. It was thus indicated that the basic B nose-inlet profile and the method of nose design could be applied to the design of nose inlets having proportions greatly different from those of the original nose-inlet shape tested.

Difficulty was experienced, however, in the application of the original B nose-inlet ordinates. The slope of the nose-inlet profile at the station at which the nose faired into the streamline body was a finite value that varied with the nose-inlet proportions assumed. It was evident that the nondimensional profile should be extended to a point at which the slope was zero (maximum-diameter station). In order to attain this extension, the B nose-inlet ordinates were considered to include the NACA 111 streamline body (to which the original nose inlet was faired) as far back as the maximum-diameter station. The resulting ordinates were developed in a nondimensional form and are plotted in figure 2.

The fairness of the extended B nose-inlet ordinates could not be determined from the measured pressure distribution presented in reference 1 because the wing-support interference affected the pressure distribution over the rear part of the nose inlet. Plots of the slope and the rate of change of slope of the extended B nose-inlet ordinates indicated a slight amount of unfairness in the region where the original B nose inlet joined the streamline body. On the assumption that the curves of slope and rate of change of slope should be fair (these two curves together specify the local radius of curvature), the two curves were faired and the resulting ordinates determined. The faired ordinates, hereinafter designated the NACA 1-series ordinates, are given in table I and are plotted in figure 2 in comparison with the extended B nose-inlet ordinates. The two curves are practically identical over the critical forward section and have only minor differences over the rear section. The resultant NACA 1-series ordinates are, therefore, essentially the original NACA B nose-inlet ordinates with the addition of a faired extension back to the maximum-diameter station.

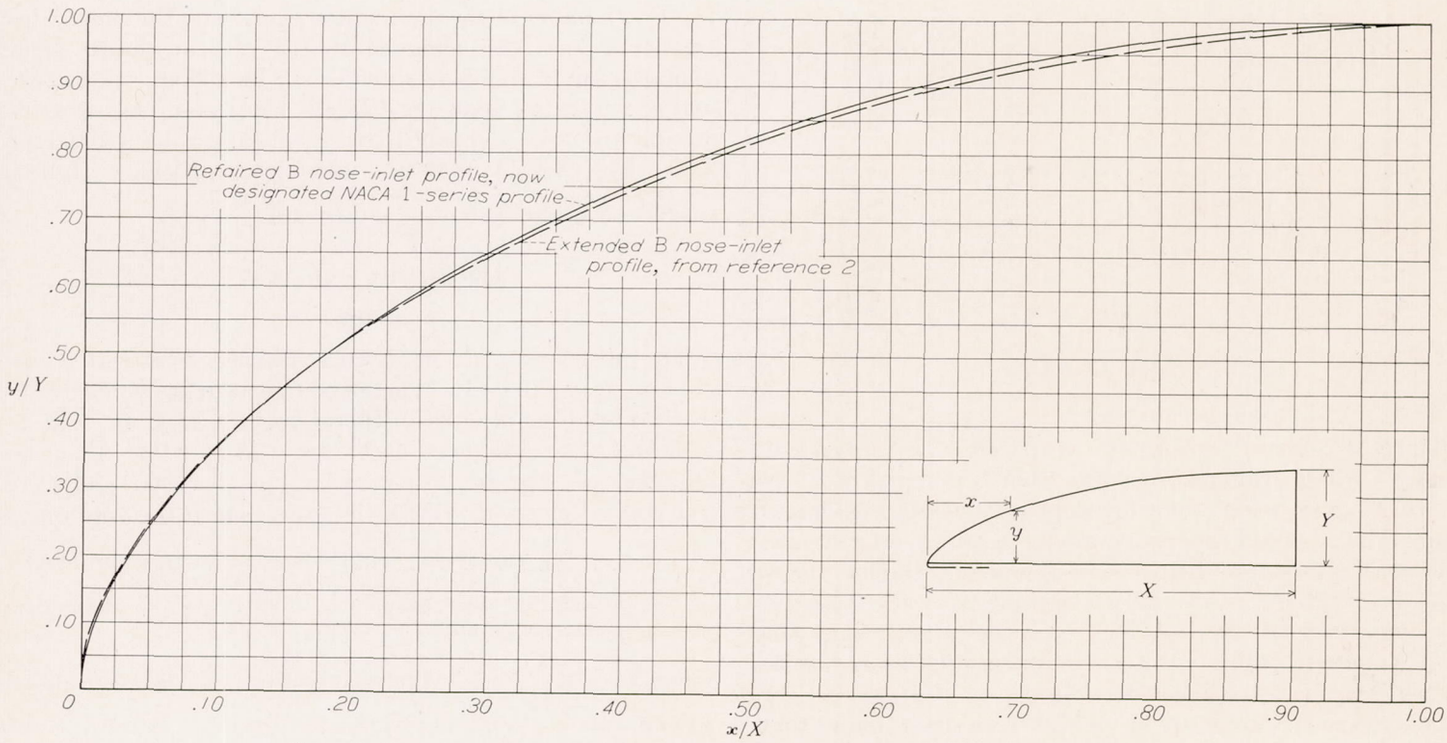

FIGURE 2.—Comparison of the extended B nose-inlet profile of reference 2 with NACA 1-series nose-inlet profile.

TABLE I
NACA 1—SERIES ORDINATES

[Ordinates in percent]

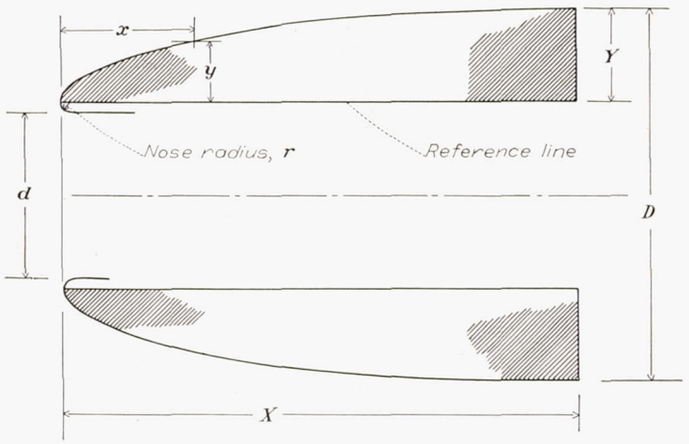

$$X=\left(\frac{X}{D}\right)D$$

$$Y=\frac{D-d}{2}-r$$

$$\text{For } r=0.025Y: Y=\frac{D-d}{2.05}=\frac{D\left(1-\frac{d}{D}\right)}{2.05}$$

x/X	y/Y	x/X	y/Y	x/X	y/Y	x/X	y/Y
0	0	13.0	41.94	34.0	69.08	60.0	89.11
.2	4.80	14.0	43.66	35.0	70.08	62.0	90.20
.4	6.63	15.0	45.30	36.0	71.05	64.0	91.23
.6	8.12	16.0	46.88	37.0	72.00	66.0	92.20
.8	9.33	17.0	48.40	38.0	72.94	68.0	93.11
1.0	10.38	18.0	49.88	39.0	73.85	70.0	93.95
1.5	12.72	19.0	51.31	40.0	74.75	72.0	94.75
2.0	14.72	20.0	52.70	41.0	75.63	74.0	95.48
2.5	16.57	21.0	54.05	42.0	76.48	76.0	96.16
3.0	18.31	22.0	55.37	43.0	77.32	78.0	96.79
3.5	19.94	23.0	56.66	44.0	78.15	80.0	97.35
4.0	21.48	24.0	57.92	45.0	78.95	82.0	97.87
4.5	22.96	25.0	59.15	46.0	79.74	84.0	98.33
5.0	24.36	26.0	60.35	47.0	80.50	86.0	98.74
6.0	27.01	27.0	61.52	48.0	81.25	88.0	99.09
7.0	29.47	28.0	62.67	49.0	81.99	90.0	99.40
8.0	31.81	29.0	63.79	50.0	82.69	92.0	99.65
9.0	34.03	30.0	64.89	52.0	84.10	94.0	99.85
10.0	36.13	31.0	65.97	54.0	85.45	96.0	99.93
11.0	38.15	32.0	67.03	56.0	86.73	98.0	99.98
12.0	40.09	33.0	68.07	58.0	87.95	100.0	100.00

Nose radius: $0.025Y$

The NACA C cowling ordinates are presented in reference 1. These cowling ordinates, derived from a systematic series of wind-tunnel tests, were developed to attain the maximum critical speed for conventional cowling proportions. The cowling pressure distribution approaches the flat shape that is optimum from the standpoint of critical speed. A comparison of the NACA C cowling profile with the NACA 1-series ordinates on a nondimensional basis (fig. 3) shows reasonable agreement. Figure 3 also shows the nondimensional profile of an NACA wing-inlet shape that is discussed in the section entitled "Wing inlets."

In figure 3 the NACA C cowling $\left(\frac{d}{D}=0.70;\ \frac{X}{D}=0.31\right)$ and the original B nose inlet $\left(\frac{d}{D}=0.38;\ \frac{X}{D}=1.85\right)$ are sketched to scale. The great difference in the proportions of these two nose inlets, which approach the optimum from the standpoint of critical speed, is evident. The critical Mach numbers of the NACA C cowling and B nose inlet are, from references 1 and 2, 0.63 and 0.84, respectively. With the nondimensional similarity of the profiles of these two nose inlets established (fig. 3), the large variation in critical speed must be a function of the nose-inlet proportions. It is indicated, therefore, that nose inlets having proportions intermediate to these two nose inlets and having critical-speed characteristics approaching the optimum can be derived from essentially the same nondimensional profile. With the NACA 1-series ordinates as a basic profile, a systematic series of wind-tunnel tests was undertaken to determine the effects of nose-inlet proportions on critical speed.

NOSE-INLET DESIGNATION

A designation system for nose inlets has been devised that incorporates the following basic proportions (see sketch in table I):

d inlet diameter
D maximum outside diameter of nose inlet
X length of nose inlet, measured from inlet to maximum-diameter station

The number designation is written in the form 1–40–150. The first number in the designation represents the series; the number 1 has been assigned to the present series. The second group of numbers specifies the inlet diameter in percent of maximum diameter d/D; the third group of numbers specifies the nose-inlet length in percent of maximum diameter X/D. The NACA 1–40–150 nose inlet, therefore, has a 1-series basic profile with $\frac{d}{D}=0.40$ and $\frac{X}{D}=1.50$.

APPARATUS AND TESTS

MODELS

The nose inlets of the NACA 1-series investigated are illustrated in table II. These nose inlets represent a systematic variation of inlet-diameter ratio d/D from 0.40 to 0.70 and of length ratio X/D from 0.30 to 2.00 All nose-inlet models were of 12-inch maximum diameter and were constructed of wood. With the exception of the nose inlets of $\frac{X}{D}=2.00$, for which the length was 24 inches, the length of the detachable nose inlets was maintained at 18 inches. This length corresponds to a value of X/D of 1.5. To nose inlets having $\frac{X}{D}<1.5$, cylindrical sections (skirts) were added to maintain the over-all length at 18 inches. Several of the nose inlets were provided with detachable skirts in order to

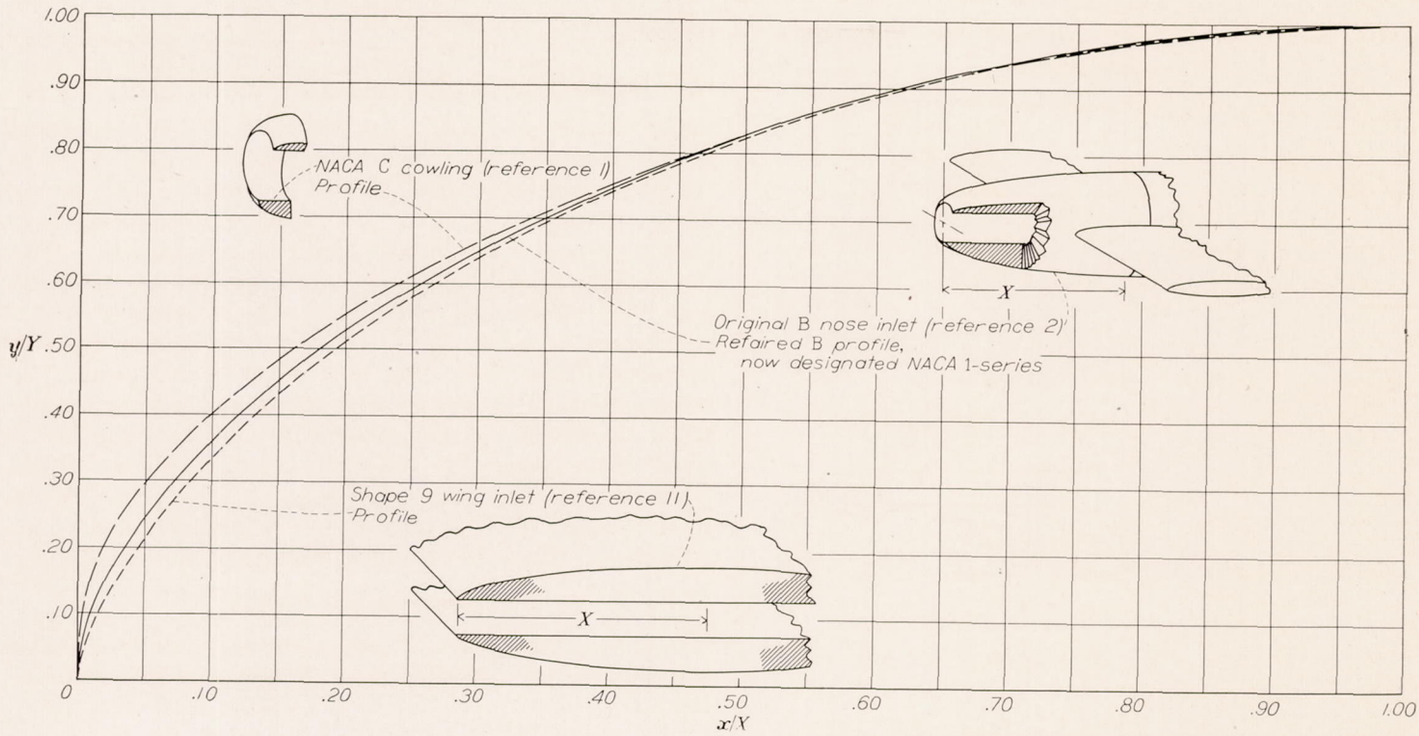

FIGURE 3.—Comparison of nondimensional profiles and proportions of three high-critical-speed air inlets from references 1, 2, and 11.

TABLE II
NACA 1—SERIES NOSE INLETS TESTED

d/D	X/D					
	2.00	1.50	1.00	.75	.50	.30
0.40	1-40-200	1-40-150				
.50	1-50-200	1-50-150	1-50-100		1-50-050	
.60	1-60-200	1-60-150	1-60-100	1-60-075	1-60-050	
.70		1-70-150	1-70-100		1-70-050	1-70-030

investigate the effects of varying fineness ratio of the test body. Scale drawings of each of the nose inlets tested are presented in figure 4, grouped according to inlet-diameter ratio. Photographs of certain of the nose inlets (with skirts), which illustrate variations in length ratio and inlet-diameter ratio, are presented in figure 5. The duct lip radius for all nose inlets tested was maintained at $0.025Y$ (table I), which is approximately the same value as in the development tests of references 1 and 2. Several minor modifications to the lip radius and internal fairing were tested. (See fig. 6.) No attempt was made to simulate an aircraft internal-flow system insofar as internal resistance and duct lines are concerned. The model ducts for the nose inlets were conical back to the parting line of the movable nose section, where all ducts had a common diameter of 7.2 inches.

In addition to the nose inlets listed in table II, the NACA C cowling was tested. Three nose inlets having $\frac{d}{D}=0.60$ and $\frac{X}{D}=1.50$ and having profiles representing deviations from the NACA 1-series profile were also tested to show the effects of such deviations. All three nose inlets, which are drawn to scale in figure 7, differ from the NACA 1-series profile in that the thickness of the forward part is greater than for the NACA 1-series profile.

Each nose inlet was provided with a row of surface static-pressure orifices, which extended along the top center line from the inlet lip to a point 3⅜ inches to the rear of the detachable nose. The pressure tubing passed from the model through the tunnel test section along the support strut and was connected to a photographically recorded multiple-tube manometer in the test chamber.

The nose inlets were mounted on a cylindrical afterbody that was supported at the tunnel center line by a single vertical streamline strut. This strut was attached to the body at a station 2 strut chords behind the removable nose

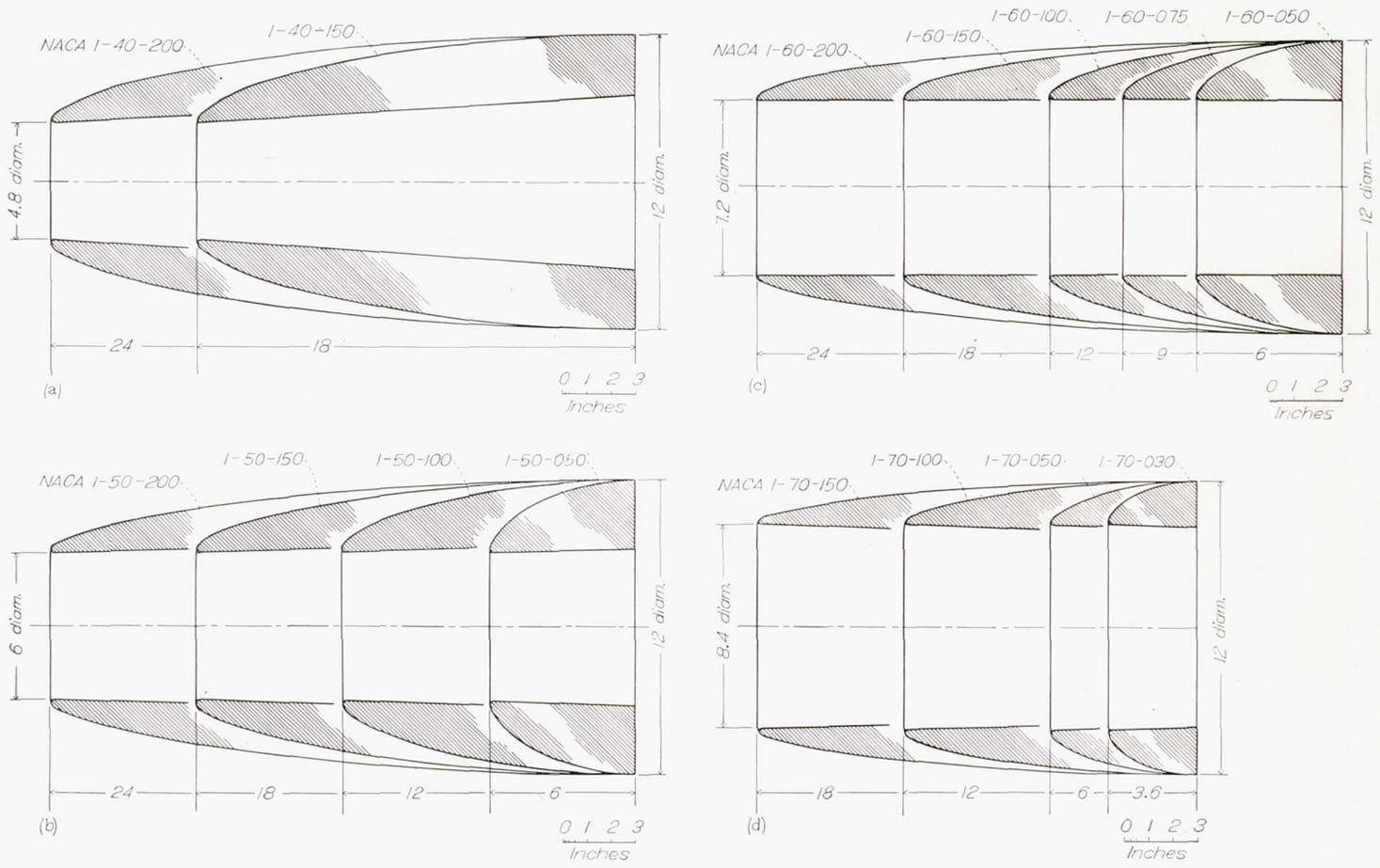

(a) $\frac{d}{D}$=0.40.

(b) $\frac{d}{D}$=0.50.

(c) $\frac{d}{D}$=0.60.

(d) $\frac{d}{D}$=0.70.

FIGURE 4.—Scale drawings of the NACA 1-series nose inlets tested.

inlet in order to minimize interference effects. A drawing of the model installation is shown in figure 8. The internal-flow system is also shown in figure 8. The duct section immediately behind the parting line of the nose inlet and body was contracted to the rake station, where a rake of total-pressure and static-pressure tubes was located for the determination of internal losses and air-flow quantity. The duct exit was located at the tail of the body and was provided with a plug-type control for varying the exit area. An electric-motor drive for the exit control was included in order that the air-flow quantity could be varied through a range during each test. A flapped exit was used for several tests to obtain high values of inlet-velocity ratio. The angle of attack of the model was varied through fixed increments by means of an internal indexing device.

EQUIPMENT AND TESTS

The Langley 8-foot high-speed tunnel, in which this investigation was conducted, is a closed-throat, circular-section, single-return tunnel. The turbulence of the air stream is low but is somewhat higher than the turbulence of free air.

The complete range of NACA 1-series nose inlets shown in table II was tested at M_0=0.30 and 0.40 through an angle-of-attack range from approximately 0° to 8° by 2° increments. Several of the nose inlets were tested through the Mach number range up to approximately M_0=0.7. The inlet-velocity ratio was varied from about 0.2 to values higher than 1.0 for the nose inlets having small values of d/D. For the nose inlets having large values of d/D, the maximum value of inlet-velocity ratio was limited by the capacity of the internal-flow system.

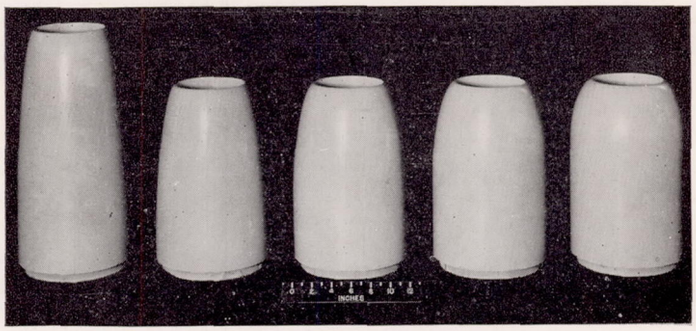

(a) $\frac{d}{D}$=0.60; $\frac{X}{D}$=2.00, 1.50, 1.00, 0.75, and 0.50, from left to right.

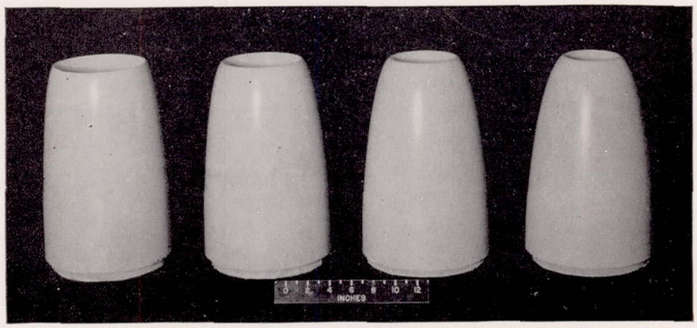

(b) $\frac{X}{D}$=1.50; $\frac{d}{D}$=0.70, 0.60, 0.50, and 0.40, from left to right.

FIGURE 5.—Details of nose inlets showing variations in inlet-diameter ratio and length ratio.

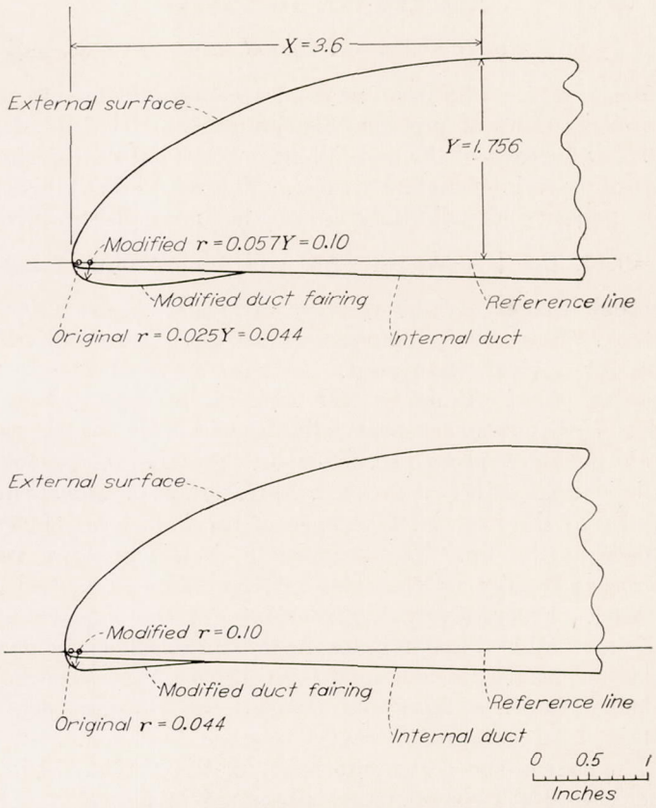

FIGURE 6.—NACA 1-70-030 nose inlet (upper sketch) and C cowling (lower sketch) with original and modified lip radii.

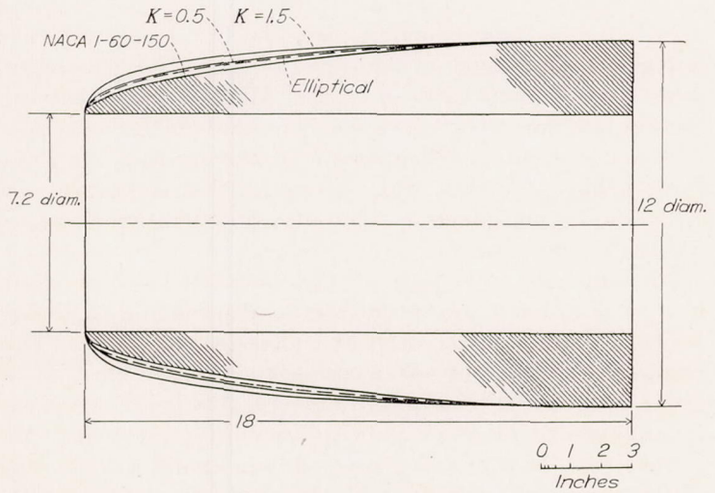

FIGURE 7.—Scale drawings of modified nose inlets tested, compared with the NACA 1-60-150 nose inlet.

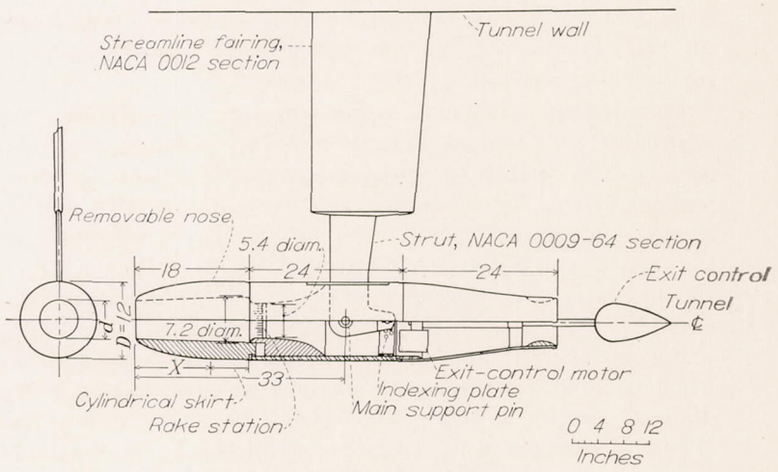

FIGURE 8.—Model installation and details.

844332—50——2

RESULTS AND DISCUSSION

BASIC NOSE-INLET CHARACTERISTICS

Basic data.—The basic nose-inlet characteristics are presented as plots of pressure distribution and critical Mach number for each of the nose inlets. These data are grouped according to inlet-diameter ratio. Figures 9 and 10 present the pressure distributions over the nose inlets having $\frac{d}{D}$=0.40, the NACA 1–40–200 and 1–40–150 nose inlets, through ranges of inlet-velocity ratio and model angle of attack. These two parameters govern the pressure distribution for a given nose inlet. At zero angle of attack the pressure distributions for the moderate-to-high values of inlet-velocity ratio are essentially flat with very low values of peak negative pressure coefficient. As the inlet-velocity ratio is progressively decreased, a pressure peak appears near the lip of the nose inlet because of the high local angle of attack of the lip. The magnitude of the pressure peak increases rapidly as the inlet-velocity ratio is further decreased. Progressively higher values of the inlet-velocity ratio are required to eliminate the pressure peak as the model angle of attack is increased. At higher values of inlet-velocity ratio, a favorable pressure distribution can be obtained through greater ranges of angle of attack.

The critical-speed characteristics for the NACA 1–40–200 and 1–40–150 nose inlets are presented in figure 11. The critical Mach numbers were determined from the measured pressure distributions by means of the Von Kármán relation (reference 4). For a given angle of attack, little change occurs in the value of the critical Mach number for values of inlet-velocity ratio in the medium-to-high range. The sharp downward break in the critical Mach number curve occurs at a value of inlet-velocity ratio below which the critical Mach number is determined by a pressure peak near the lip. Further decrease in inlet-velocity ratio produces a rapid decrease in critical Mach number.

An important effect of an increase in angle of attack (fig. 11) is to shift the knee of the critical Mach number curve to progressively higher values of inlet-velocity ratio. A comparison of the critical-speed characteristics for two angles of attack shows only small differences between the values of the critical speed above the knees of the two curves; below the knees of the curves, however, marked differences are noted.

Figures 12 to 27 present pressure distributions and critical Mach number characteristics for the nose inlets having inlet-diameter ratios of 0.50, 0.60, and 0.70. In general, the effects of changes in inlet-velocity ratio and angle of attack are similar to those described for the NACA 1–40–200 and 1–40–150 nose inlets.

The effects of inlet proportions.—The critical Mach number curves for the series of nose inlets tested have been grouped for constant angles of attack, according to inlet-diameter ratio and length ratio, to illustrate the effects of these parameters on the critical Mach number characteristics. Figure 28 shows the effects of length ratio on critical Mach number. For a given inlet-diameter ratio, an increase in maximum critical Mach number is shown to occur with increases in length ratio. An increase in length ratio, however, causes the knee of the critical Mach number curve to occur at progressively higher values of inlet-velocity ratio and thereby reduces the inlet-velocity-ratio range for maximum critical speed. A wider range for maximum critical speed is therefore obtained for the lower values of length ratio but with an important sacrifice in the value of maximum critical Mach number.

Figure 29 shows the effect of inlet-diameter ratio on critical Mach number characteristics. A decrease in the value of inlet-diameter ratio for a given length ratio shifts the knee of the critical Mach number curve to lower values of the inlet-velocity ratio and thereby increases the extent of the inlet-velocity-ratio range for maximum critical speed. The effect of inlet-diameter ratio on maximum critical speed is small at large values of length ratio. For extremely low values of length ratio, a significant decrease in maximum critical Mach number occurs with decrease in the value of inlet-diameter ratio. These data thus indicate that the length ratio is the more important of these two parameters in governing the maximum critical speed; the inlet-diameter ratio is, in general, secondary. For a given length ratio, however, the inlet-diameter ratio governs the position of the knee of the critical Mach number curve.

In figure 28 envelope curves have been drawn tangent to the knees of the critical Mach number curves. A summary plot of the envelope curves alone is presented in figure 30 for α=0°, 2°, and 4° for each of the d/D groups. Inasmuch as the knee of the critical Mach number curve corresponds to the point or conditions at which the nose-inlet pressure distribution is approximately flat, the envelope curve has important significance in that any point on the curve represents the optimum value of critical Mach number that can be obtained for specified values of inlet-diameter ratio and inlet-velocity ratio. Comparison of the envelopes for the three angles of attack (fig. 30) shows that important decreases in critical Mach number occur in operation at angles of attack other than 0°.

It is apparent from figure 28 that only one value of length ratio X/D will give the optimum critical speed at a particular value of inlet-diameter ratio and inlet-velocity ratio. This point on the envelope curve corresponds to the knee in the critical Mach number curve; therefore, this point represents the minimum value of inlet-velocity ratio at which the particular nose inlet will possess an essentially flat pressure distribution and a critical Mach number approaching its maximum.

In flight the level high-speed condition will usually govern the inlet design, for not only will the flight Mach number be a maximum but also the inlet-velocity ratio will usually be a minimum. The design of a nose inlet to satisfy given critical Mach number requirements must therefore be based on the minimum inlet-velocity ratio.

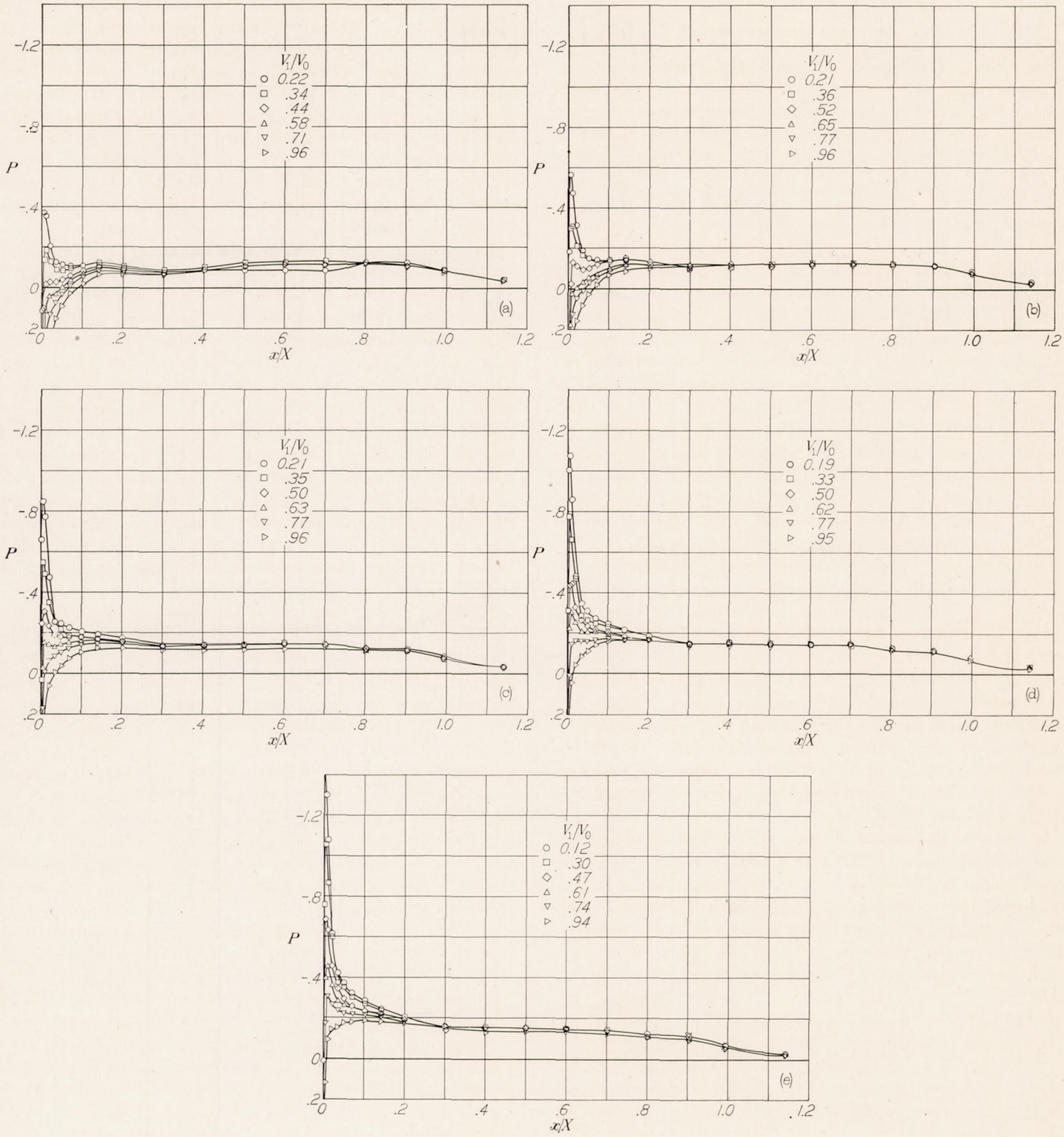

(a) $\alpha=-0.2°$. (b) $\alpha=1.9°$.
(c) $\alpha=3.9°$. (d) $\alpha=5.8°$.
(e) $\alpha=7.8°$.

FIGURE 9.—Pressure distributions over the NACA 1–40–200 nose inlet. $M_0=0.40$.

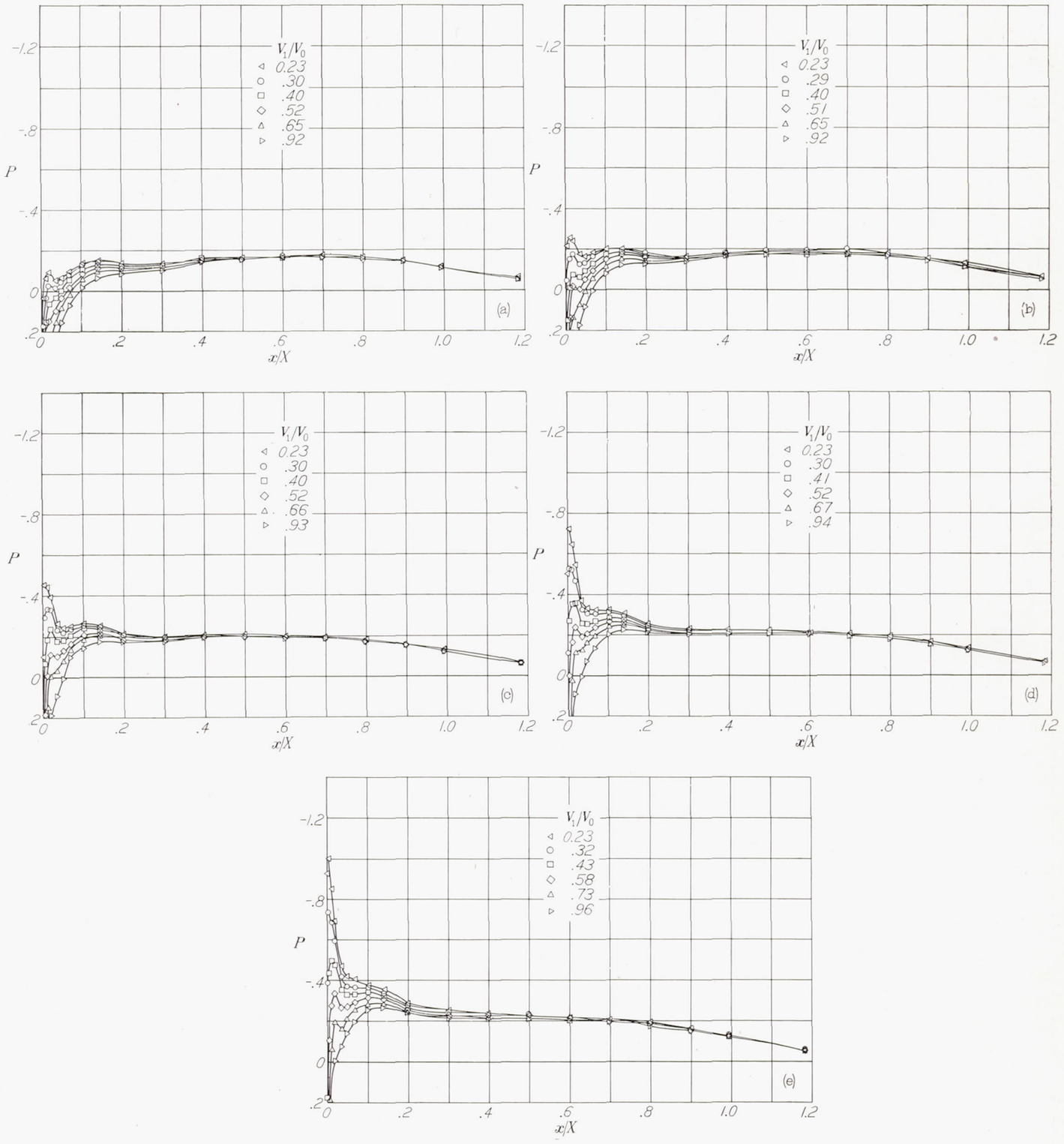

(a) $\alpha = -0.1°$. (b) $\alpha = 1.8°$.
(c) $\alpha = 3.8°$. (d) $\alpha = 5.8°$.
(e) $\alpha = 7.7°$.

FIGURE 10.—Pressure distributions over the NACA 1-40-150 nose inlet.
$M_0 = 0.4$

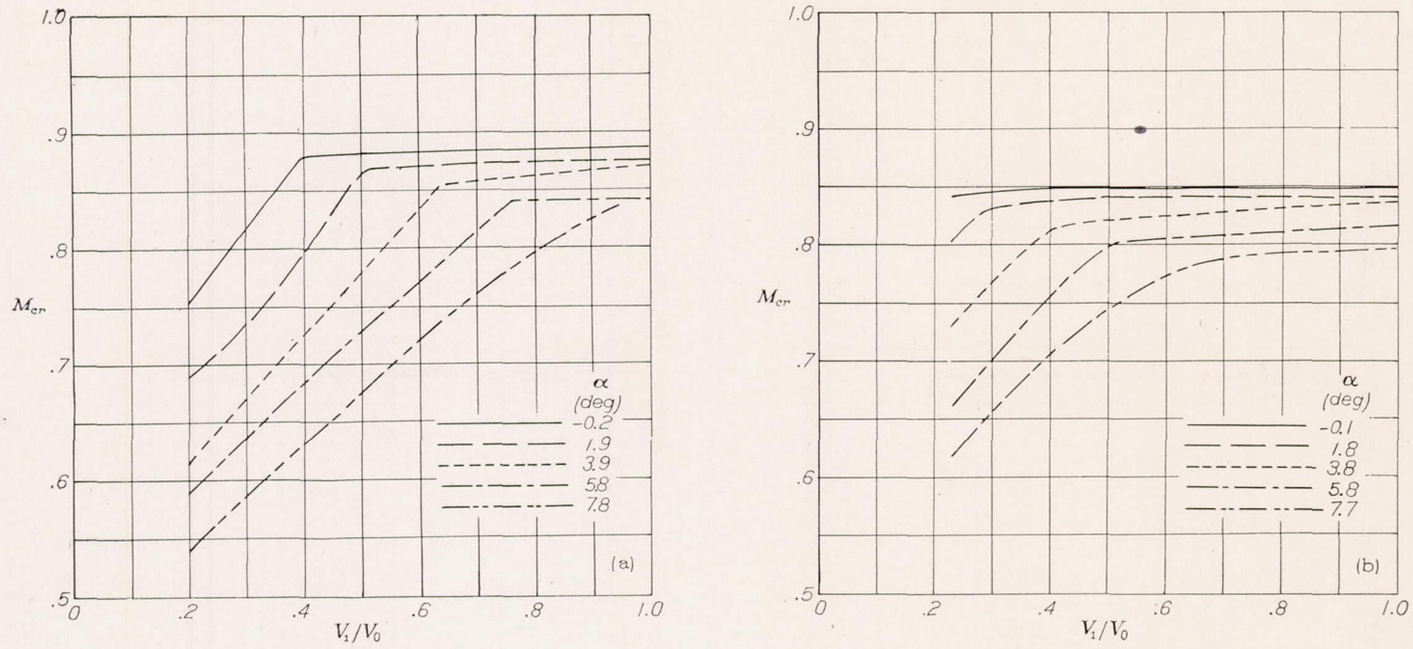

(a) NACA 1–40–200 nose inlet.

(b) NACA 1–40–150 nose inlet.

FIGURE 11.—Critical Mach numbers for the NACA 1-series nose inlets having an inlet-diameter ratio of 0.40.

SELECTION CHARTS

Basis and composition.—The envelope curves for the NACA 1-series nose inlets tested (figs. 28 and 30) have been arranged in the form of selection charts in figure 31, from which nose-inlet proportions can be determined for a specified critical Mach number and corresponding minimum air-flow quantity. The inlet-velocity ratio, which cannot be fixed for a given air quantity until the entrance diameter is known, has been replaced by the mass-flow coefficient $\frac{m}{\rho_0 F V_0}$, which is an independent design quantity. The mass-flow coefficient is related to the inlet-velocity ratio by the following equation:

$$\frac{m}{\rho_0 F V_0}=\left(\frac{d}{D}\right)^2\left(\frac{V_1}{V_0}\right)\left[\frac{\gamma-1}{2}M_0^2-\frac{\gamma-1}{2}M_0^2\left(\frac{V_1}{V_0}\right)^2+1\right]^{\frac{1}{\gamma-1}}$$

Figure 32 is a plot of inlet-velocity ratio against mass-flow coefficient for various values of d/D and M_0. The curves for Mach numbers less than 0.50 have been omitted. The curves for incompressible flow ($M_0=0$) can be added to this figure as straight lines between the origin and the points at which the curves converge at $\frac{V_1}{V_0}=1.0$. The inlet-velocity ratios for the envelope curves from figure 30 have been converted to mass-flow coefficients at the corresponding value of M_{cr} by means of figure 32.

The solid lines in the lower half of the selection chart (fig. 31) are the envelope curves from figure 30. The interjacent dashed curves represent the envelopes for intermediate values of d/D and were obtained from cross plots of the experimental data. The envelope curves have been extended beyond the limits of the data by only a small amount. Some additional extrapolation may be judiciously performed on the selection chart, if necessary, through reference to figure 28. The dashed curves intersecting the main curves on the selection chart are lines of constant inlet-velocity ratio for corresponding values of $\frac{m}{\rho_0 F V_0}$, d/D, and M_{cr} on this chart. The solid curves on the upper half of the selection chart are plots of the value of X/D required for an NACA 1-series nose inlet having the maximum critical Mach number for a particular value of inlet-diameter ratio and mass-flow coefficient.

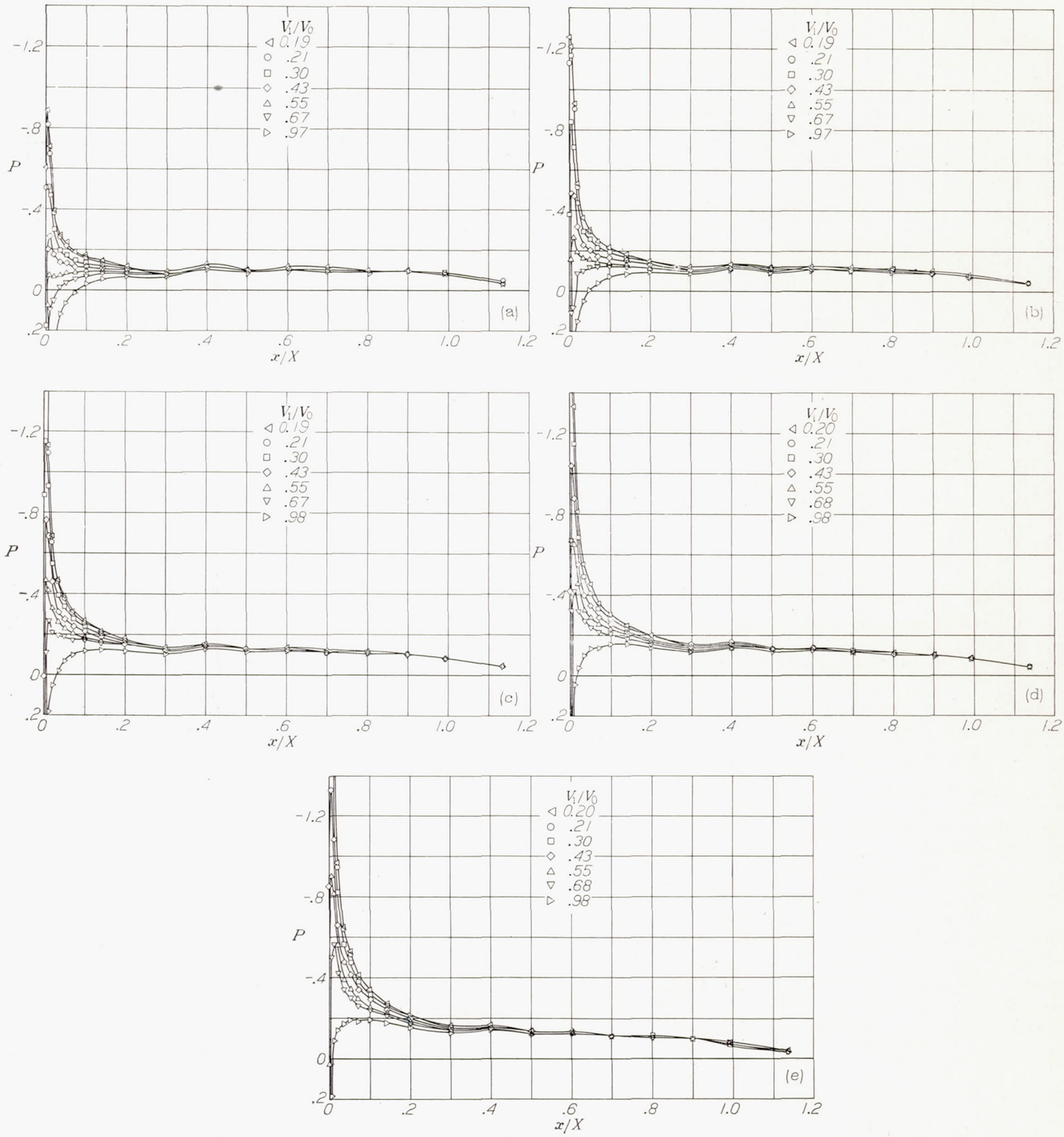

(a) $\alpha = -0.1°$. (b) $\alpha = 1.8°$.
(c) $\alpha = 3.9°$. (d) $\alpha = 5.8°$.
(e) $\alpha = 7.9°$.

FIGURE 12.—Pressure distributions over the NACA 1–50–200 nose inlet. $M_0 = 0.40$.

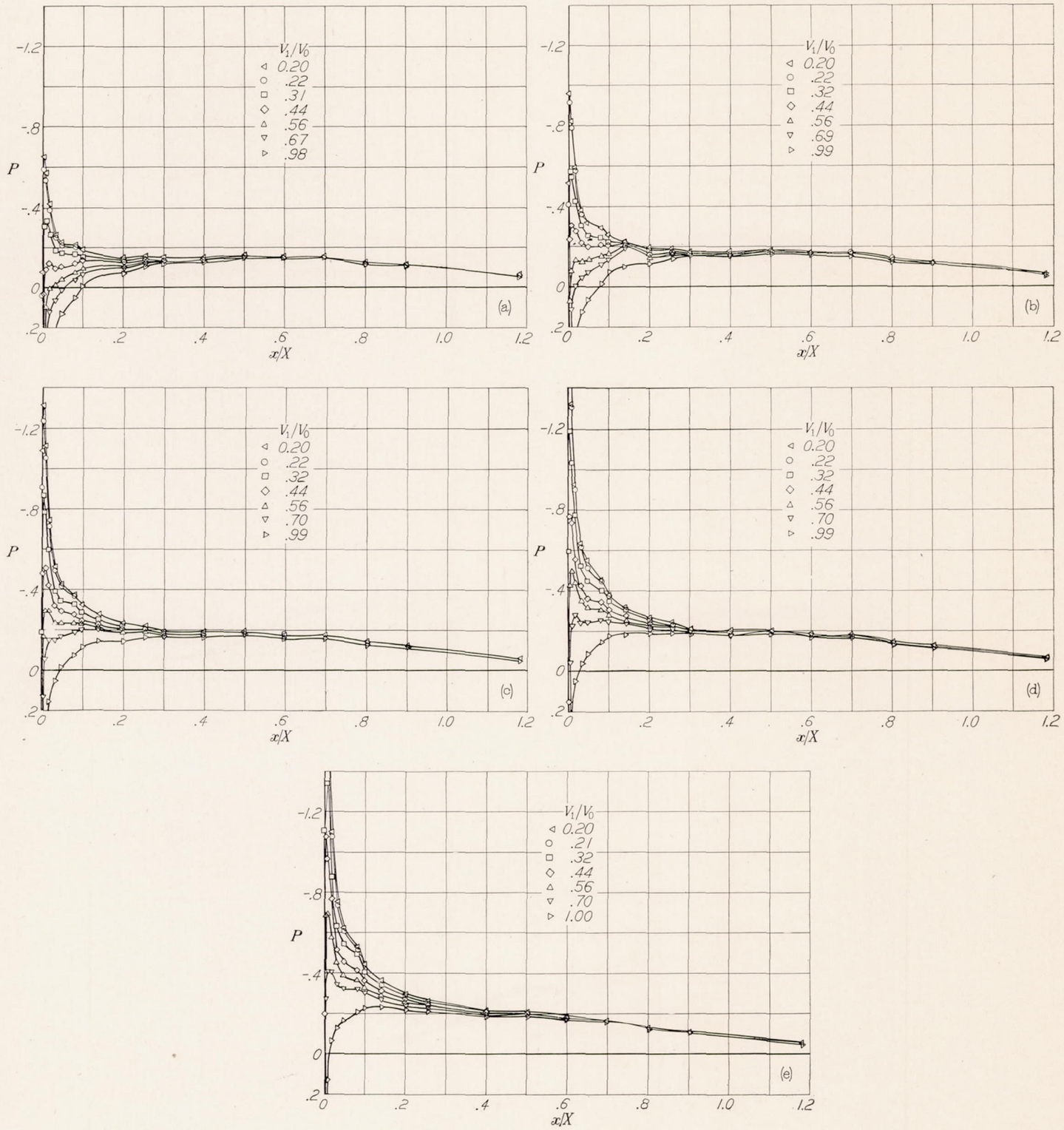

(a) $\alpha = -0.2°$. (b) $\alpha = 1.8°$.
(c) $\alpha = 3.9°$. (d) $\alpha = 5.8°$.
(e) $\alpha = 7.8°$.

FIGURE 13.—Pressure distributions over the NACA 1–50–150 nose inlet. $M_0 = 0.40$.

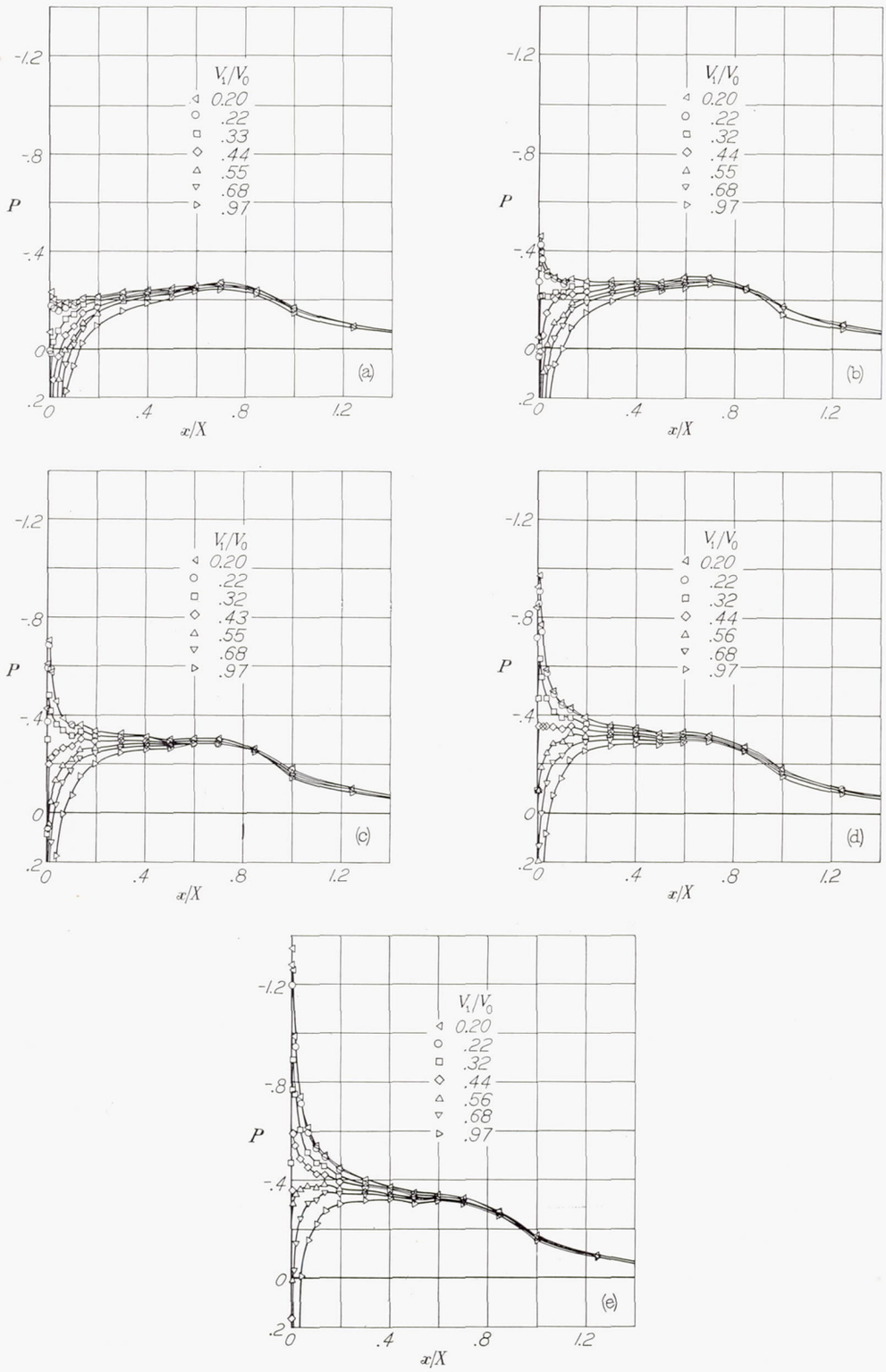

(a) $\alpha = -0.2°$. (b) $\alpha = 1.8°$.
(c) $\alpha = 3.9°$. (d) $\alpha = 5.8°$.
(e) $\alpha = 7.8°$.

FIGURE 14.—Pressure distributions over the NACA 1–50–100 nose inlet. $M_0 = 0.40$.

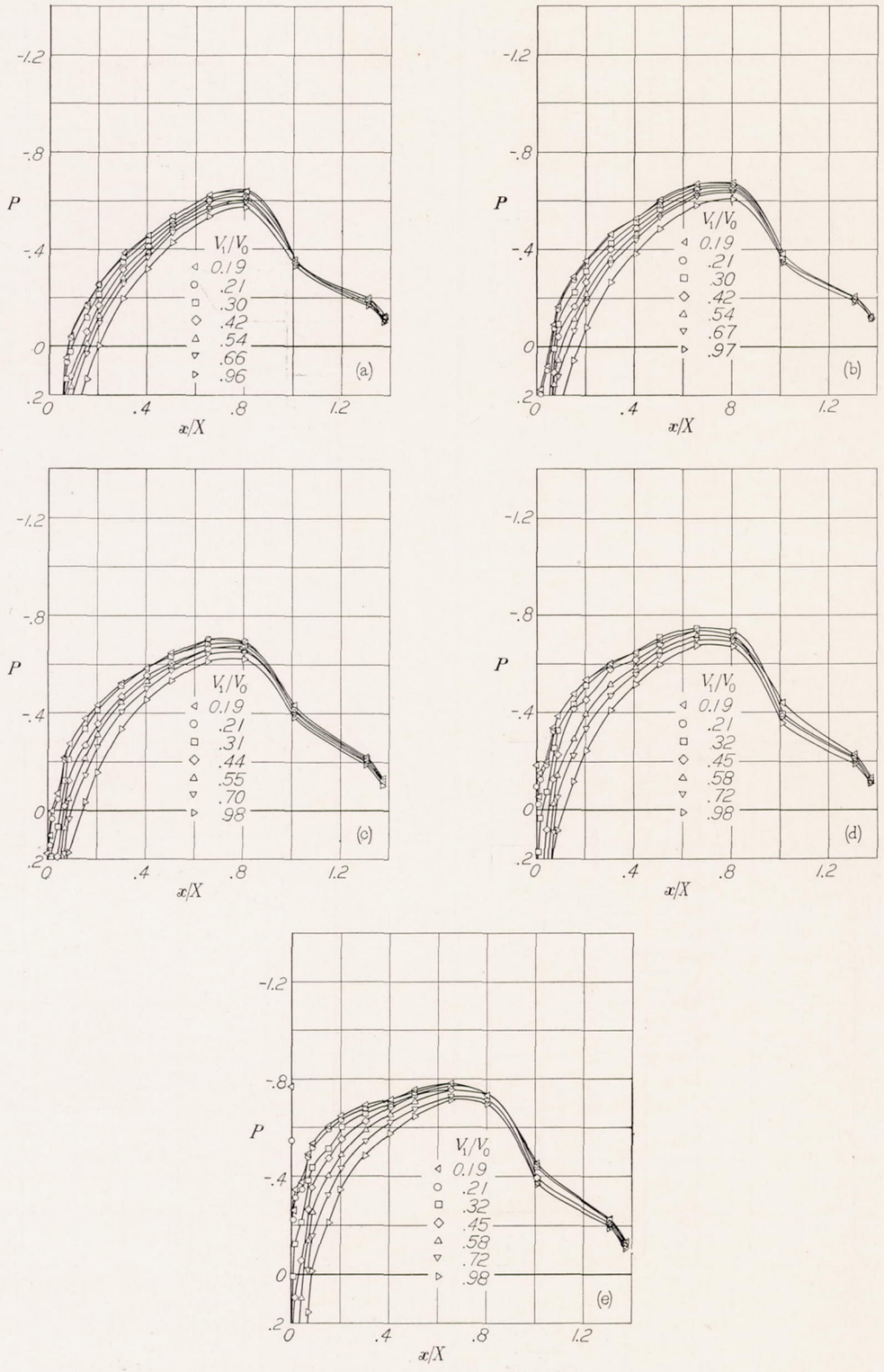

(a) $\alpha=-0.1°$. (b) $\alpha=1.8°$.
(c) $\alpha=3.9°$. (d) $\alpha=5.8°$.
(e) $\alpha=7.8°$.

FIGURE 15.—Pressure distributions over the NACA 1–50–050 nose inlet, $M_0=0.40$.

844332—50——3

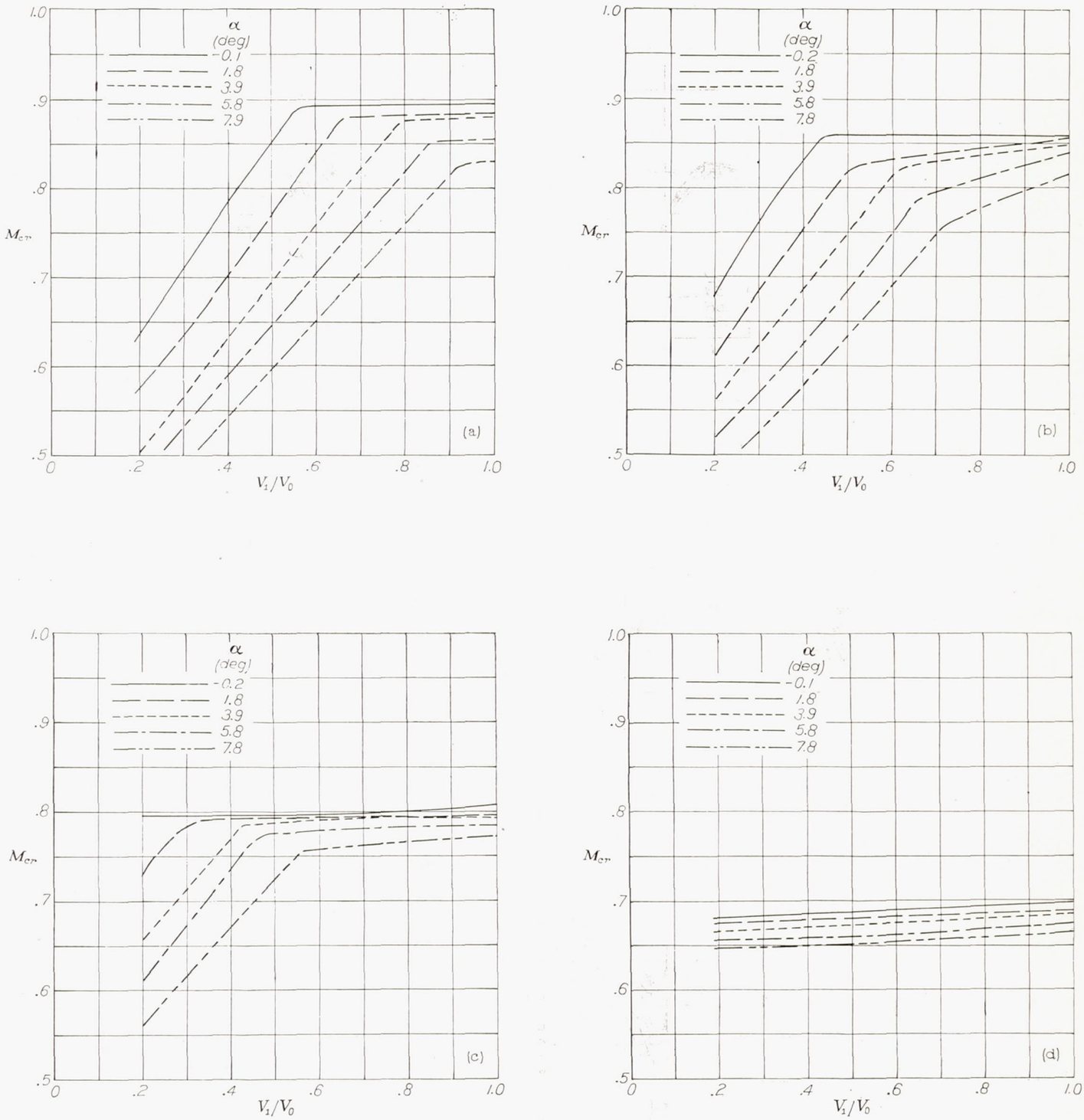

(a) NACA 1–50–200 nose inlet. (b) NACA 1–50–150 nose inlet.
(c) NACA 1–50–100 nose inlet. (d) NACA 1–50–050 nose inlet.

FIGURE 16.—Critical Mach numbers for the NACA 1-series nose inlets having an inlet-diameter ratio of 0.50.

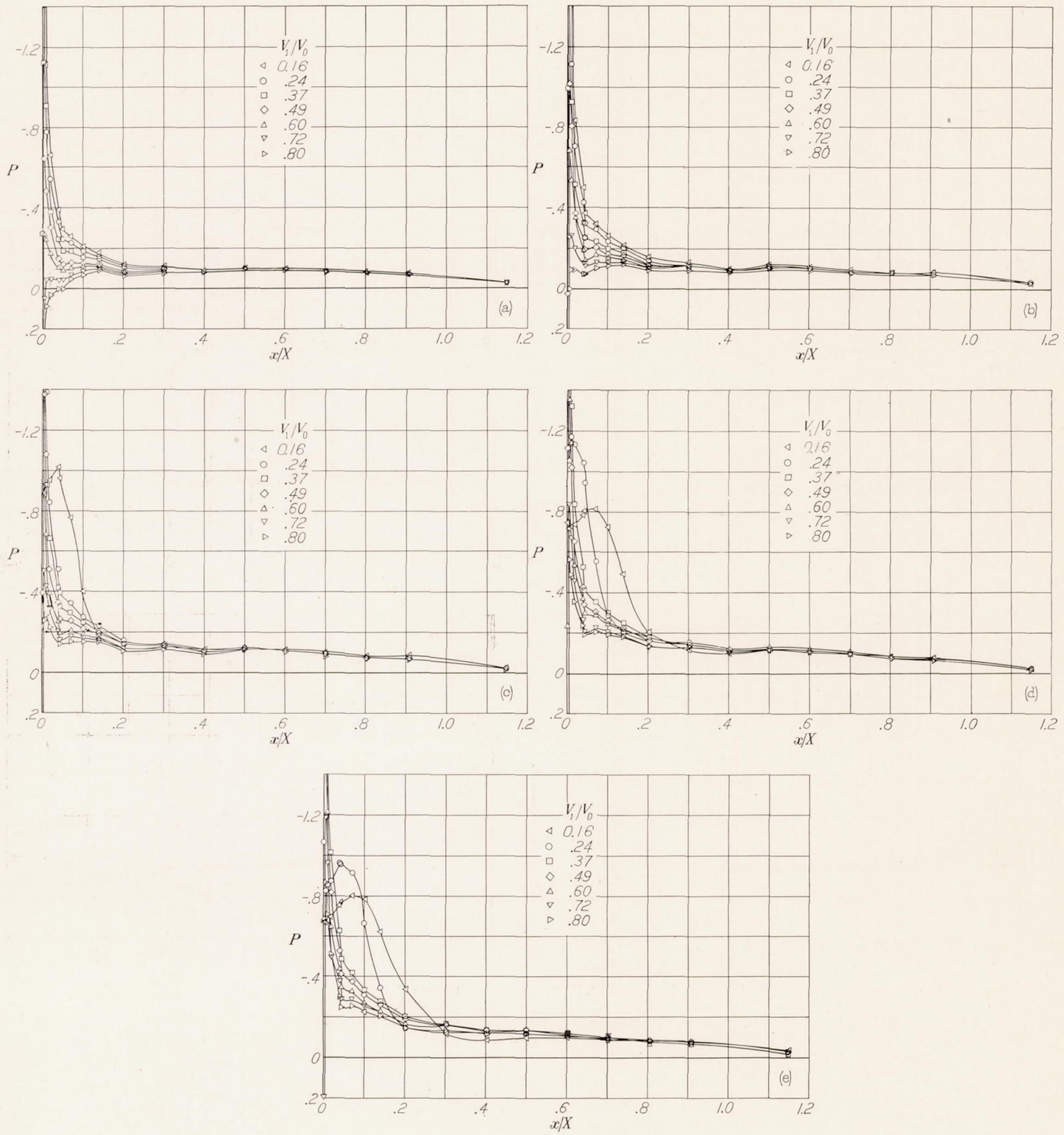

(a) $\alpha = -0.1°$. (b) $\alpha = 1.9°$.
(c) $\alpha = 3.9°$. (d) $\alpha = 5.9°$.
(e) $\alpha = 7.9°$.

FIGURE 17.—Pressure distributions over the NACA 1–60–200 nose inlet. $M_0 = 0.30$.

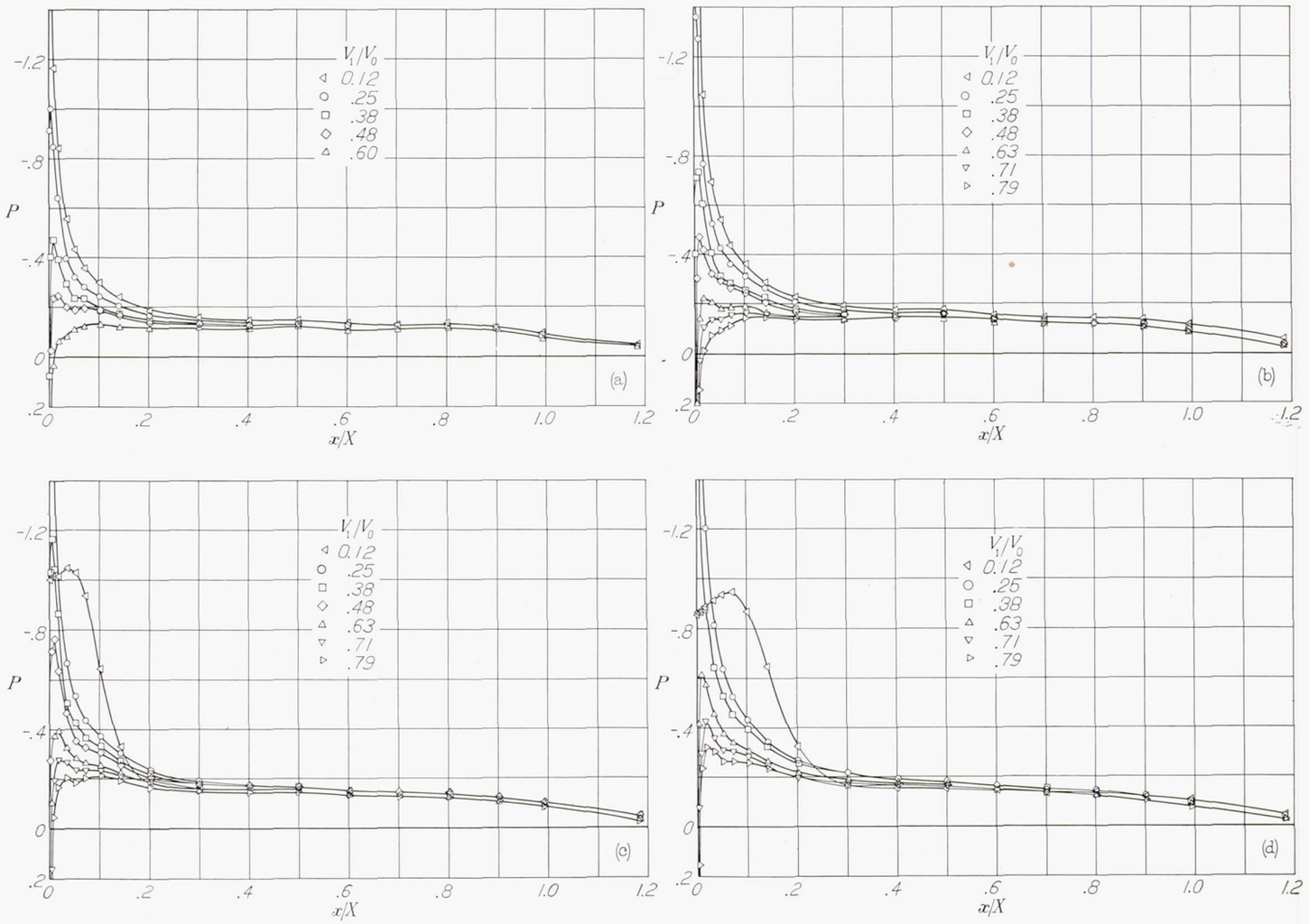

(a) $\alpha = -0.1°$. (b) $\alpha = 1.8°$.
(c) $\alpha = 3.9°$. (d) $\alpha = 5.9°$.

FIGURE 18.—Pressure distributions over the NACA 1–60–150 nose inlet.
$M_0 = 0.30$.

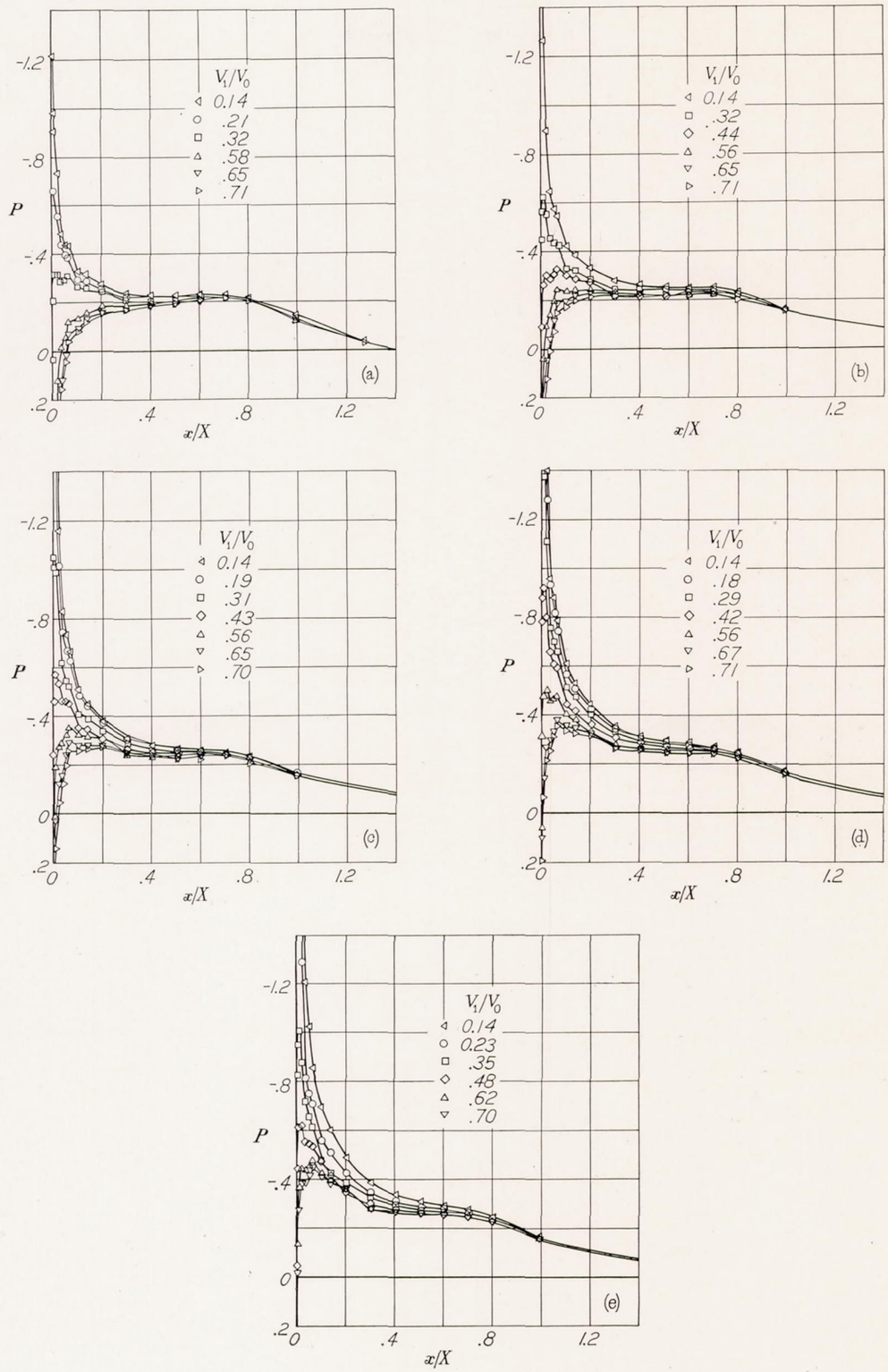

(a) $\alpha=-0.2°$. (b) $\alpha=1.9°$.
(c) $\alpha=3.9°$. (d) $\alpha=5.8°$.
(e) $\alpha=7.8°$.

FIGURE 19.—Pressure distributions over the NACA 1-60-100 nose inlet. $M_0=0.40$.

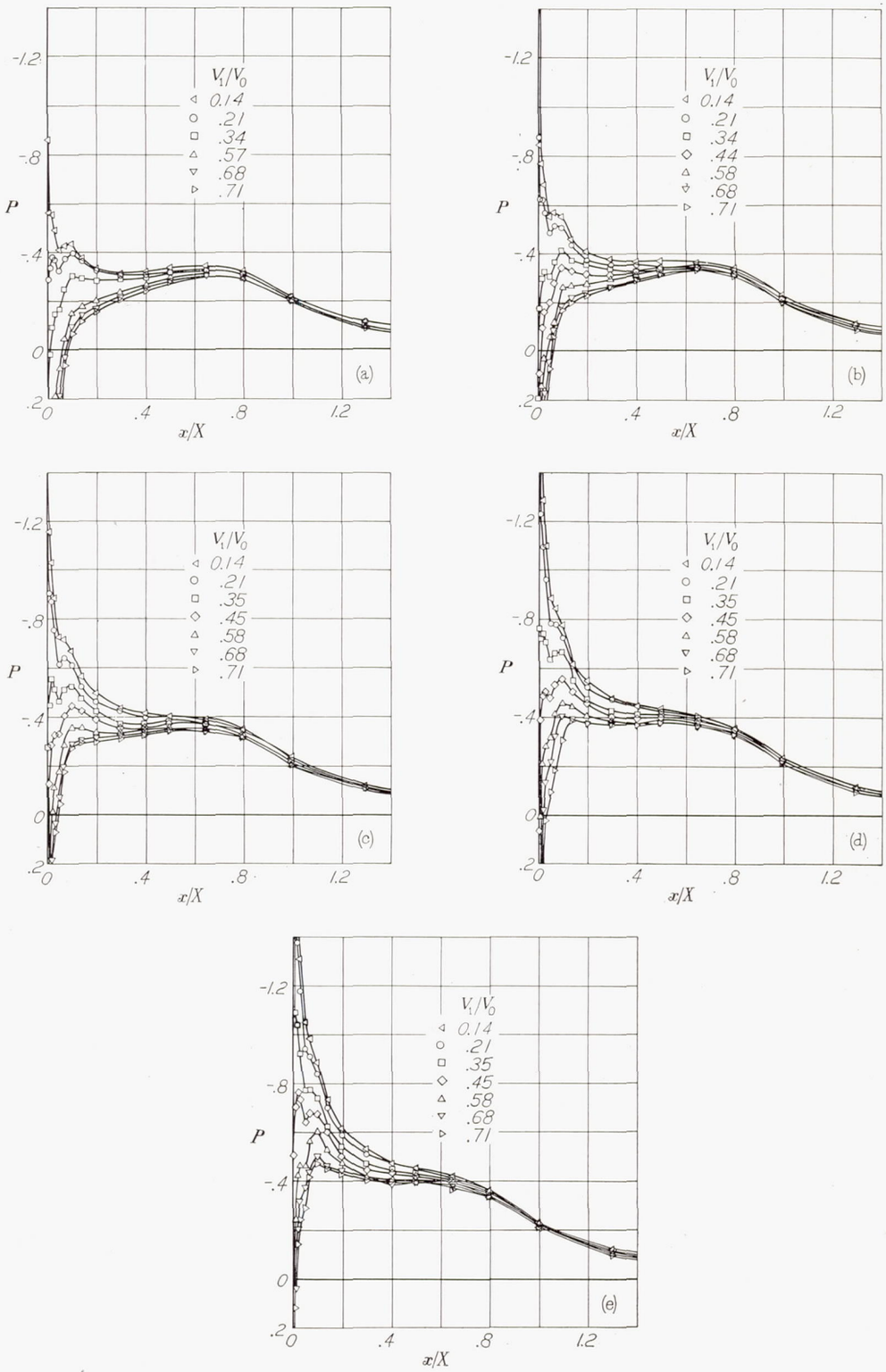

(a) $\alpha = -0.2°$. (b) $\alpha = 1.8°$.
(c) $\alpha = 3.8°$. (d) $\alpha = 5.8°$.
(e) $\alpha = 7.8°$.

FIGURE 20.—Pressure distributions over the NACA 1-60-075 nose inlet.
$M_0 = 0.40$.

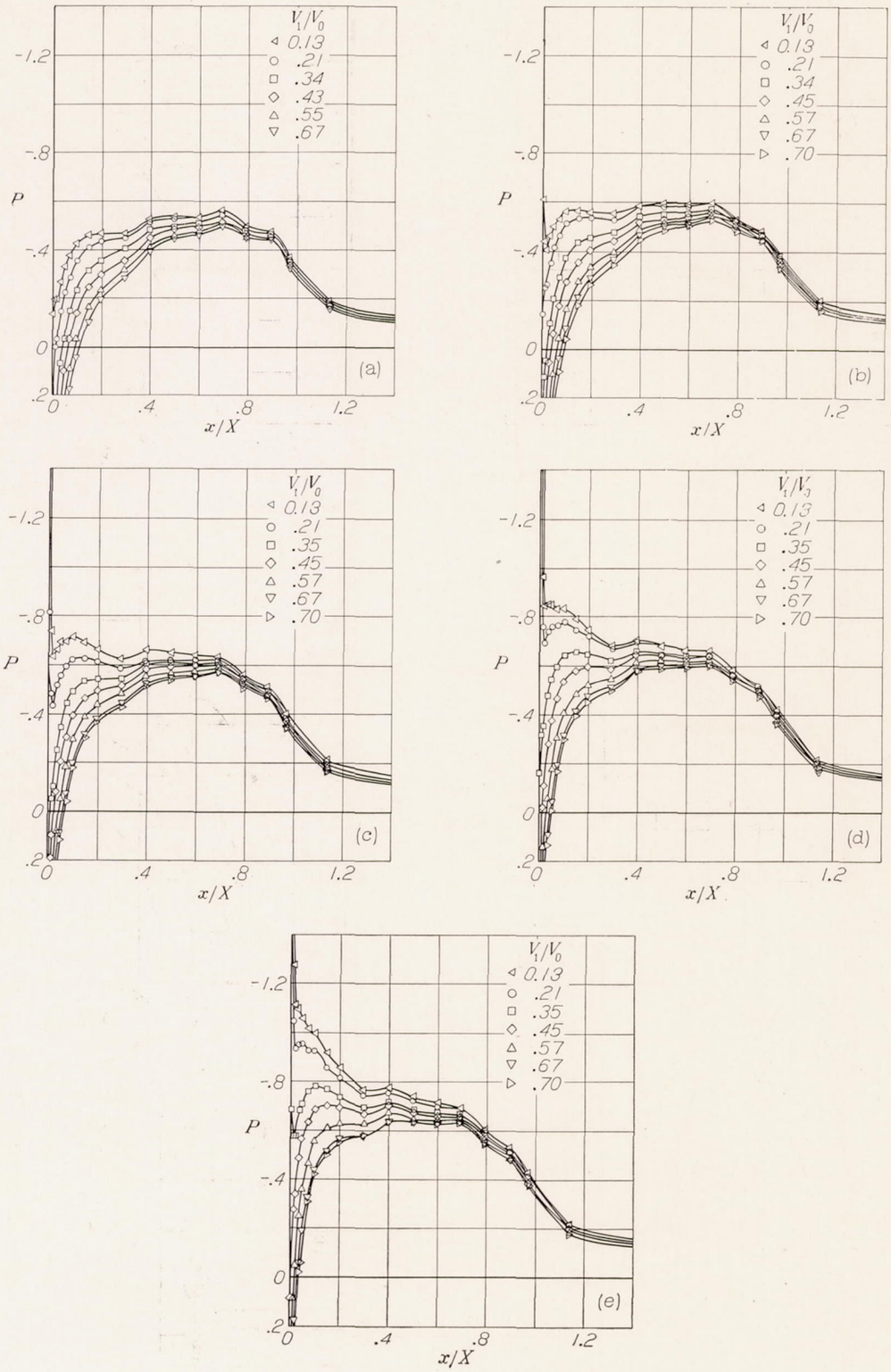

(a) $\alpha=-0.2°$. (b) $\alpha=1.8°$.
(c) $\alpha=3.8°$. (d) $\alpha=5.8°$.
(e) $\alpha=7.8°$.

FIGURE 21.—Pressure distributions over the NACA 1–60–050 nose inlet. $M_0=0.40$.

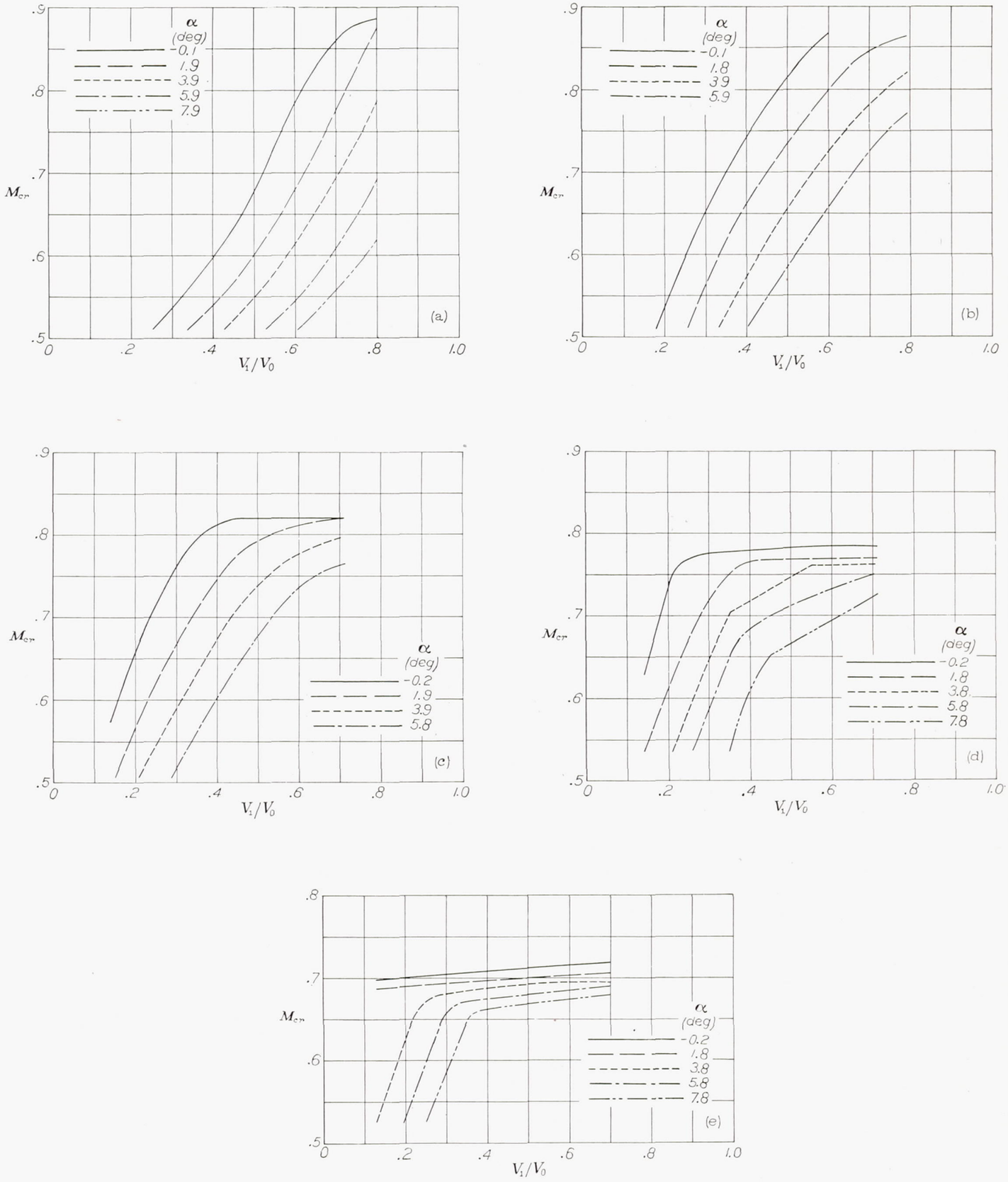

(a) NACA 1-60-200 nose inlet.
(b) NACA 1-60-150 nose inlet.
(c) NACA 1-60-100 nose inlet.
(d) NACA 1-60-075 nose inlet.
(e) NACA 1-60-050 nose inlet.

FIGURE 22.—Critical Mach numbers for the NACA 1-series nose inlets having an inlet-diameter ratio of 0.60.

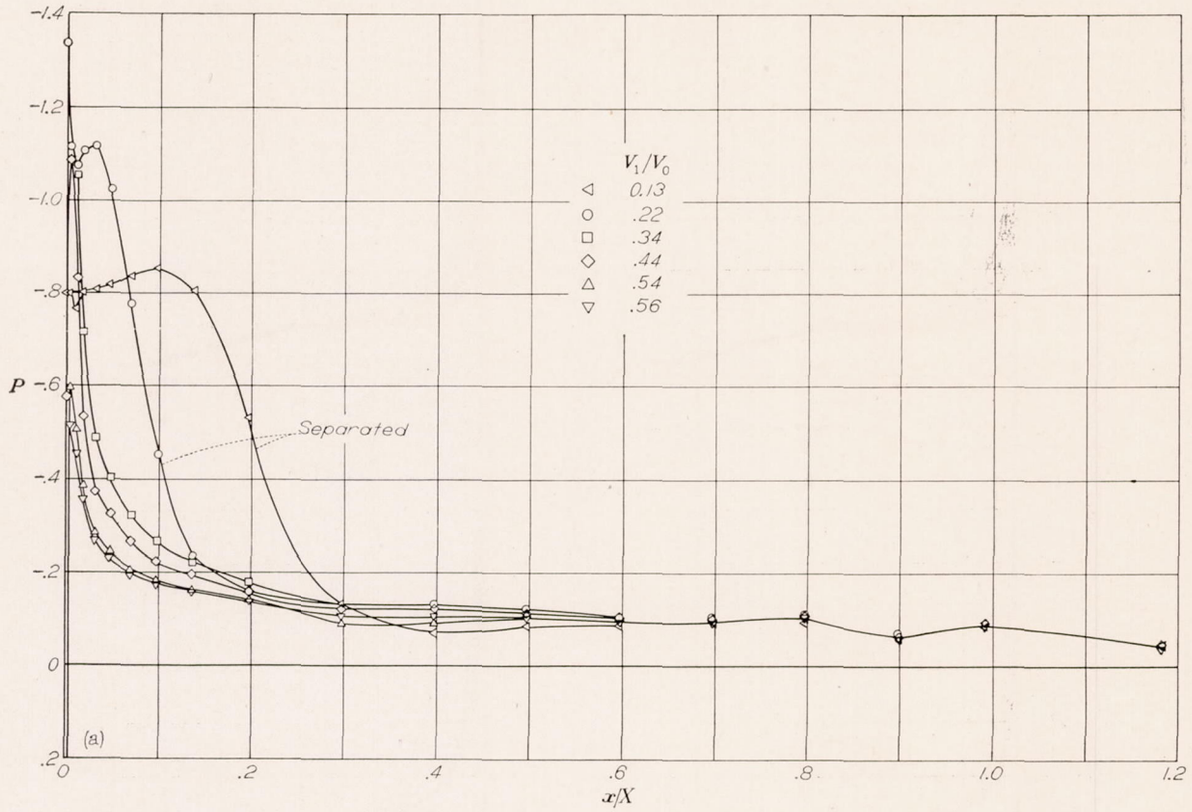

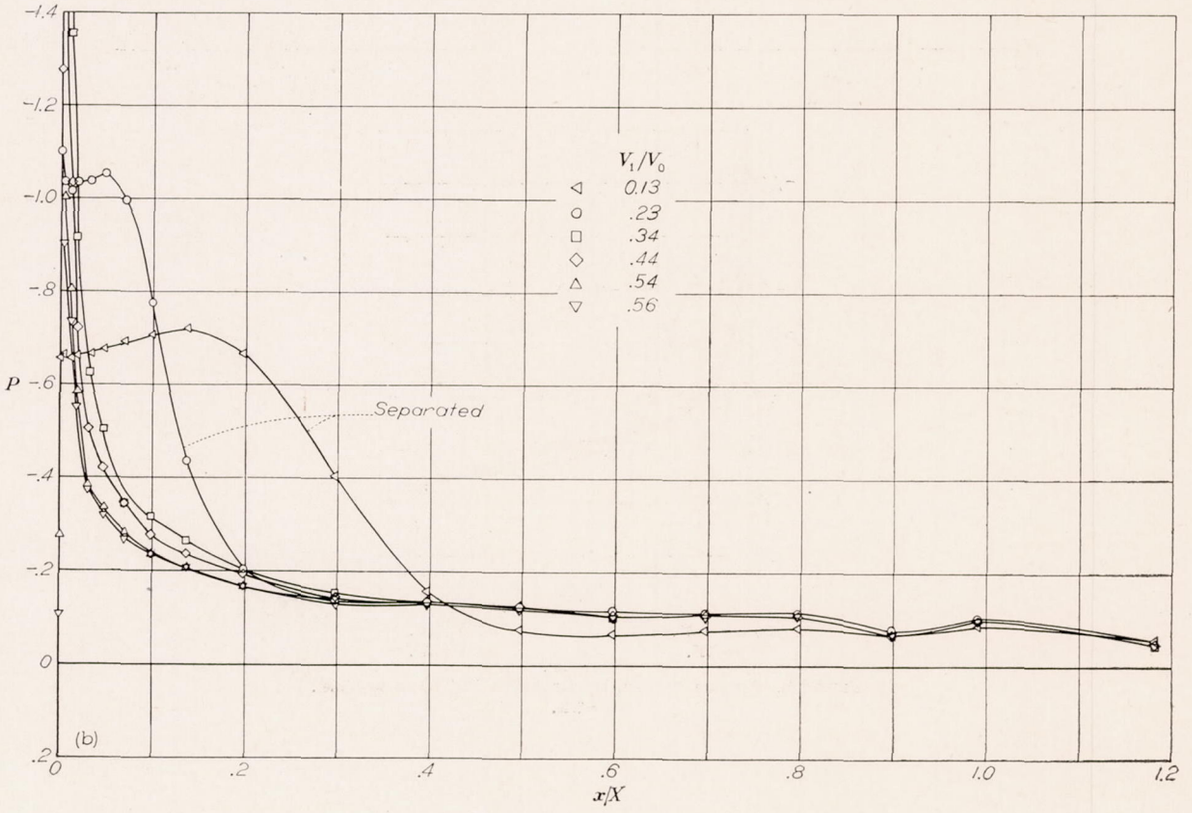

(a) $\alpha = -0.1°$.
(b) $\alpha = 1.8°$.

FIGURE 23.—Pressure distributions over the NACA 1-70-150 nose inlet.
$M_0 = 0.40$.

844332—50——4

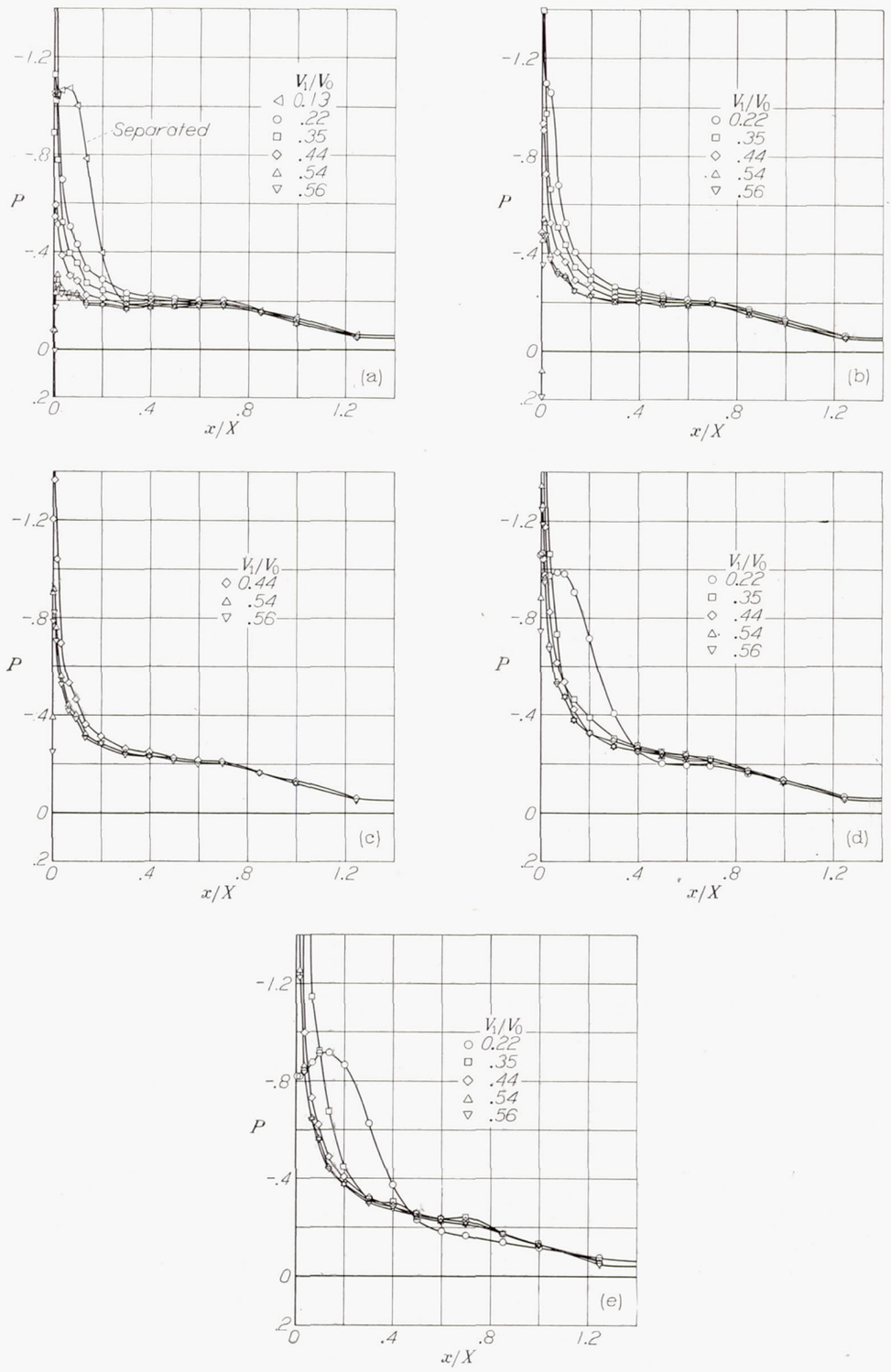

(a) $\alpha = -0.1°$. (b) $\alpha = 1.8°$.
(c) $\alpha = 3.8°$. (d) $\alpha = 5.8°$.
(e) $\alpha = 7.8°$.

FIGURE 24.—Pressure distributions over the NACA 1–70–100 nose inlet. $M_0 = 0.40$.

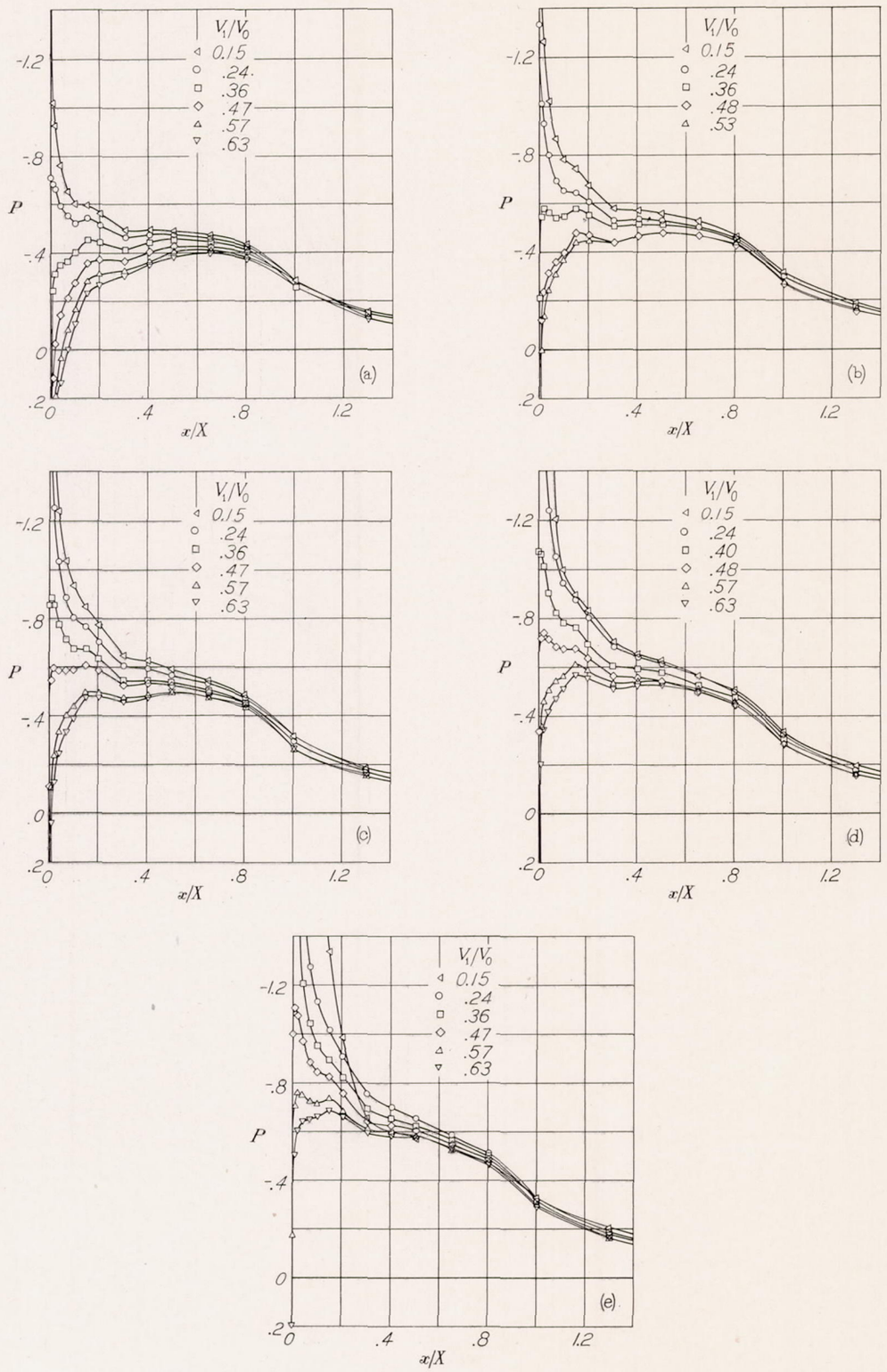

(a) $\alpha=-0.1°$. (b) $\alpha=1.8°$.
(c) $\alpha=3.8°$. (d) $\alpha=5.7°$.
(e) $\alpha=7.9°$.

FIGURE 25.—Pressure distributions over the NACA 1-70-050 nose inlet.
$M_0=0.30$.

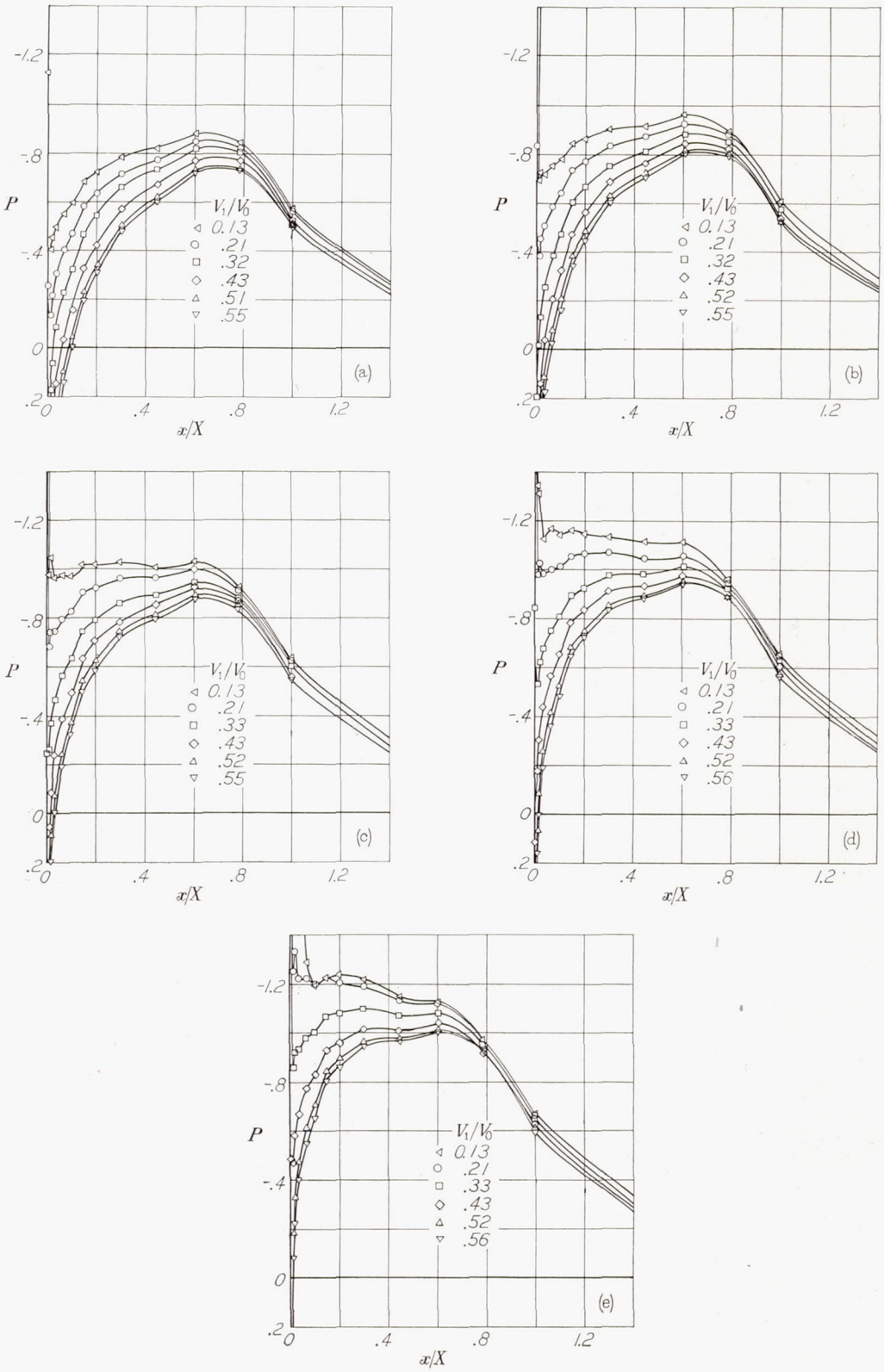

(a) $\alpha=-0.1°$. (b) $\alpha=1.8°$.
(c) $\alpha=3.8°$. (d) $\alpha=5.8°$.
(e) $\alpha=7.8°$.

FIGURE 26.—Pressure distributions over the NACA 1-70-030 nose inlet. $M_0=0.40$.

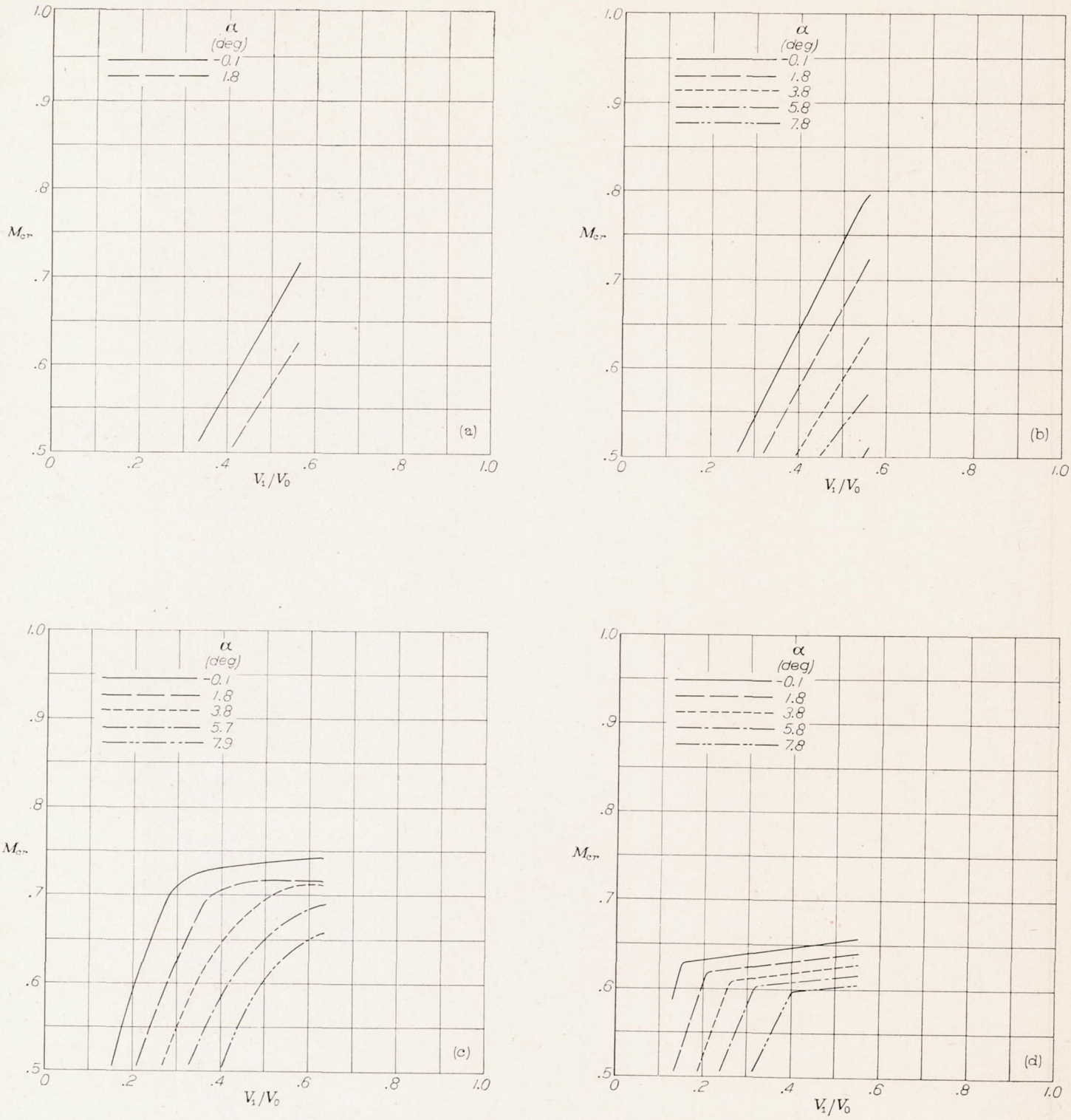

(a) NACA 1–70–150 nose inlet. (b) NACA 1–70–100 nose inlet.
(c) NACA 1–70–050 nose inlet. (d) NACA 1–70–030 nose inlet.

FIGURE 27.—Critical Mach numbers for the NACA 1-series nose inlets having an inlet-diameter ratio of 0.70.

844332—50——5

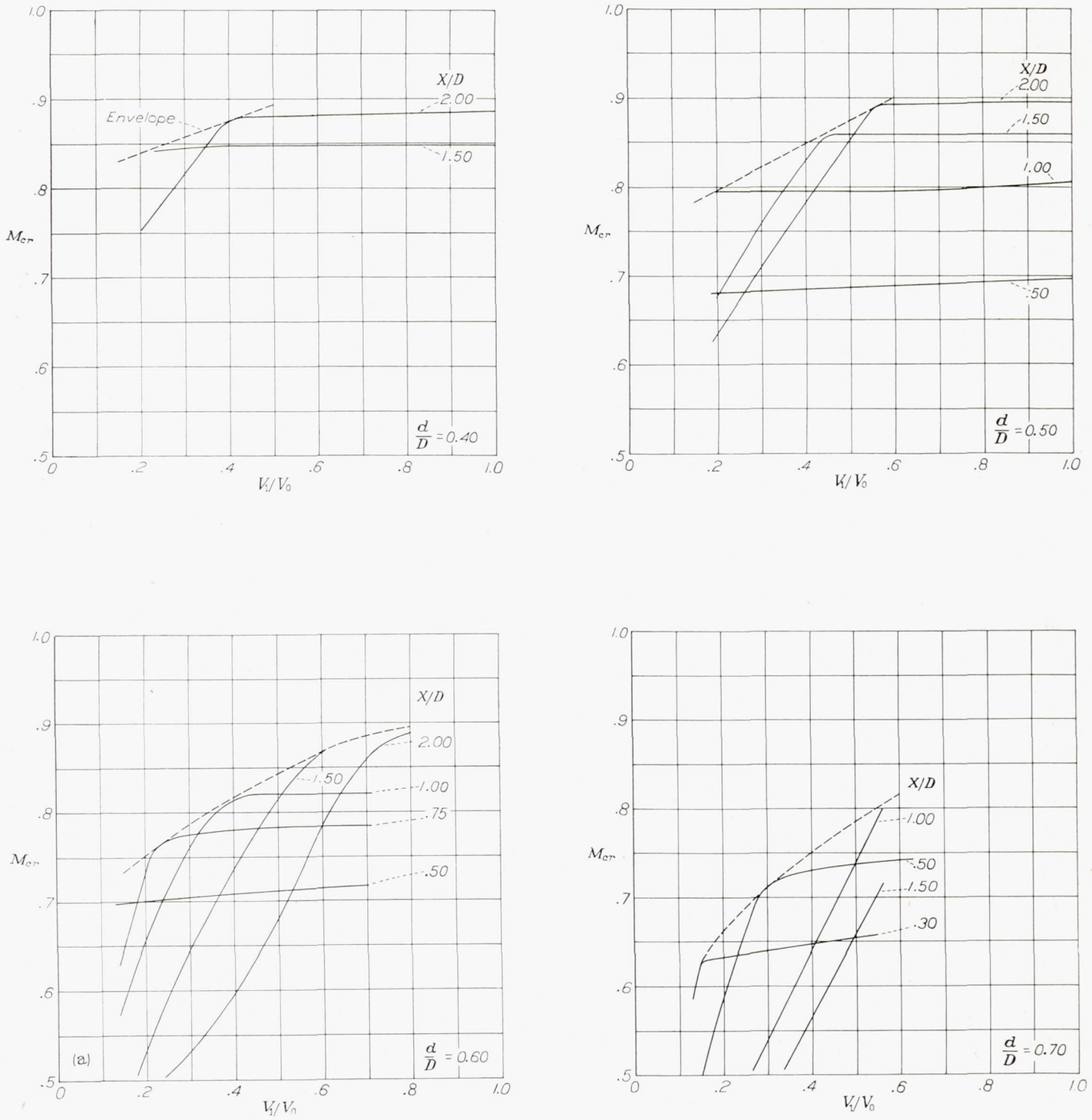

(a) $\alpha=0°$ (nominal).

FIGURE 28.—Critical Mach number characteristics of NACA 1-series nose inlets tested, grouped according to inlet-diameter ratio.

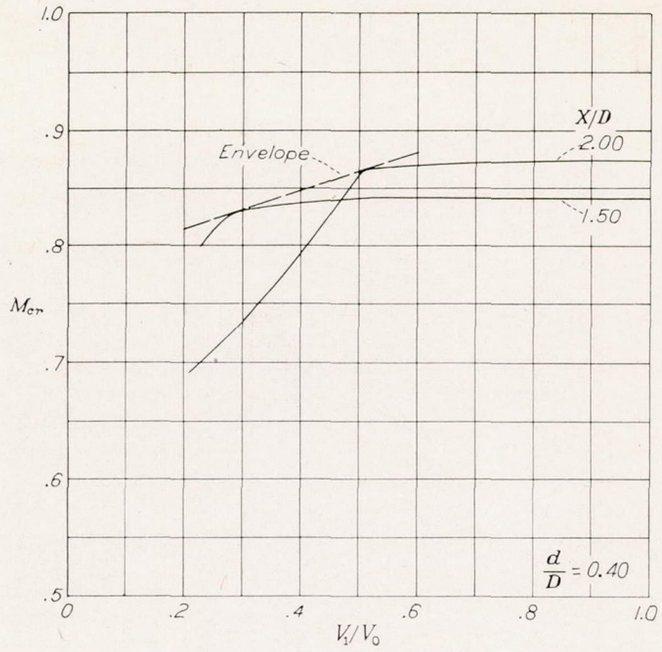

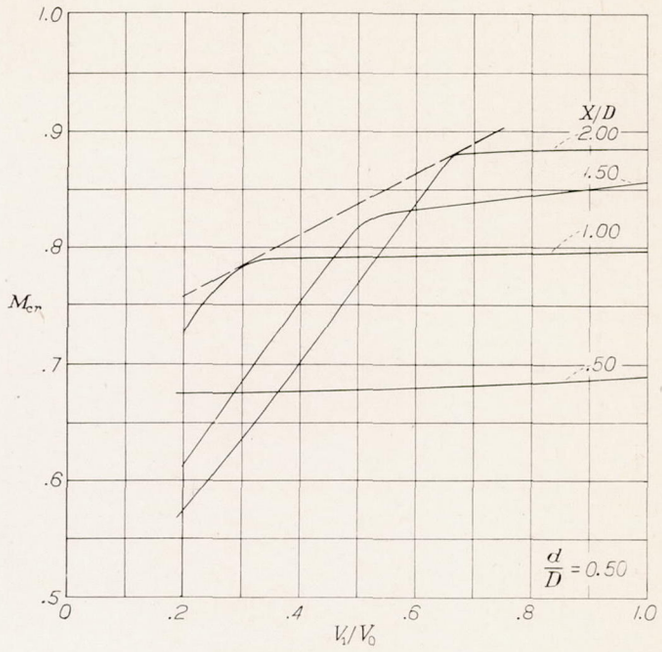

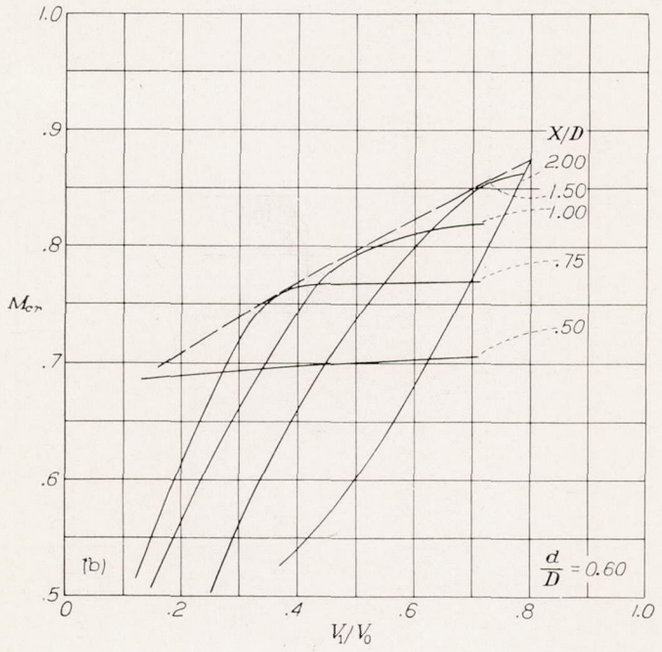

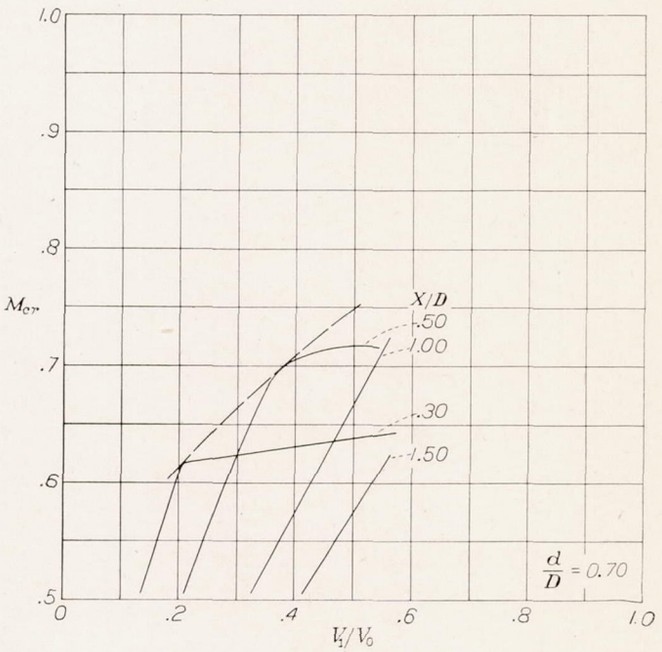

(b) α=2° (nominal).

FIGURE 28.—Continued.

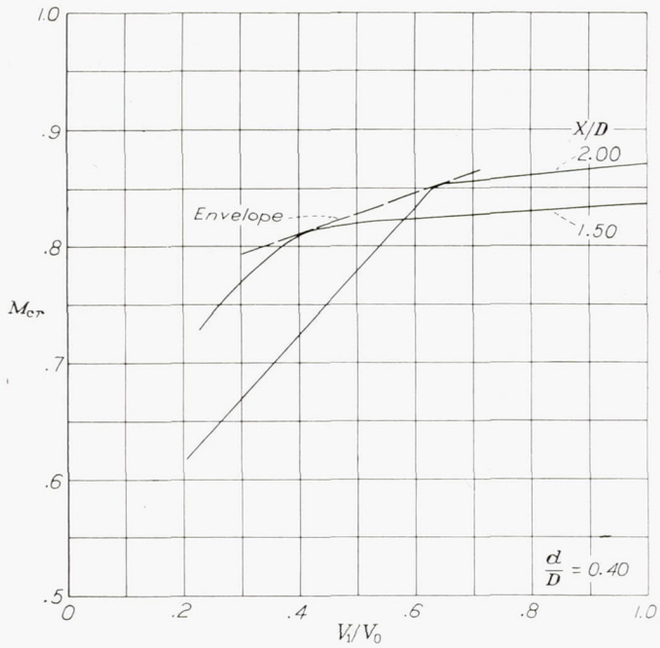

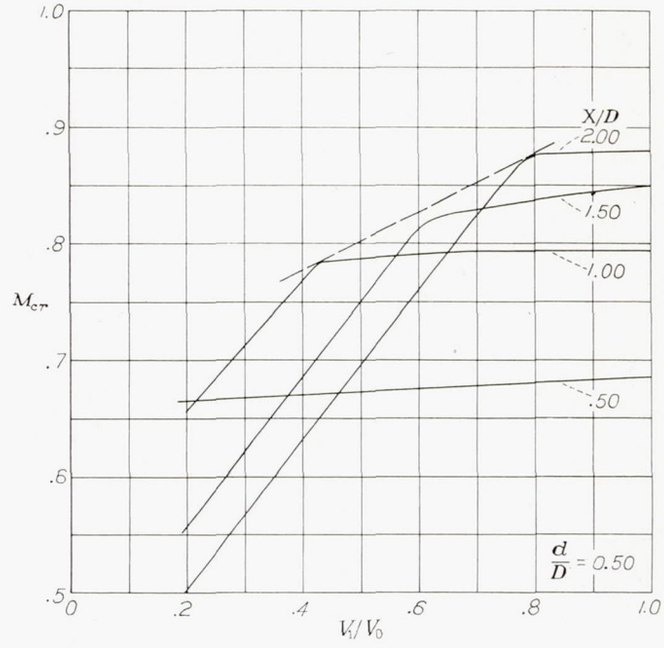

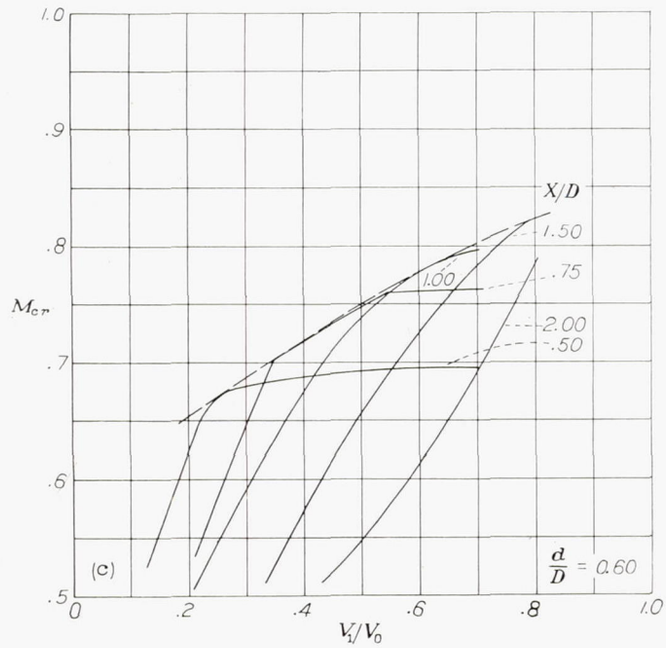

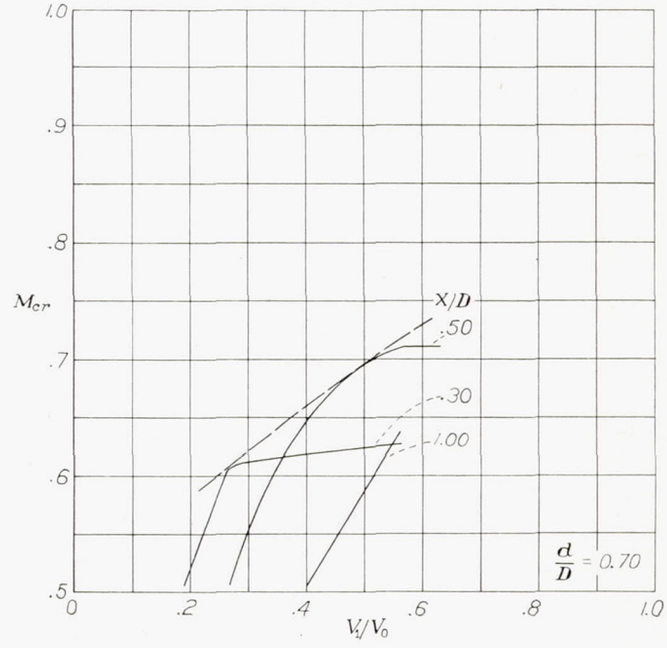

(c) $\alpha = 4°_{a}$ (nominal).

FIGURE 28.—Concluded.

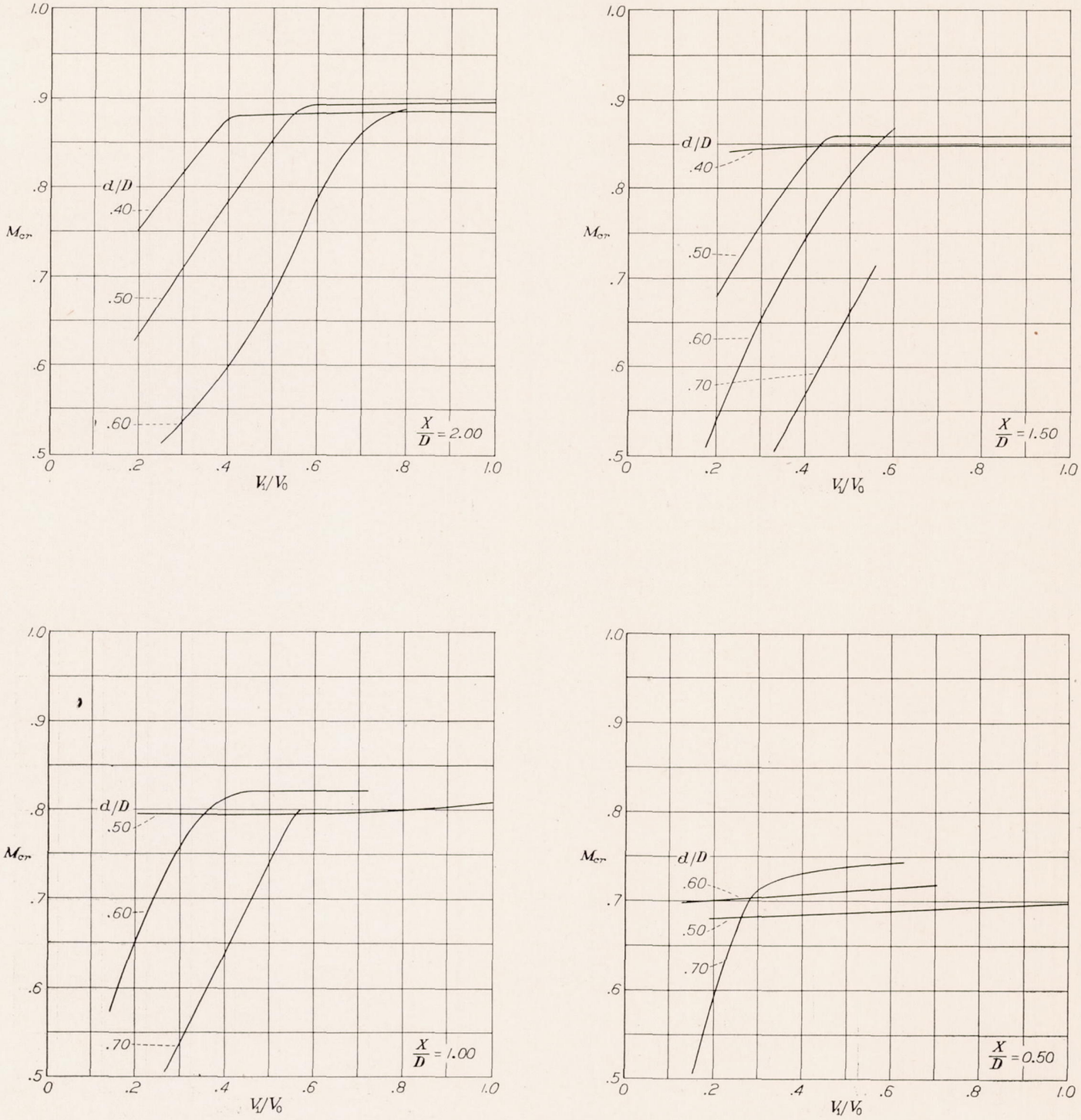

FIGURE 29.—Critical Mach number characteristics of NACA 1-series nose inlets tested, grouped according to length ratio. $\alpha=0°$.

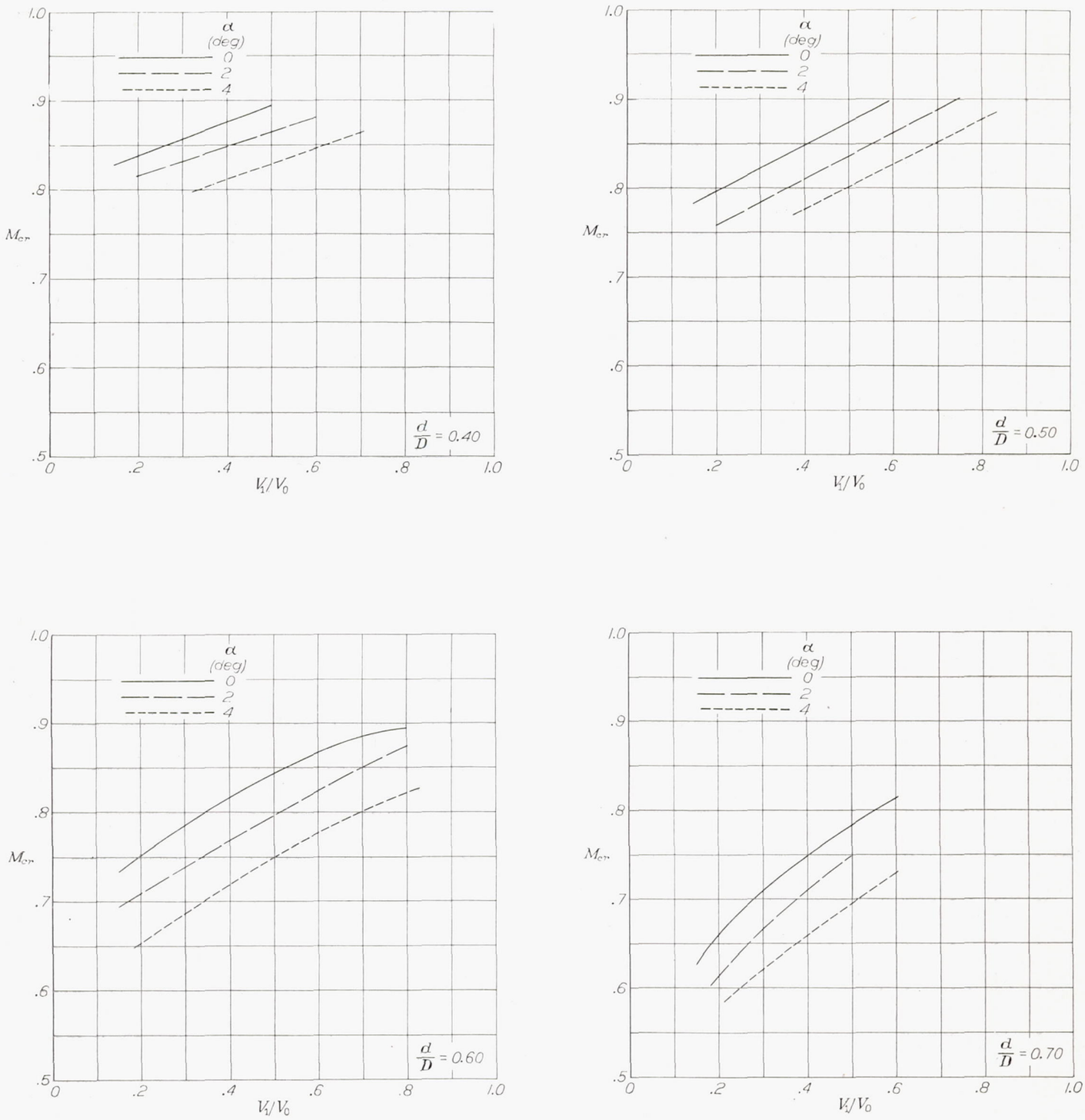

FIGURE 30.—Envelope curves for NACA 1-series nose inlets at three angles of attack. (From fig. 28.)

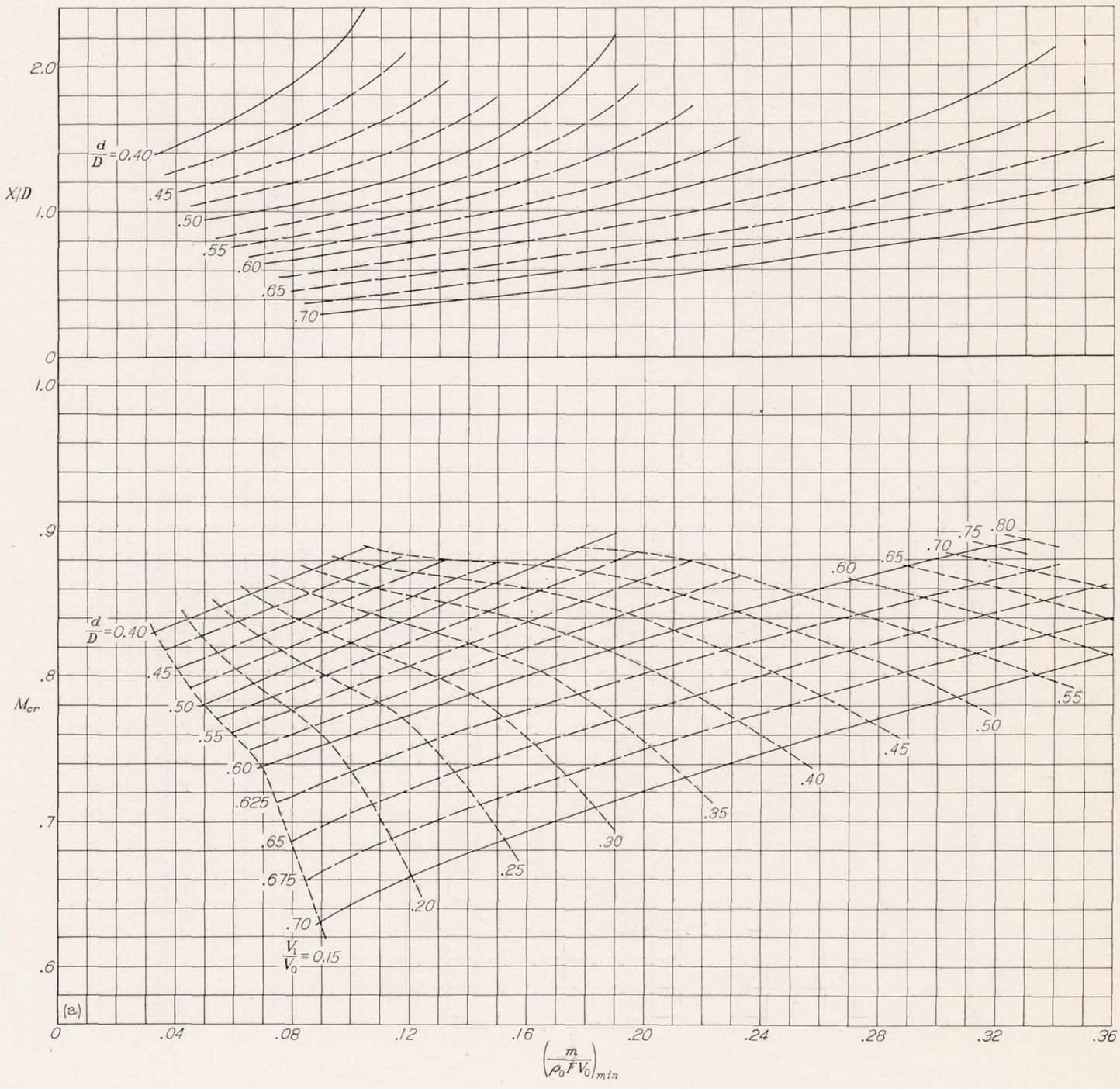

(a) $\alpha = 0°$.

FIGURE 31.—Selection charts for NACA 1-series nose inlets.

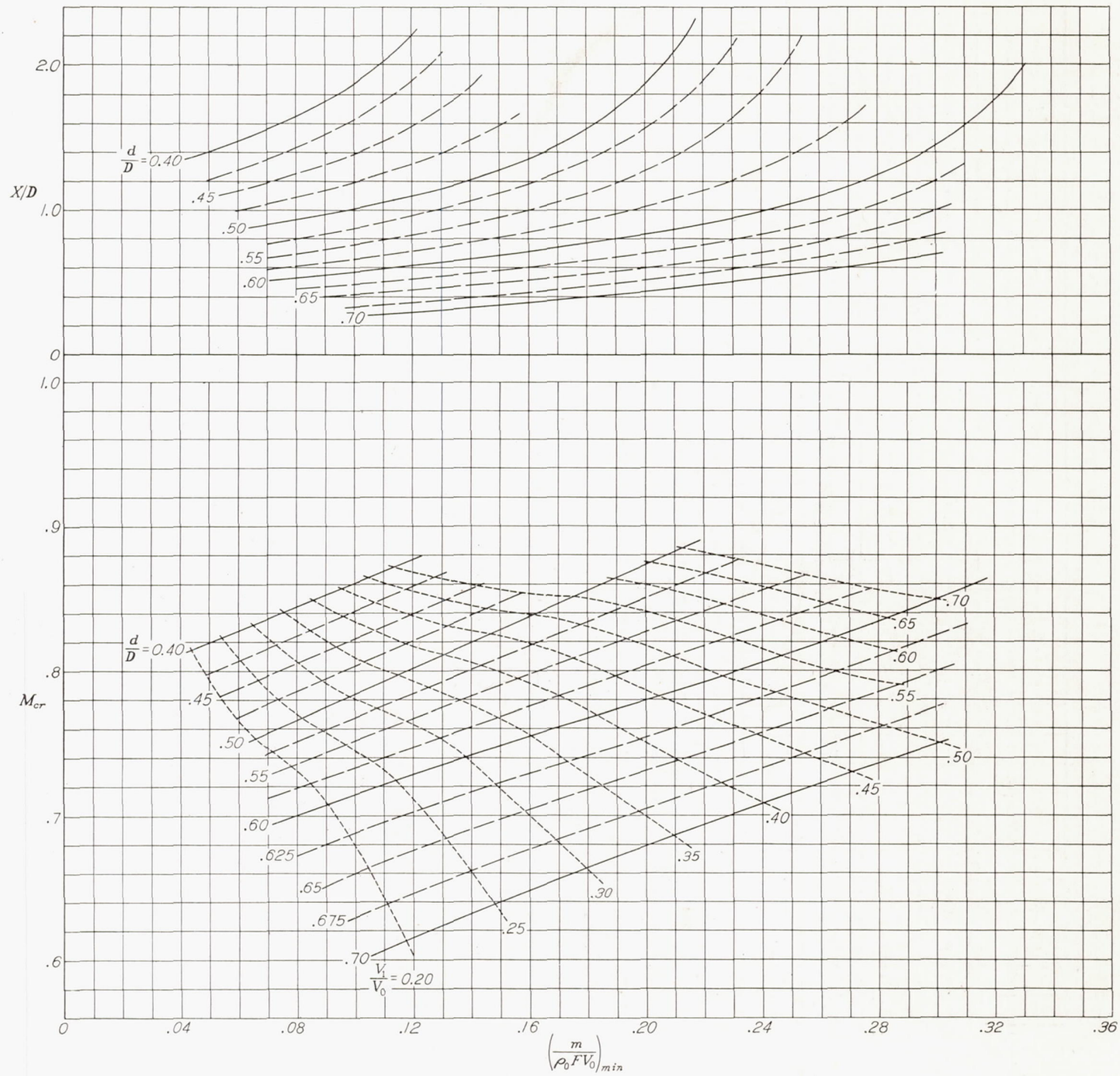

(b) $\alpha = 2°$.

FIGURE 31.—Concluded.

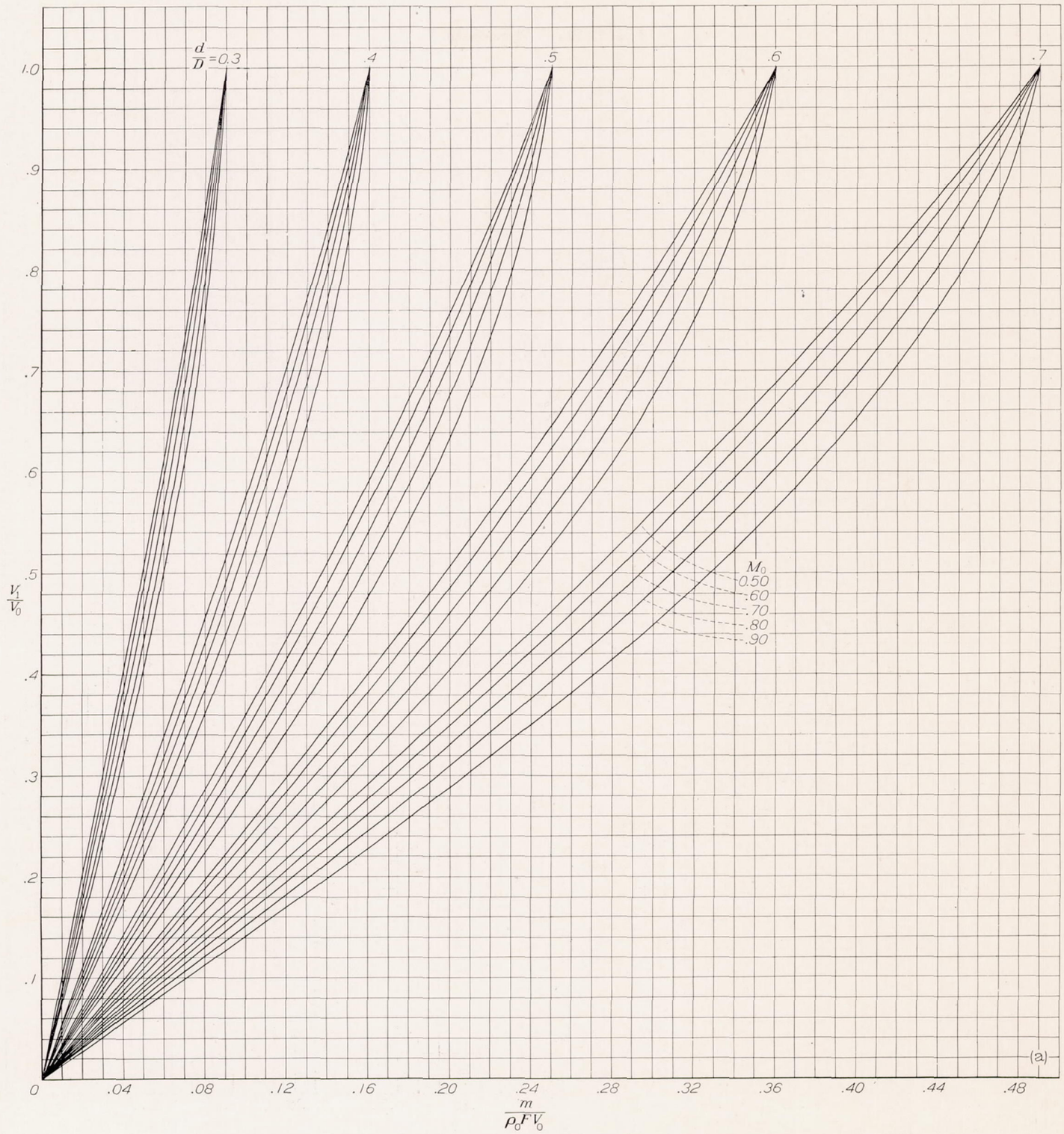

FIGURE 32.—Variation of mass-flow coefficient with inlet-velocity ratio for a given Mach number.

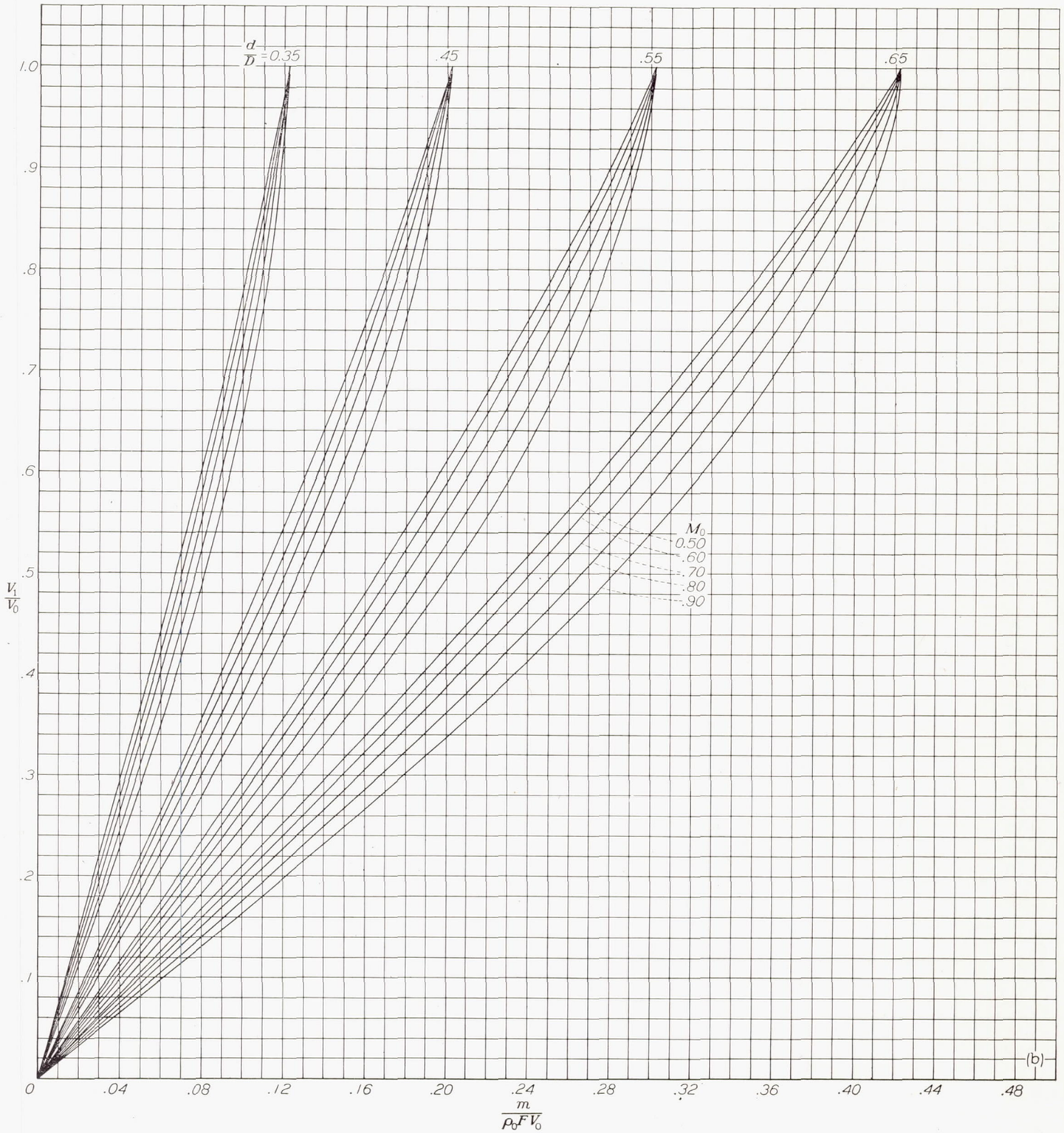

FIGURE 32.—Concluded.

Use of charts.—The selection charts have two principal applications: (1) selection of nose-inlet proportions, for use with the NACA 1-series ordinates, that will attain a specified design critical Mach number and satisfy specified air requirements; (2) determination of critical Mach number and minimum-flow conditions for an NACA 1-series nose inlet of given proportions. In general, these two applications pertain to the high-speed and cruise conditions, respectively. The selection of proportions of a nose inlet will usually be governed by the high-speed condition. It will then be desirable to check the selected proportions for other flight conditions, such as the cruise condition, for which the design angle of attack, mass-flow coefficient, and flight Mach number will be somewhat different. The high-angle-of-attack (low-speed) flight conditions are also of interest from considerations of external and internal separation. (These items are discussed in the section entitled "Detail Considerations.")

The design data specifying the selection parameters are the design speed and altitude, the corresponding air requirement, and the frontal area of the body to which the nose inlet is being applied. The use of the charts is illustrated by means of an example. The following design conditions and quantities will be assumed for a typical jet-propulsion installation:

Circular-fuselage cross-sectional area, F, sq ft	20
Operating altitude, ft	35,000
Density at altitude, ρ_0, slug/cu ft	0.000736

	High-speed condition	Cruise condition
Free-stream velocity, V_0, fps	807	661
mph	550	450
Free-stream Mach number, M_0	0.83	0.68
Angle of attack, α, deg	0	2
Air required, lb/sec	50	45
Mass-flow coefficient, $\frac{m}{\rho_0 F V_0}$	0.130	0.143

The proportions for the nose inlet to meet the high-speed conditions are found by entering the selection chart for $\alpha=0°$ (fig. 31 (a)) at the bottom with the value of mass-flow coefficient $\left(\frac{m}{\rho_0 F V_0}\right)_{min}=0.130$ and proceeding vertically upward to the value of $M_{cr}=0.83$. At this point the value of inlet-diameter ratio d/D can be read along with the value of inlet-velocity ratio V_1/V_0 corresponding to the values of d/D, $\left(\frac{m}{\rho_0 F V_0}\right)_{min}$, and M_{cr} for this point. By continuing vertically to the top section of the chart, the required value of length ratio X/D can be read for the value of d/D obtained previously. The proportions for the nose inlet that will give a critical Mach number equal to the high-speed-flight Mach number are

$$\left.\begin{aligned}\frac{d}{D}&=0.526\\ \frac{X}{D}&=1.16\end{aligned}\right\}\text{ Selection I}$$

The corresponding value of $\left(\frac{V_1}{V_0}\right)_{min}=0.35$ may be read from the selection chart.

The nose inlet selected for the high-speed condition (selection I) should now be checked to determine whether it will satisfy the specified cruise requirements. This check can be made by entering the top half of the selection chart for $\alpha=2°$ (fig. 31 (b)) with $\frac{X}{D}=1.16$, proceeding across to the value $\frac{d}{D}=0.526$, and then moving vertically downward to the same value of d/D on the lower half of the chart. At this point the value of $\left(\frac{m}{\rho_0 F V_0}\right)_{min}$ and the corresponding value of M_{cr} can be read. By this procedure the following results for the cruise condition are obtained:

$$M_{cr}=0.815$$

$$\left(\frac{m}{\rho_0 F V_0}\right)_{min}=0.159$$

$$\left(\frac{V_1}{V_0}\right)_{min}=0.44$$

In figure 33 (a) a scale drawing of this NACA 1-series nose inlet (selection I) is presented for illustration along with the critical Mach number curves estimated from figure 28 for $\alpha=0°$ and $\alpha=2°$ (the high-speed and cruise conditions, respectively). Also noted on this figure are points representing the two specified design requirements. The design high-speed requirement falls on the knee of the curve for $\alpha=0°$ because the selection charts are based on the knee. The fact that the design cruise requirement falls below the estimated critical Mach number curve for $\alpha=2°$ indicates that the critical speed for the nose inlet selected exceeds the cruise requirement. The cruise requirement point, however, represents a value of mass-flow coefficient below the minimum value indicated by the knee of the curve. Operation of the selected nose inlet at the cruise condition will therefore produce at the lip of the inlet a pressure peak, which may be undesirable from the standpoint of drag.

It is evident that some margin may be desirable between the design operating requirements and the nose-inlet selection conditions. An inspection of figure 33 (a) indicates that a margin of $\frac{m}{\rho_0 F V_0}$ of the order of 0.02 may be desirable to eliminate the pressure peak in the cruise condition. The design selection parameters for the high-speed condition then become

$$\left(\frac{m}{\rho_0 F V_0}\right)_{min}=0.130-0.02=0.110$$

$$M_{cr}=0.83$$

From the selection chart for the high-speed condition (fig. 31 (a)), by the method outlined for selection I, the following results are obtained:

$$\left.\begin{aligned}\frac{d}{D}&=0.50\\ \frac{X}{D}&=1.20\\ \left(\frac{V_1}{V_0}\right)_{min}&=0.33\end{aligned}\right\}\text{ Selection II}$$

For the cruise condition for these values of X/D and d/D, from figure 31 (b),

$$M_{cr}=0.819$$

$$\left(\frac{m}{\rho_0 F V_0}\right)_{min}=0.138$$

$$\left(\frac{V_1}{V_0}\right)_{min}=0.42$$

The estimated critical Mach number curves and the points corresponding to the design requirements are shown with a scale drawing of this nose inlet in figure 33 (b). For the cruise condition, the required value of the mass-flow coefficient is higher than the minimum value represented by the knee of the curve. Introduction of this margin in $\frac{m}{\rho_0 F V_0}$ involves a decrease in the value of the inlet-diameter ratio and a corresponding increase in inlet-velocity ratio but only a small change in the value of the length ratio.

In the design of some installations, a margin between the design high-speed Mach number and the critical Mach number of the nose inlet may be desirable in addition to the margin in mass-flow coefficient illustrated by selection II. With a margin of 0.02 assumed for M_{cr} and with the same margin in mass-flow coefficient assumed as for selection II, the design selection parameters become

$$\left(\frac{m}{\rho_0 F V_0}\right)_{min}=0.110$$

$$M_{cr}=0.83+0.02=0.85$$

From the selection chart for the high-speed condition (fig. 31 (a)), the following results are obtained:

$$\left.\begin{aligned}\frac{d}{D}&=0.47\\ \frac{X}{D}&=1.45\\ \left(\frac{V_1}{V_0}\right)_{min}&=0.37\end{aligned}\right\}\text{ Selection III}$$

For the cruise condition (fig. 31 (b)), for these values of X/D and d/D,

$$M_{cr}=0.834$$

$$\left(\frac{m}{\rho_0 F V_0}\right)_{min}=0.128$$

$$\left(\frac{V_1}{V_0}\right)_{min}=0.45$$

The estimated critical Mach number curves and the points corresponding to the design requirements are shown with a scale drawing of this nose inlet in figure 33 (c). For both the cruise and the high-speed conditions a margin now exists between the design values and the required operating values of M_{cr} and $\left(\frac{m}{\rho_0 F V_0}\right)_{min}$. Introduction of these margins results in a nose inlet having a smaller inlet-diameter ratio and a greater length ratio than those of the nose inlet selected for the original design conditions (selection I). The decreased inlet-diameter ratio involves a corresponding increase in

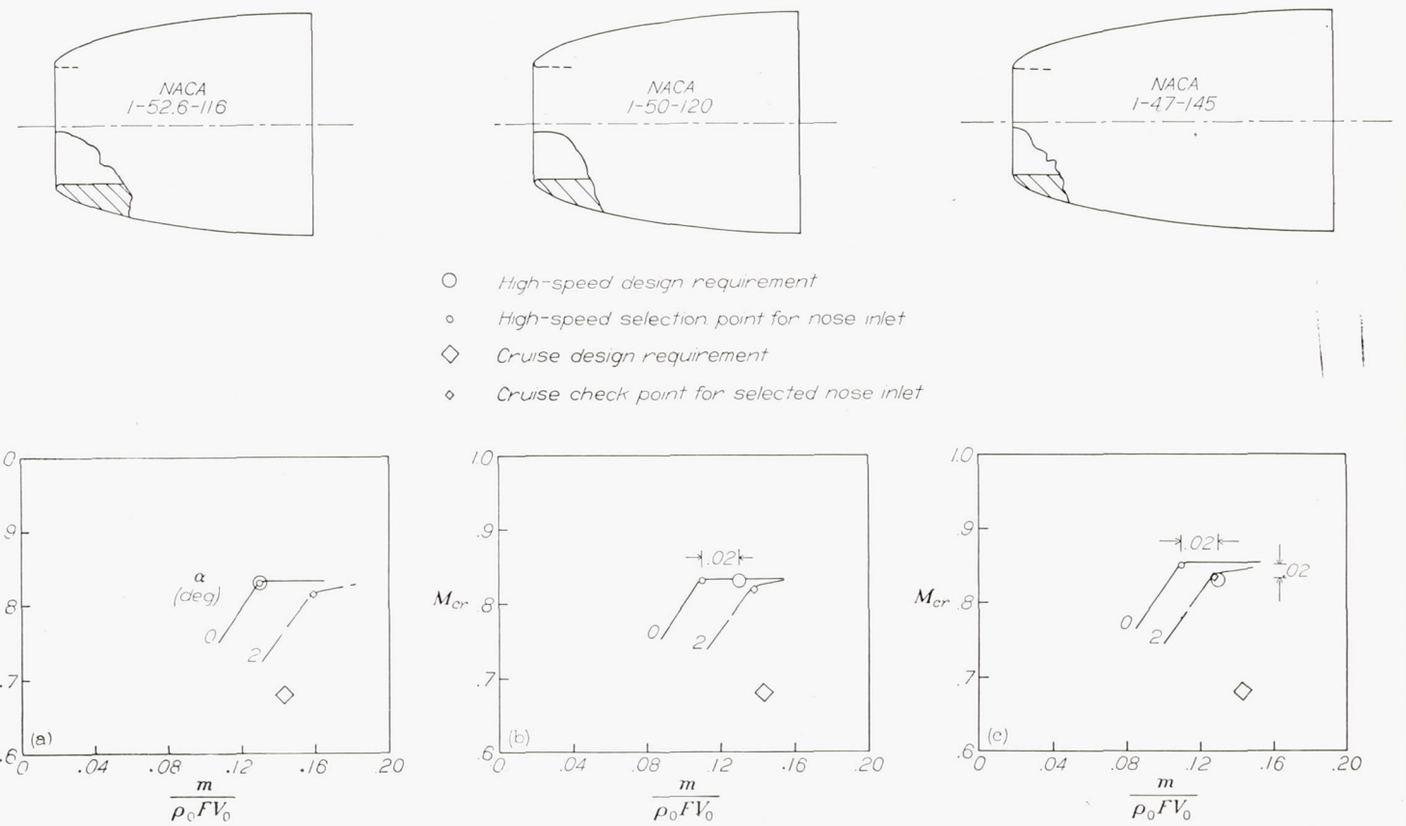

(a) Selection I. (b) Selection II. (c) Selection III.

FIGURE 33.—Comparison of three NACA 1-series nose inlets selected for one application. (See example in text.) Curves are estimated.

inlet-velocity ratio, which may be detrimental from the standpoint of internal losses. In order to determine the amount of design margin that may be used, therefore, the characteristics of the internal-flow system must be considered.

Several important qualifications should be noted concerning the application of the selection charts. The selection charts for the NACA 1-series nose inlets are based on the knee of the critical Mach number curve for a given nose inlet. The application of these charts to the design of a nose inlet for a given critical Mach number will therefore result in a nose inlet having the minimum value of X/D and the maximum value of d/D that can be used. The proportions given by the selection charts represent limiting values rather than optimum values; consequently, in installations for which values of length and diameter ratios are not restricted, the proportions can be varied from the limiting values in the directions indicated in the example previously presented.

For an NACA 1-series nose inlet having arbitrary proportions, the critical Mach number characteristics at $\alpha=0°$ and 2° may be checked against the operating requirements by means of the selection charts in a manner similar to that employed in checking the cruise condition for selection I of the example. For conditions to which the selection charts do not apply, reference can be made to figures 28 and 29 and to the figures presenting critical Mach number data for the nose inlets tested for estimation of the characteristics of the particular nose inlet involved.

Certain combinations of nose-inlet proportions within the range of the series tested cannot be checked for critical speed and operating conditions by means of the selection chart of figure 31; for example, the NACA 1–50–050 nose inlet, which was tested in the present investigation, cannot be found by entering the upper part of the selection chart with its proportions. Figure 15 shows that the characteristic flat pressure distribution is not obtained with this nose inlet at any value of inlet-velocity ratio. Examination of the curves for the nose inlets of $\frac{d}{D}=0.50$ (fig. 28) shows that the critical-speed curve for this nose inlet falls far below the envelope curve even if the envelope and critical-speed curves are extrapolated to $\frac{V_1}{V_0}=0$. For an inlet-diameter ratio of 0.50, therefore, this nose inlet has a considerably shorter length than that required to obtain the critical speed indicated by the envelope curve even at $\frac{V_1}{V_0}=0$. This nose inlet therefore does not appear on the selection charts because, as the chart shows, larger values of length ratio should be used for this value of inlet-diameter ratio.

DESIGN APPLICATION

The NACA 1-series ordinates.—The selection charts presented are based on nose inlets designed from the NACA 1-series ordinates. These ordinates have been shown in the section entitled "Design Analysis" to approach closely the optimum from the standpoint of critical speed for a wide range of nose-inlet proportions. Any departure from the nondimensional NACA 1-series ordinates (table I) may appreciably lower the value of the maximum critical Mach number and alter the shape of the critical Mach number curve. The results of tests of several nose inlets having profiles that differ from the NACA 1-series ordinates are presented in the section entitled "Effects of variations in basic profile."

The small degree of waviness evident in some of the pressure distributions for several of the nose inlets is believed to be due to very small deviations in profile. Because the models were constructed of wood and were of relatively small size (12-in. diameter), exact dimensional control of the profile was difficult. It is believed, however, that, inasmuch as these deviations are small, the effects on maximum critical Mach number and the shape of the critical Mach number curve will likewise be small. Nose inlets based on the NACA 1-series ordinates should therefore closely approach the optimum from the standpoint of critical speed for the particular proportions selected.

It should be noted that the selection of an NACA 1-series nose inlet of proportions that exactly satisfy given conditions results in a pressure distribution approaching a flat shape. Although optimum from the standpoint of critical speed, such a pressure distribution is not the most desirable from the standpoint of attaining laminar flow. The pressure distributions at inlet-velocity ratios above the design value, however, tend to approach the type of distribution characteristic of those permitting laminar flow. The introduction of margin in the design value of $\frac{m}{\rho_0 F V_0}$, as shown in the example, will therefore tend to provide a more favorable pressure distribution from the standpoint of attaining laminar flow.

Cowlings.—In order to compare the critical-speed characteristics of the NACA 1-series nose inlets with the NACA C cowling of reference 1, a model of the NACA C cowling was tested on the model shown in figure 8. The pressure distributions and critical Mach number characteristics are presented in figures 34 and 35, respectively. The value of critical speed obtained for this cowling agrees closely with the value determined in the tests of reference 1. The proportions of this cowling are $\frac{d}{D}=0.70$ and $\frac{X}{D}=0.31$; therefore, this cowling is closely comparable in proportions to the NACA 1–70–030 nose inlet. The critical-speed characteristics of this nose inlet and the NACA C cowling are compared in figure 36. The critical Mach number of the NACA C cowling is shown to be between 0.005 and 0.01 higher than that for the NACA 1–70–030 nose inlet. Approximately one-half this difference can be shown (by cross plots of the experimental data) to be due to the slightly greater length ratio of the NACA C cowling $\left(\frac{X}{D}=0.31\right)$; the remainder must be ascribed to the slight difference between the basic nondimensional ordinates for the NACA C cowling and the NACA 1-series ordinates. (See fig. 3.) The fact that the remaining difference is small indicates that the NACA C cowling ordinates and 1-series ordinates will yield nose inlets of approximately equal critical speed. An inspection of the pressure distributions, however, indicates that, for nose inlets of proportions similar to those of short cowlings, an increase in thickness near the lip, such as is provided by the NACA C cowling ordinates, may be beneficial.

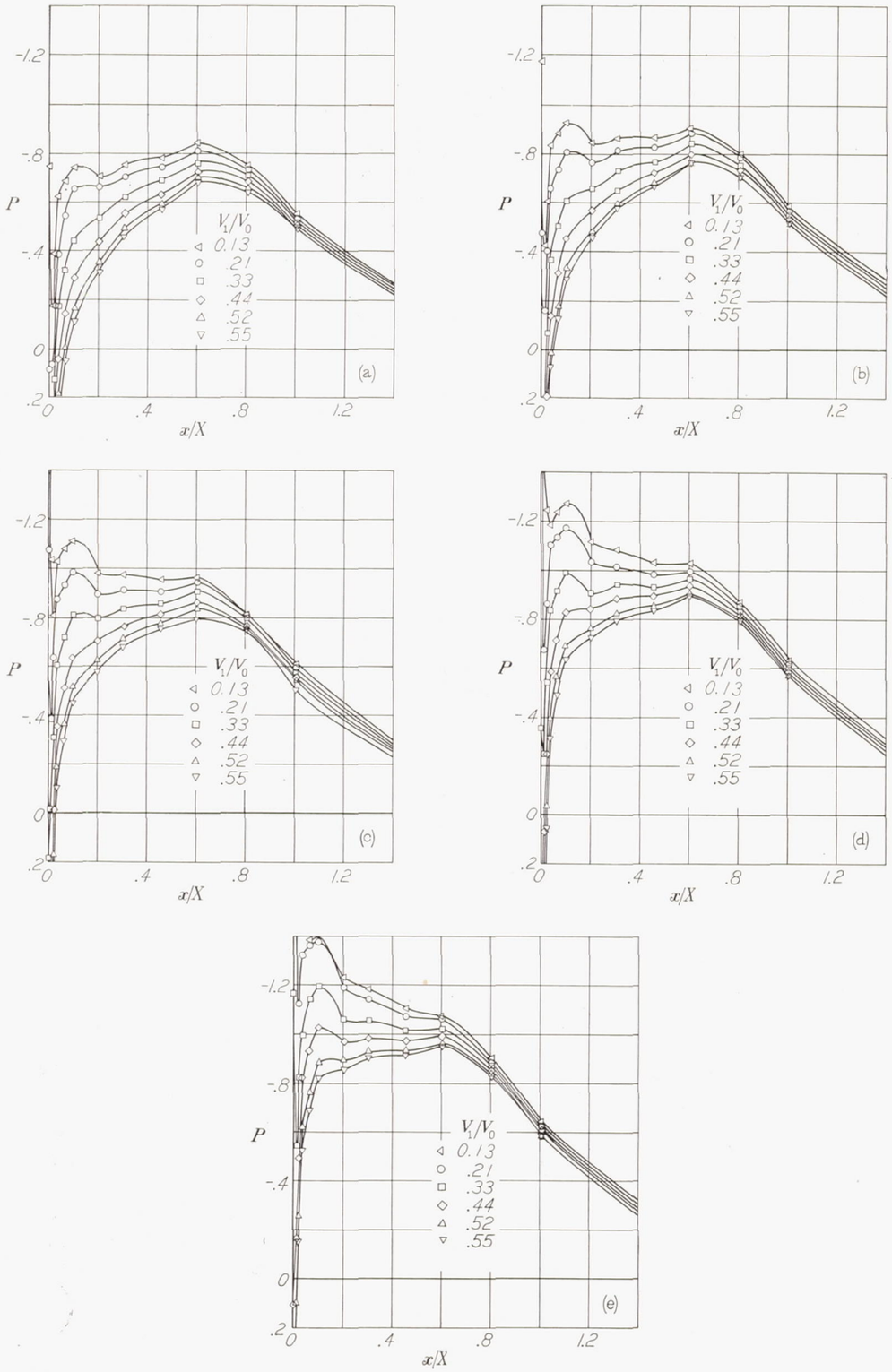

(a) $\alpha = -0.1°$. (b) $\alpha = 1.8°$.
(c) $\alpha = 3.8°$. (d) $\alpha = 5.8°$.
(e) $\alpha = 7.9°$.

FIGURE 34.—Pressure distributions over the NACA C cowling. $M_0 = 0.40$.

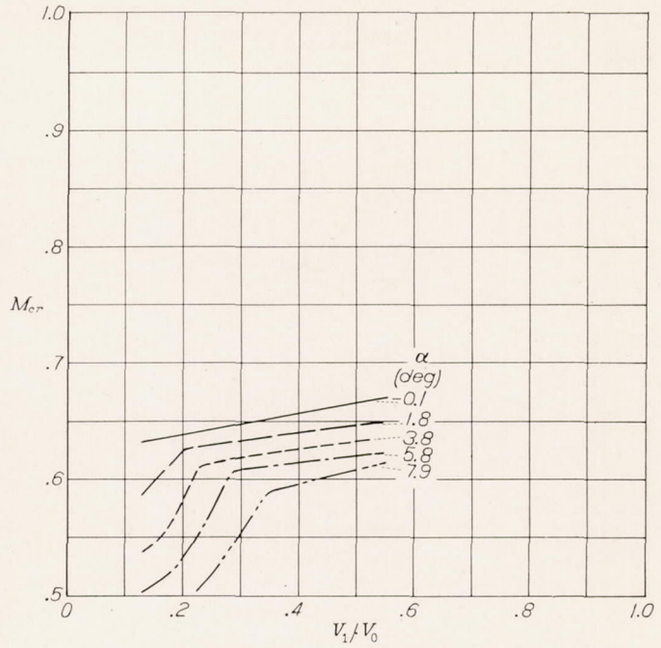

FIGURE 35.—Critical Mach numbers for the NACA C cowling.

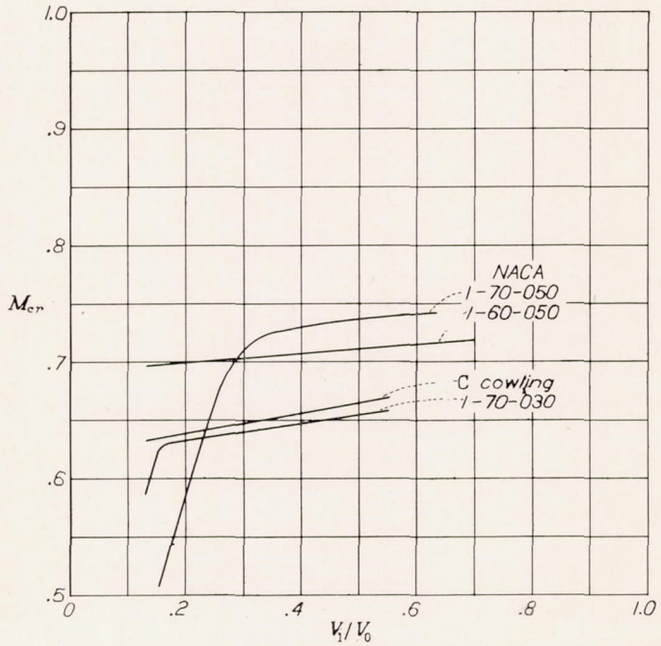

FIGURE 36.—Comparison of critical Mach number characteristics of NACA C cowling and 1-series nose inlets. $\alpha=0°$.

The critical Mach number curves for the NACA 1–70–050 and 1–60–050 nose inlets have been added to figure 36 to show the effects of small variations in proportions for short-cowling-type nose inlets and to illustrate the changes in proportions that must be made in order to obtain cowlings having critical Mach numbers above that of the NACA C cowling. These data show that the simultaneous increase in the length ratio and decrease in inlet-diameter ratio by appropriate increments will yield cowlings of higher critical speed than the NACA C cowling for comparable inlet-velocity-ratio and angle-of-attack ranges. Selection of nose-inlet proportions in this range may be made by means of the selection charts previously presented (fig. 31).

Effect of propeller spinners.—The effect of a propeller spinner on the critical Mach number of a cowling and on the internal flow must be considered in the design of a cowling for a tractor propeller installation. Several cowling shapes have been developed by the NACA for use with large spinners (references 5 and 6). The data from tests of these cowlings have been analyzed in relation to data in the present report.

Shown in figure 37 are the NACA D_l cowling (cowl 2 of reference 5) and the NACA D_s cowling (reference 6), which were developed for use with the spinners shown. For comparison of profiles, NACA 1–series cowlings of similar proportions have been superimposed. The profiles of both the D_l and D_s cowlings fall somewhat under the NACA 1–series profile near the lip, but good agreement with the NACA 1–series profiles is evident. Inasmuch as the profiles are generally comparable, the characteristics of the cowlings developed for use with spinners may be compared with the characteristics of the NACA 1–series open-nose cowlings to establish qualitatively the effects of the propeller spinners.

Pressure distributions over the NACA D_l and D_s cowlings from data in references 5 and 6 are presented in figure 38. The pressure distributions for both cowlings do not possess the flat contour that is characteristic of the pressure distributions for the NACA 1–series nose inlets. Inasmuch as no high pressure peaks exist, however, small modifications to the cowling contours would probably suffice to obtain essentially flat pressure distributions.

The critical Mach numbers of the NACA D_l and D_s cowlings at $\alpha=0°$ are shown in figure 39 for several values of inlet-velocity ratio. Also shown in this figure are the estimated critical Mach number curves for the corresponding NACA 1–series cowlings (without spinners) taken from figure 31 for the proportions shown in figure 37. The maximum critical Mach numbers of the NACA D_s and D_l cowlings are in good agreement with those of the corresponding NACA 1–series open-nose cowlings. The effect of a spinner on the maximum critical speed of a cowling is evidently small.

Figure 39 (b) shows also values of critical Mach number from unpublished tests of a full-scale NACA D_s cowling installation with spinner in place and with spinner removed. These data show that the cowling without spinner is operating at an inlet-velocity ratio well below the knee of the critical Mach number curve and consequently possesses a high pressure peak at the lip and a corresponding low critical speed.

FIGURE 37.—NACA cowlings developed for use with large spinners. NACA 1-series cowlings of similar proportions superimposed for comparison of profiles.

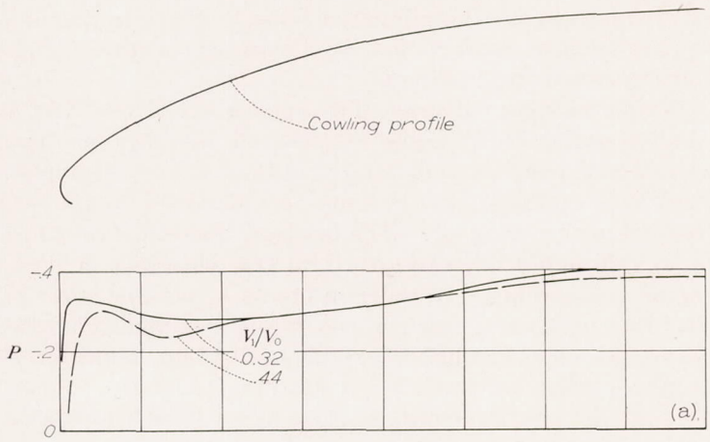

(a) NACA D_l cowling.

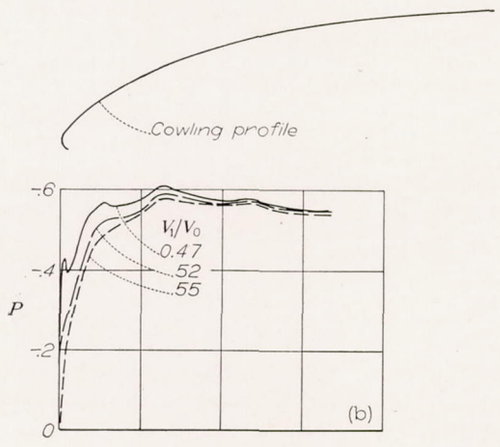

(b) NACA D_s cowling.

FIGURE 38.—Pressure distributions over NACA D_l and D_s cowlings. (Data from references 5 and 6.) $\alpha=0°$.

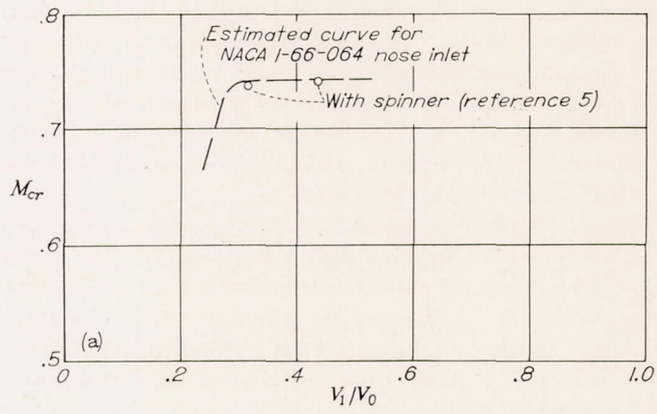

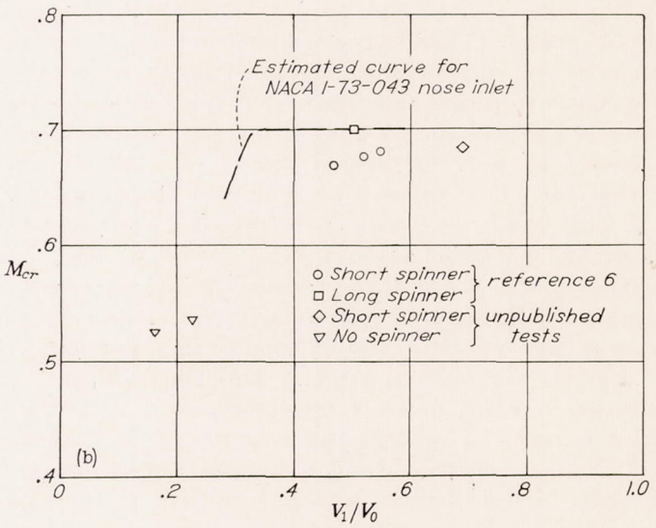

(a) NACA D_l cowling.
(b) NACA D_s cowling.

FIGURE 39.—Critical Mach numbers for NACA D_l and D_s cowlings. Estimated curves for NACA 1-series cowlings shown in figure 37 included for comparison. $\alpha=0°$.

The principal effect of the spinner in the case of the NACA D_l and D_s cowlings is therefore to raise the inlet-velocity ratio for the design air-flow quantity; this increase permits the cowling to operate in the range of inlet-velocity ratio for maximum critical speed.

The effect of a spinner on the inlet-velocity ratio at which the knee of the critical Mach number curve occurs is not accurately predictable from existing data. The data tend to indicate, however, that the knee will occur at a value of inlet-velocity ratio equal to or slightly less than the value for the open-nose condition. The addition of a spinner to a cowling thus permits (but does not necessarily require) an increase in d/D as a consequence of the increased inlet-velocity ratio. This fact may be of advantage in selecting a high-critical-speed cowling of minimum frontal area (discussed in section entitled "Sample cowling designs").

In the design of a cowling with a spinner, consideration must be given to the fact that a minimum value of inlet-velocity ratio exists below which unstable flow at the cowling entrance occurs. Values of the minimum inlet-velocity ratio for stable entrance flow and high cooling-pressure recovery have been determined from tests of specific installations. The data of references 6 and 7 indicate a value of minimum inlet-velocity ratio of the order of 0.4 for a cowling with spinner but no propeller; reference 6 and the results of unpublished flight tests indicate a value of the order of 0.35 for a cowling with spinner and rotating propeller. The use of suitable propeller cuffs has been found to improve entrance-flow stability at low values of inlet-velocity ratio and has been shown to permit satisfactory operation at inlet-velocity ratios as low as 0.30. A general investigation, however, is necessary to provide definite values of minimum inlet-velocity ratio for various cowling-spinner configurations.

It will usually be desirable to design a cowling for the lowest value of inlet-velocity ratio consistent with stable entrance flow because of the increase in diffuser losses that occurs with increase in inlet-velocity ratio. An optimum value of inlet-velocity ratio or spinner size therefore exists for a given cowling installation. This fact is illustrated in reference 7, which presents the results of investigations in which spinners of several sizes were tested in conjunction with NACA cowlings through limited ranges of air-flow quantity. This reference shows that, from the standpoint of internal total-pressure recovery, an optimum spinner size exists for a given cowling. Use of a spinner smaller or larger than the optimum was shown to result in increased total-pressure losses.

In summary, the foregoing analysis indicates that no important changes in maximum critical speeds of cowlings selected from the design charts presented herein will occur when a propeller spinner is added. In addition, the available data tend to indicate that the knee of the critical Mach number curve will occur at approximately the same value of inlet-velocity ratio for a cowling with or without a spinner; further investigation is required, however, to establish definitely the location of the knee of the curve. The inlet-diameter ratio d/D of a cowling may therefore be increased above the open-nose design value, if desired, in order to take advantage of the increase in inlet-velocity ratio produced by the addition of the spinner. With a spinner, however, a minimum value of inlet-velocity ratio exists for stable entrance conditions. The spinner diameter should therefore be adjusted to keep the operating value of inlet-velocity ratio slightly above this minimum value. (The selection of a cowling-spinner combination is illustrated in the sample cowling designs that follow.)

Sample cowling designs.—The application of the NACA 1-series ordinates to high-critical-speed cowlings for two typical radial engines is illustrated in the following examples. For these examples, the cowlings are designed to provide only cylinder cooling air. The fuselage diameter is assumed to be sufficiently large to assure internal clearance between engine and cowling. In order to obtain a specified value of clearance between engine and cowling, a trial-and-error procedure for determining the value of fuselage diameter is required. The assumed design conditions and the proportions of the cowlings selected from figure 31 are presented in the following table:

Maximum diameter of fuselage or nacelle, D, ft	5.0
Operating altitude, ft	35,000
Free-stream density at altitude, ρ_0, slug/cu ft	0.000736
Design maximum velocity, V_0,	
fps	733
mph	500
Design critical Mach number, M_{cr}, corresponding to V_0 above	0.76
Cowling angle of attack, deg	0

	Two-row radial engine	Four-row radial engine
Cylinder cooling mass flow, m, slugs/sec	0.64	1.22
Mass-flow coefficient, $\frac{m}{\rho_0 F V_0}$	0.06	0.115
From figure 31 (a), for the above values of critical Mach number and mass-flow coefficient:		
d/D	0.55	0.61
X/D	0.75	0.73
$(V_1/V_0)_{min}$	0.15	0.24

The cowling profiles were computed from table I and are drawn to scale in figure 40 along with the corresponding engine installations. In the preceding section it was pointed out that the inlet-velocity ratio should not fall below approximately 0.3 when a spinner is used with a cuffed propeller. With the assumption of a cuffed propeller, the spinner sizes for the two cowlings have been selected to raise the inlet-velocity ratios to 0.3. The resulting spinner diameters are 23 inches and 16 inches for the cowlings shown in figures 40 (a) and 40 (b), respectively.

These two examples show that cowlings designed for critical Mach numbers above that of the NACA C cowling are characterized by a smaller inlet-diameter ratio and a

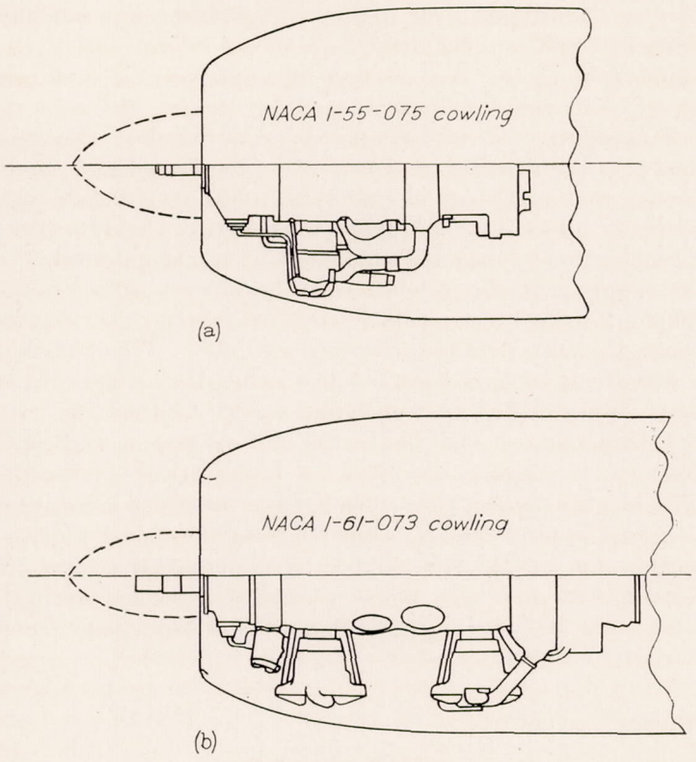

(a) Two-row radial engine.
(b) Four-row radial engine.

FIGURE 40.—Examples of NACA 1-series cowlings designed to provide only cylinder cooling air for two typical radial engines. Internal cowling shape omitted; design critical Mach number, 0.76.

greater length ratio. The length of the propeller shaft on these engines necessitates the location of the engine ahead of the maximum-diameter station of these high-critical-speed cowlings. The maximum diameters of these cowlings are therefore greater than the minimum diameter that might otherwise be used. The increases in frontal area above the minimum area (for the same internal clearance between engine and cowling) for the cowlings in figures 40 (a) and 40 (b), are approximately 26 and 20 percent, respectively. Such an increase in frontal area may not be significant in the case of installations for which the fuselage or nacelle diameter is governed by factors other than the engine diameter but will present an important increase in frontal area and drag in installations for which the minimum fuselage or nacelle diameter is governed only by the engine diameter. This excess frontal area may be reduced by use of an extended propeller shaft or a hollow spinner such as that used in the NACA high-speed cowling (reference 8), which was derived from the B nose ordinates.

The cowling proportions given by the design charts (for use with the NACA 1-series ordinates) represent the minimum length ratio and the maximum inlet-diameter ratio for given requirements. The addition of the spinners, however, has increased the inlet-velocity ratios of the sample cowlings; this increase makes possible (but not mandatory) an increase in the inlet-diameter ratio. This change is of particular interest as an additional method of reducing the excess frontal area because, as the value of d/D is increased, the maximum diameter of the cowling can be decreased. Inasmuch as the inlet-velocity ratio for the cowling with spinner has been raised above the value for the cowling without spinner, a fictitious value of mass-flow coefficient higher than the design value can in effect be assumed and the cowling proportions can be determined from the selection charts on the basis of this value. The spinner frontal area must then be chosen to make the inlet-velocity ratio the desired value without actually increasing the mass-flow coefficient above the original design value.

The proportions of an NACA 1-series cowling designed for operation with a spinner at an inlet-velocity ratio of 0.3 will now be selected for the four-row engine for which the requirements were previously presented. The selection may be made by entering the design chart (fig. 31 (a)) at the left side with the value of $M_{cr}=0.76$ and proceeding horizontally across the chart to the line for $\frac{V_1}{V_0}=0.30$. At this point the value of d/D can be read; then, by moving vertically upward to the top section of the chart, the value of X/D can be read at the value of d/D previously obtained. The results thus determined are

$$\frac{d}{D}=0.64$$

$$\frac{X}{D}=0.73$$

$$\left(\frac{V_1}{V_0}\right)_{min}=0.30$$

$$\left(\frac{m}{\rho_0 F V_0}\right)_{min}=0.159$$

The area occupied by the spinner must be sufficient to make the inlet-velocity ratio 0.30 at the original specified value of mass-flow coefficient, 0.115. The spinner diameter is then 20 inches. The excess frontal area of this cowling over the minimum area that could be used (for the same engine clearance) is approximately 18 percent, slightly less than the excess frontal area of the cowling shown in figure 40 (b).

In some cases, further decreases in excess frontal area may be desired; in others, a spinner larger than that given by the procedure outlined may be required from considerations of propeller hub size as, for example, for cowlings designed for use with gas turbines of small diameter. In such cases the inlet-velocity ratio can be further increased in order to make possible a further increase in inlet-diameter ratio and spinner size. The increased inlet-velocity ratio will, however, tend to increase losses in the diffuser.

It is to be emphasized that the procedure presented for designing NACA 1-series cowlings for use with propeller spinners is based on the analysis of the results of limited investigations. Future general investigations of cowling-spinner combinations may therefore lead to some refinements of this procedure; in addition, some small modifications to the NACA 1-series ordinates may be found necessary for use with spinners. In general, however, the procedure outlined is believed to be satisfactory, particularly for installations including the use of a spinner of conservative size.

Air scoops.—The application of the NACA 1-series profile to air scoops has been demonstrated in the tests of reference 9. In this investigation a large scoop was designed as a semicircular body of revolution and located near the longitudinal midposition on the lower surface of a fighter-type fuselage. Provision for removing the fuselage boundary layer was included. The critical Mach number curves for three radial planes of the scoop (taken from fig. 20 (b) of reference 9) are shown in figure 41. The estimated critical Mach number curve for a nose inlet of inlet-diameter ratio and length ratio equal to those of the scoop has been obtained by means of figures 28 (a) and 32 (a) and added to figure 41 for comparison. Marked similarity between shapes of the estimated curve and the curves measured for the bottom and 60° planes of the scoop is noted. The knees of the curves occur at approximately the same value of inlet-velocity ratio. The critical Mach number curves for the scoop are lower than the curves for the corresponding nose inlet throughout the inlet-velocity-ratio range because of the effect of the flow field of the wing and fuselage on which the scoop was located. It is thus indicated that the proportions for high-critical-speed air scoops may be obtained from the selection chart (fig. 31), with allowance for an estimated loss in critical speed due to interference effects. Additional tests of such air scoops are needed to provide more detailed design information concerning the application of the NACA 1-series profile to high-critical-speed air scoops.

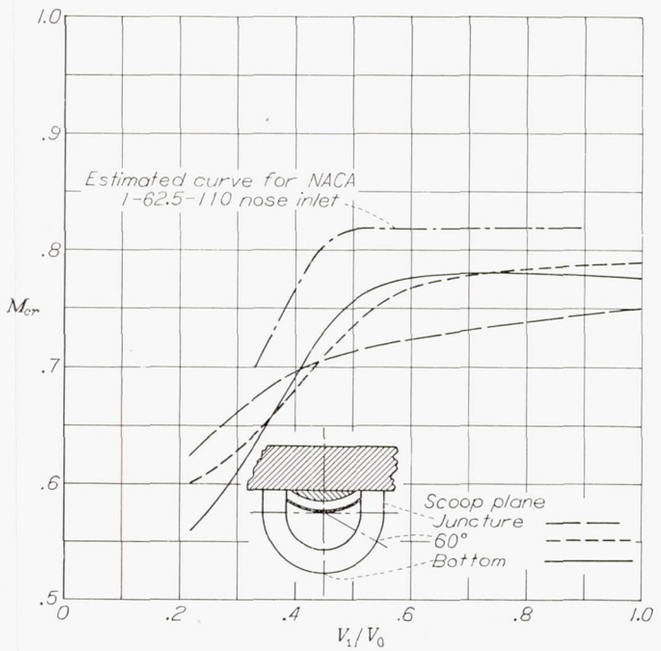

FIGURE 41.—Comparison of critical speeds for air scoop (from fig. 20(b) of reference 9) and corresponding nose inlet, both designed from NACA 1-series ordinates. $\alpha=0°$.

Wing inlets.—An analysis presented in reference 10 shows that pressure distributions over two-dimensional and three-dimensional bodies of identical thickness distribution will generally have similar shapes. Reference 10 shows, for example, that in incompressible flow with motion parallel to the major axis the velocity distribution about a prolate spheroid is equal to a constant times the velocity distribution about the corresponding elliptical cylinder. This constant is a function of only the thickness ratio. For shapes other than elliptical, the corresponding velocity ratios for two- and three-dimensional bodies do not remain a constant; however, for shapes developed for high critical speeds, the ratio of velocities may be considered to approach a constant as a first approximation. Inasmuch as the velocity distributions for similar two- and three-dimensional bodies are related, some similarity between profiles developed for optimum critical speed for two-dimensional wing inlets and three-dimensional nose inlets might be expected.

The profile of a symmetrical two-dimensional wing inlet (shape 9) is presented in reference 11. High-speed tests of this shape (reference 12) show, for medium values of inlet-velocity ratio, a pressure distribution approaching that of the three-dimensional NACA 1–series nose inlets. Figure 3 presents the nondimensional profile of shape 9 wing inlet for comparison with the NACA 1–series profile. Close agreement is noted. The nondimensional profiles for two-dimensional and three-dimensional air inlets developed to approach the optimum from the standpoint of critical speed are thus shown to be essentially similar. The NACA 1–series ordinates thus may have application to the experimental development of high-critical-speed two-dimensional wing inlets.

It is of interest to compare the relation between the measured critical speed of the shape 9 wing inlet and the critical speed estimated for a three-dimensional nose inlet from the present paper with the factors for converting from three-dimensional to two-dimensional flows derived from reference 10. The comparison shows that the measured critical speed of the wing inlet is appreciably lower than that which would be predicted by the use of data from the present paper and from reference 10. Although general agreement was previously noted as to the shape of the corresponding pressure distributions for similar two-dimensional and three-dimensional profiles, numerical agreement as to the magnitude of the peak pressures should not necessarily be expected inasmuch as the results of reference 10 apply only to solid bodies of elliptical profile with no consideration for admitting air at the leading edge.

Gun hoods.—Low-drag hoods for gun openings have been developed in reference 13 from the nose A ordinates presented in reference 2. The design of these gun-opening hoods or of gun-barrel fairings from which the gun barrel does not protrude can be determined by the nose-inlet selection charts

(fig. 31). For such applications the envelope curves of figure 31 may have to be extrapolated to low values of mass-flow ratio. The proportions of the inlet section of the hood can be selected from this figure in the usual manner; however, the design critical Mach number should include consideration of the induced-velocity field existing at the point of application.

DETAIL CONSIDERATIONS

Comparison of critical speeds obtained by experiment and by extrapolation.—The NACA 1–50–150 and 1–70–050 nose inlets, which are representative of a long nose inlet and a short cowling-type nose inlet, respectively, were tested through the Mach number range to approximately $M_0=0.7$ in order to compare the experimental variation in peak negative pressure coefficient with the theoretical variation (the Von Kármán relation, reference 4) assumed in the present paper for the determination of critical speeds. Figures 42 (a) and 43 (a) show the variation of measured peak negative pressure coefficient with Mach number for the NACA 1–50–150 and 1–70–050 nose inlets at constant values of inlet-velocity ratio. The lowest values of peak negative pressure coefficient follow approximately the theoretical increase with Mach number; however, the high values of peak negative pressure coefficient do not follow the theoretical variation. (See figs. 13 and 25 for the pressure distributions over these nose inlets.) This effect has been observed in previous investigations in which sharp pressure peaks occurred over relatively sharp inlet lips (reference 12).

The failure of the variation of peak negative pressure coefficient to follow the theoretical variation may be due in part to the fact that, in compressible flows, the inlet-velocity ratio may not be the basic parameter which accurately defines the local flow angle at the inlet lip. Another parameter, the mass-flow coefficient $\frac{m}{\rho_0 F V_0}$, reduces to A_0/F, the ratio of the area of the stream tube for mass flow m at free-stream conditions to the frontal area F. This parameter therefore expresses the amount that the stream tube must expand in approaching the inlet and thereby tends to govern the local angle of flow at the lip. Figures 42 (b) and 43 (b) present the variation of peak negative pressure coefficient with Mach number for constant values of the mass-flow coefficient. For low values of the peak negative pressure coefficient, little difference exists between the theoretical and experimental variations with Mach number for constant values of V_1/V_0 or of $\frac{m}{\rho_0 F V_0}$. For higher values of peak pressure, the experimental variation with Mach number for both parameters differs considerably from the theoretical variation; however, the variation for a constant value of the mass-flow coefficient more closely approaches the theoretical variation.

Comparisons of the critical Mach number characteristics obtained from high-speed data (figs. 42 and 43) and from extrapolation of data obtained at $M_0=0.40$ and $M_0=0.30$ (figs. 16 (b) and 27 (c)) are presented in figures 44 and 45. At high values of inlet-velocity ratio, the measured critical Mach numbers for both nose inlets are equal to or slightly greater than the critical Mach numbers estimated from the tests at $M_0=0.40$ and $M_0=0.30$. For both nose inlets the knees of the experimental critical Mach number curves occur at lower values of inlet-velocity ratio than those of the curves obtained by extrapolation. Below the knees of the curves, therefore, the measured critical speeds are appreciably higher than the values obtained by extrapolation from $M_0=0.40$ and $M_0=0.30$. The critical-speed data presented for the series of nose inlets tested are therefore indicated to be conservative by a small amount in the inlet-velocity-ratio range recommended for operation and by a larger amount for inlet-velocity ratios below the recommended range.

External separation.—The pressure distributions presented for the nose inlets tested have shown external-flow separation to occur over certain of the nose inlets at low inlet-velocity ratios and high angles of attack. The pressure distributions over the nose inlets tested having values of d/D of 0.40 and 0.50 (figs. 9, 10, and 12 to 15) show no discernible separation through the test ranges. Certain of the nose inlets having values of d/D of 0.60 and 0.70 (figs. 17 to 21 and 23 to 26), however, show severe external separation or stall at the inlet lip; for example, the pressure distributions for the NACA 1–70–150 nose inlet (fig. 23) clearly indicate separated flow at low values of inlet-velocity ratio. Figure 46 shows the critical Mach number characteristics for the NACA 1–70–150 nose inlet (taken from fig. 27 (a)), to which the curve of M_{cr} has been extended into the separated range. The values of critical Mach number in this range of inlet-velocity ratio do not have their usual significance, because the flow has separated and the drag will have reached excessive values even at low speeds.

The inlet-velocity ratio below which separation occurs has been obtained from figures similar to figure 46 for the various nose inlets tested and the results are plotted in figure 47. Also shown in figure 47 is a dashed curve indicating the value of V_1/V_0 at the knee of the critical Mach number curves ($\alpha=0°$) for the various values of X/D and d/D. A nose inlet derived from the selection chart (fig. 31) will operate at inlet-velocity ratios equal to or greater than the value given by the dashed curve in figure 47 for two reasons: (1) the selection charts are based on the knee of the critical Mach number curve; (2) for most cases, the nose inlet will be selected on the basis of high-speed conditions at which the inlet-velocity ratio is a minimum. The curve of design minimum inlet-velocity ratio falls above the separation curves for all but the very low values of X/D. Figure 47 indicates, therefore, that external separation will not occur, in general, for NACA 1-series nose inlets designed from the selection charts in the present paper with the possible exception of nose inlets having very low values of X/D or operating at very high angles of attack. By means of figure 47 the approximate inlet-velocity ratio below which separation can be expected can be estimated for an NACA 1-series nose inlet of proportions in the ranges shown.

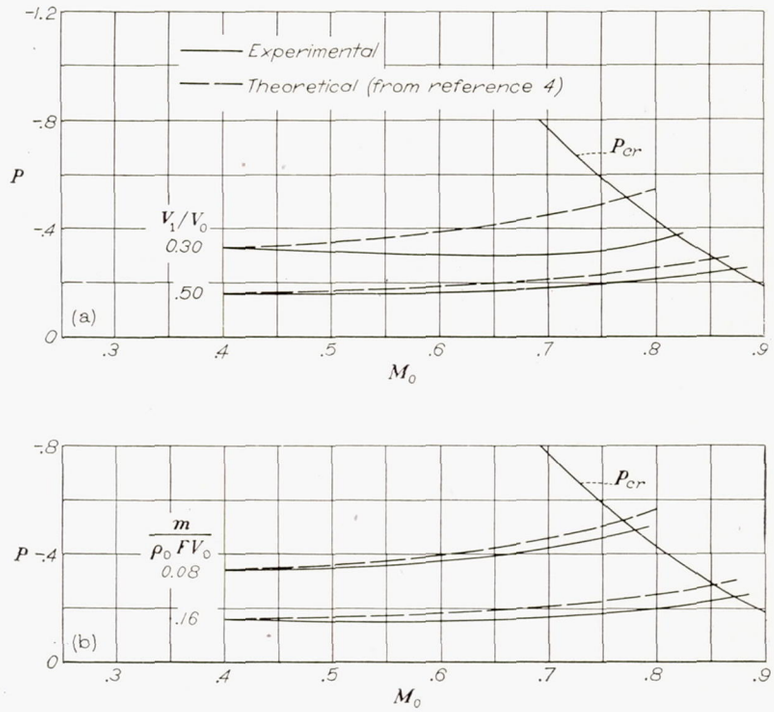

(a) Constant values of V_1/V_0.

(b) Constant values of $\frac{m}{\rho_0 F V_0}$.

FIGURE 42.—Variation of peak negative pressure coefficient with Mach number for the NACA 1–50–150 nose inlet. $\alpha=0.2°$.

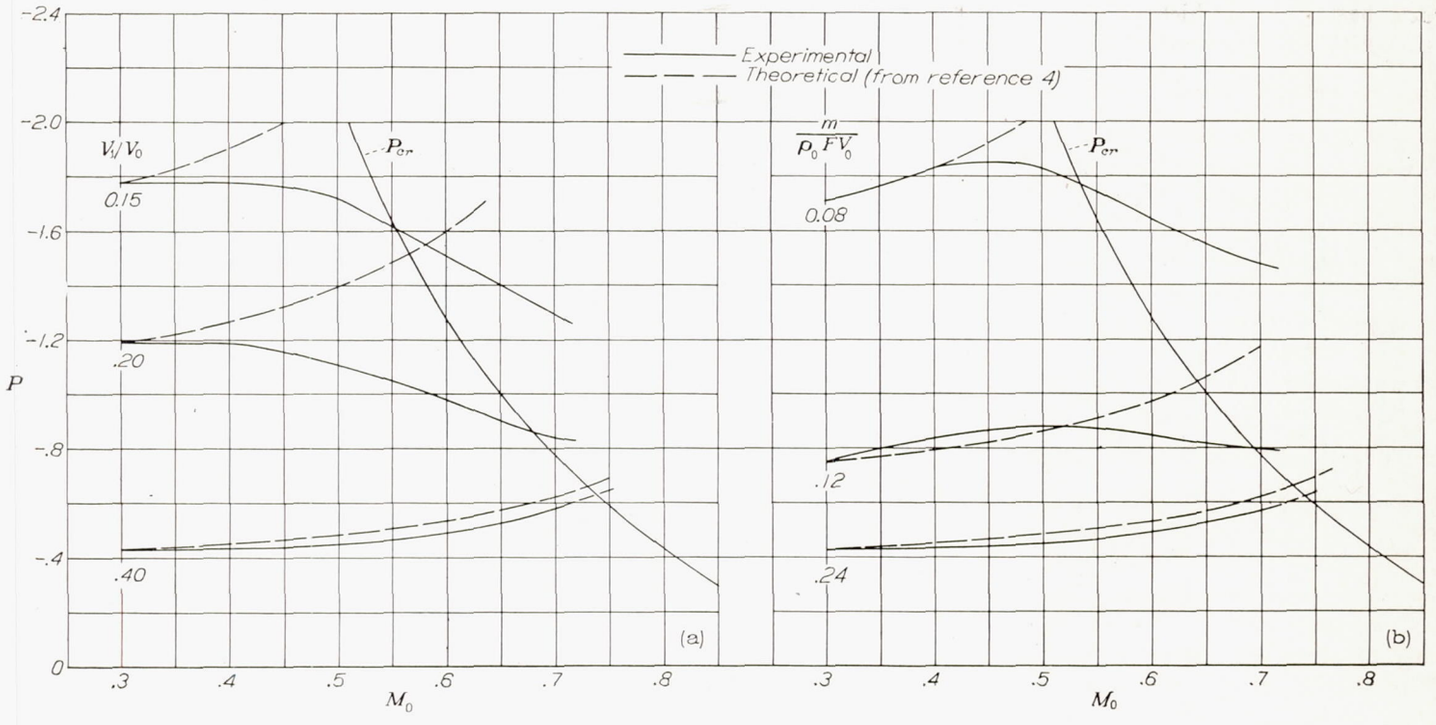

(a) Constant values of V_1/V_0.

(b) Constant values of $\frac{m}{\rho_0 F V_0}$.

FIGURE 43.—Variation of peak negative pressure coefficient with Mach number for the NACA 1–70–050 nose inlet. $\alpha=0.1°$.

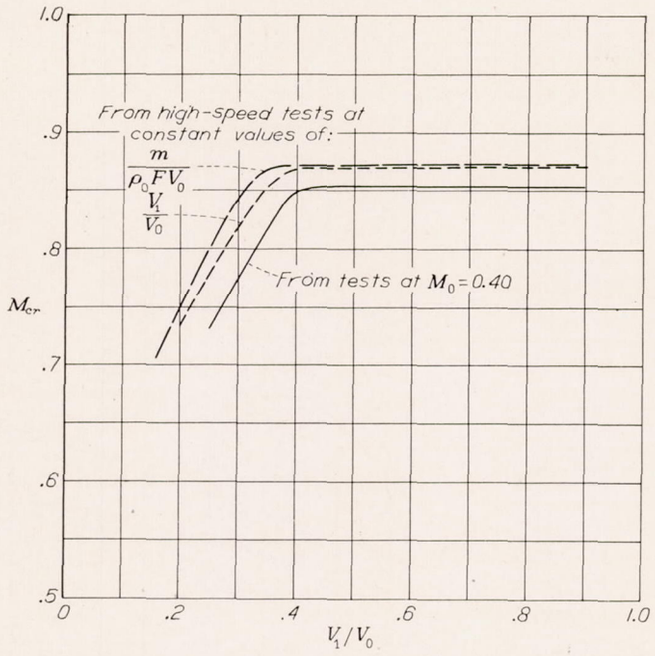

FIGURE 44.—Critical Mach numbers obtained from tests at $M_0=0.40$ (fig. 16(b)) and from tests at high speed (fig. 42) for the NACA 1–50–150 nose inlet. $\alpha=0.2°$.

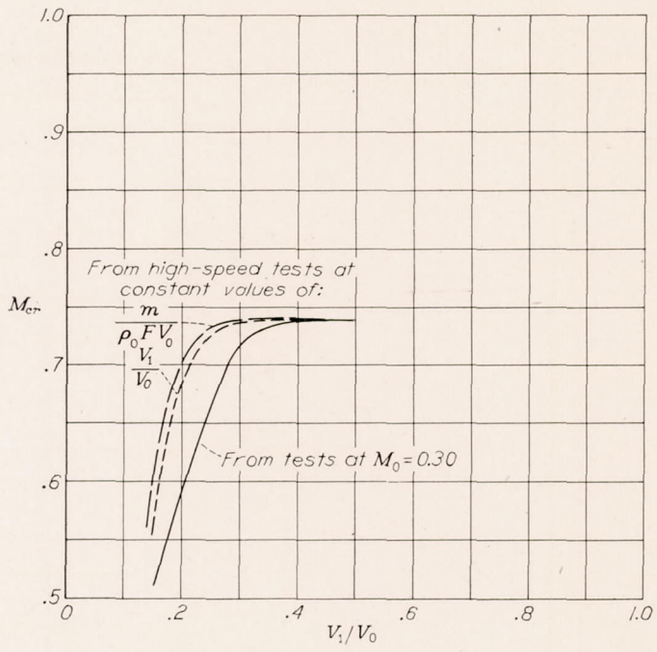

FIGURE 45.—Critical Mach numbers obtained from tests at $M_0=0.30$ (fig. 27 (c)) and from tests at high speed (fig. 43) for the NACA 1–70–050 nose inlet. $\alpha=0.1°$.

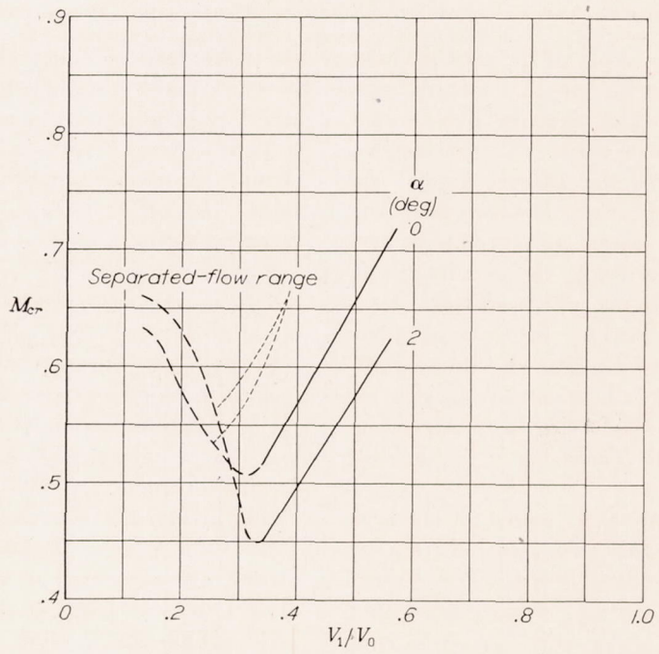

FIGURE 46.—Critical Mach numbers for the NACA 1–70–150 nose inlet. Separated-flow range included.

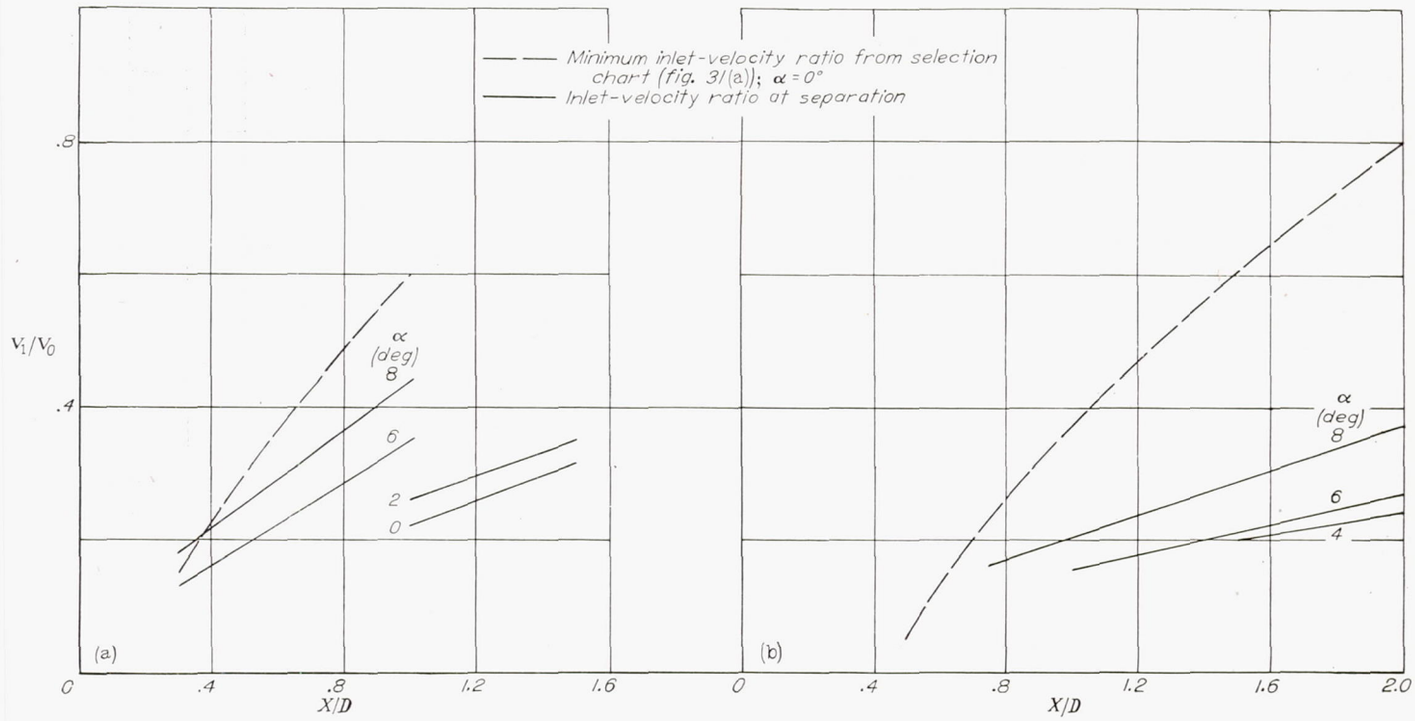

(a) $\frac{d}{D}$=0.70. (b) $\frac{d}{D}$=0.60.

FIGURE 47.—Inlet-velocity ratio below which external separation occurs. M_0=0.30 and 0.40.

The phenomenon shown in figure 46 is of general interest with regard to investigations of specific air-inlet installations in which the critical speed of an inlet may be determined for only one value of inlet-velocity ratio. The measured (or estimated) critical speed may be deceptively high if the flow is separated, and incorrect conclusions concerning the efficacy of the inlet may result. Drag measurements and tuft surveys may be useful in verifying the results of an investigation of critical Mach number. In addition, comparison of critical Mach number values for several inlet-velocity ratios will generally serve to define the flow conditions. The critical Mach number will normally increase or remain constant with increasing inlet-velocity ratio; a decrease in critical Mach number with increasing V_1/V_0 (fig. 46) generally indicates flow separation.

Internal losses.—Internal total-pressure losses for the nose inlets tested were measured at the rake station (fig. 8) through the ranges of inlet-velocity ratio and angle of attack. Inasmuch as the diameter at the end of the nose-inlet duct and the over-all length of the nose plus skirt was held constant for all tests, a corresponding value of diffuser angle θ existed for each value of inlet-diameter ratio. For nose inlets with d/D values of 0.40, 0.50, and 0.60, the values of diffuser angle were 7.6°, 3.8°, and 0°, respectively.

A typical total-pressure-loss profile at the rake station is shown in figure 48. The total-pressure loss has been computed as a fraction of inlet dynamic pressure q_1. The total-pressure losses obtained for the NACA 1–40–150, 1–50–150, and 1–60–150 nose inlets from integration of figures similar to figure 48 are shown in figures 49 (a), (b), and (c), respectively. A comparison of the magnitude of the pressure losses shows the effect of an increase in inlet-velocity ratio for constant diffuser angles.

Figure 50 shows the variation of total-pressure loss with diffuser angle θ for given values of inlet-velocity ratio and angle of attack. The adverse effect of large diffuser angles is illustrated. Figure 51 shows the variation of total-pressure loss with angle of attack for two values of inlet-velocity ratio. This figure illustrates the increase of total-pressure loss that occurs at high angles of attack for the large values of diffuser angle.

The integrated total-pressure losses for the NACA 1–50–150, 1–50–100, and 1–50–050 nose inlets at two angles of attack are presented in figure 52. Inasmuch as the value of X/D is a measure of the radius of curvature of the nose-inlet profile for a given value of d/D, comparison of the internal total-pressure losses for these nose inlets indicates the effect of external curvature. The large external radius of curvature combined with the relatively small internal radius is shown by the data for the NACA 1–50–050 nose inlet to lead to internal separation at high values of inlet-velocity ratio and angle of attack.

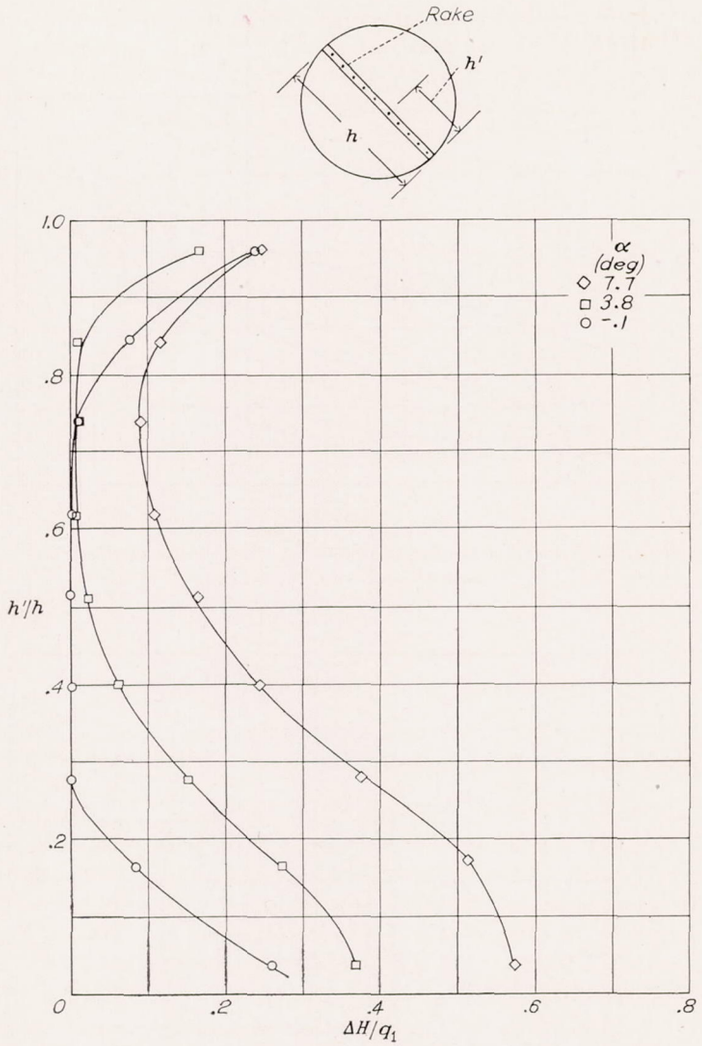

FIGURE 48.—Typical profile of internal total-pressure loss at rake station. NACA 1–40–150 nose inlet; $\frac{V_1}{V_0}$=0.93; M_0=0.40; θ=7.6°.

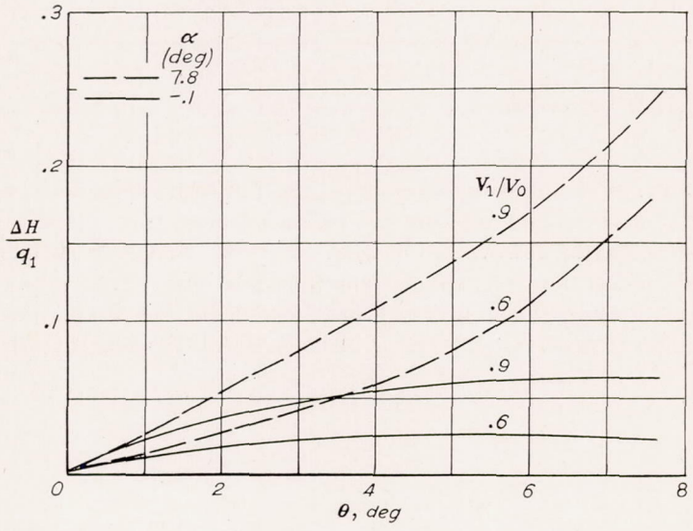

FIGURE 50.—Variation of internal total-pressure loss with diffuser angle. $\frac{X}{D}$=1.5; M_0=0.40.

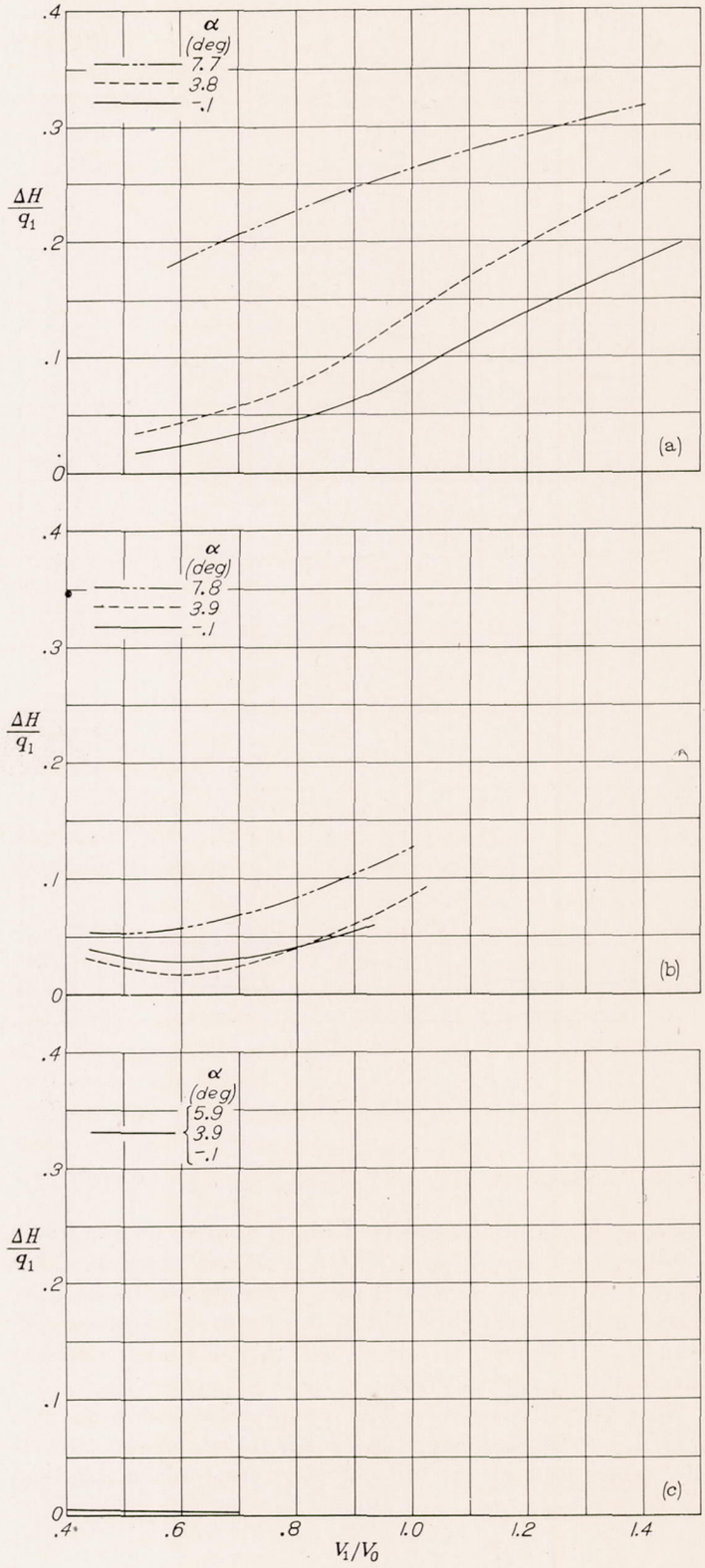

(a) NACA 1–40–150 nose inlet (θ=7.6°).
(b) NACA 1–50–150 nose inlet (θ=3.8°).
(c) NACA 1–60–150 nose inlet (θ=0°).

FIGURE 49.—Variation of internal total-pressure loss with inlet-velocity ratio for nose inlets of $\frac{X}{D}$=1.5. M_0=0.40.

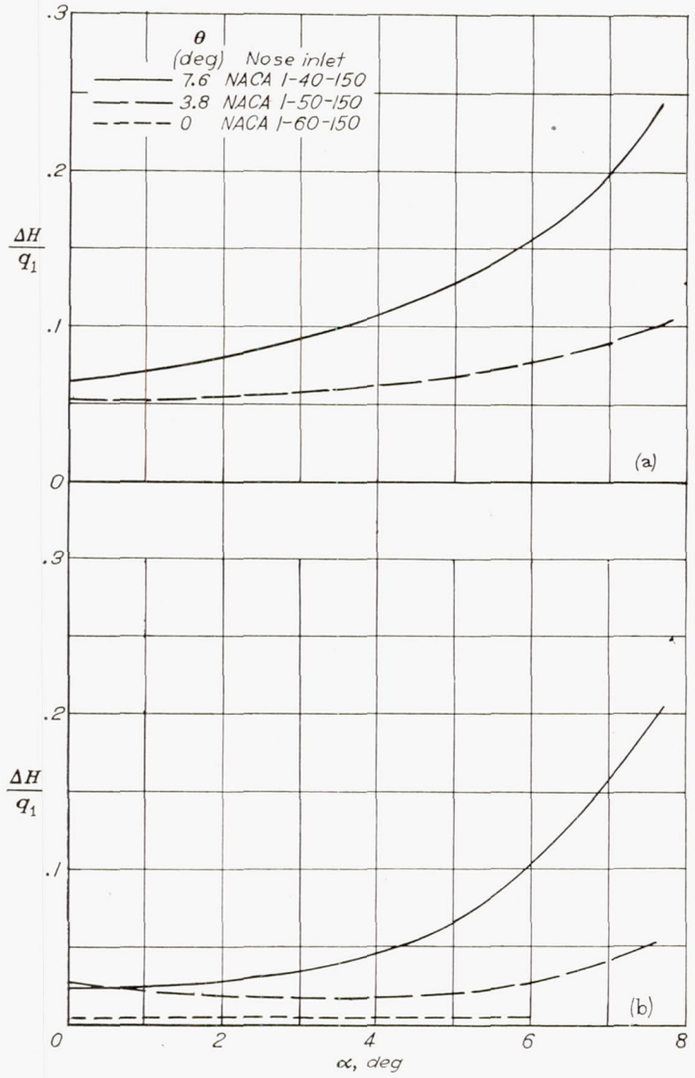

(a) $\frac{V_1}{V_0}$=0.9.

(b) $\frac{V_1}{V_0}$=0.6.

FIGURE 51.—Variation of internal total-pressure loss with angle of attack. $\frac{X}{D}$=1.5; M_0=0.40

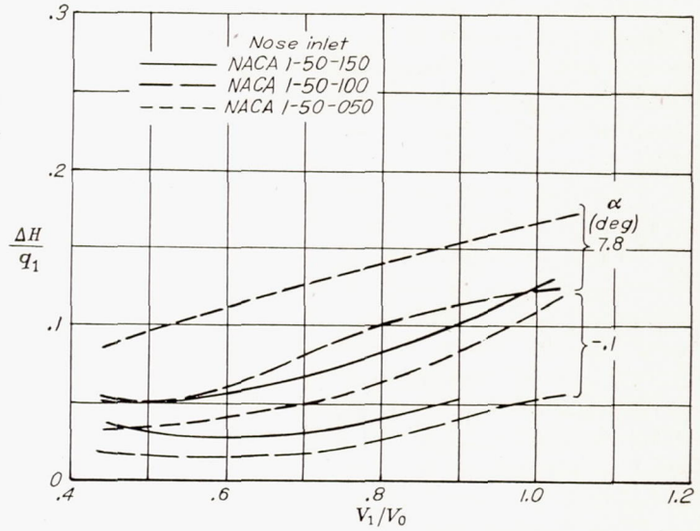

FIGURE 52.—Variation of internal total-pressure loss with inlet-velocity ratio for nose inlets of $\frac{d}{D}$=0.5. M_0=0.40; θ=3.8°.

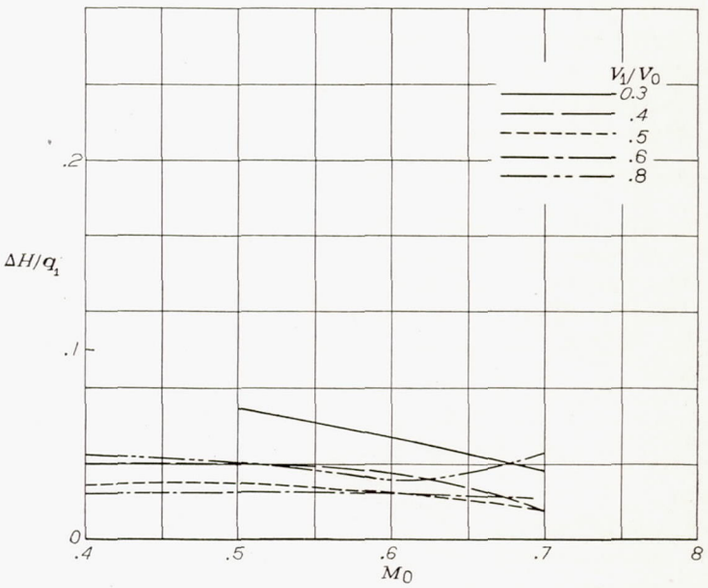

FIGURE 53.—Mach number effects on total-pressure loss for θ=3.8°. NACA 1–50–150 nose inlet; α=−0.1°.

Figure 53 shows the effects of Mach number on integrated total-pressure loss for the NACA 1–50–150 nose inlet. A slight decrease in internal losses generally occurs with increase in Mach number within the range of tests for this diffuser. It should be noted that the maximum entrance Mach number is about 0.56.

Nose-inlet lip radius.—The internal lip radius for the NACA 1-series nose inlets tested was maintained at 0.025Y, the value used in the development tests of references 1 and 2. From considerations of external-pressure distributions, this nose radius appears to be satisfactory for the nose inlets having low values of d/D. For the NACA 1–70–030 nose inlet, however, the pressure distributions (fig. 26) show that a sharp local pressure peak occurs at the lip at low values of inlet-velocity ratio. The NACA C cowling (fig. 34)

also shows a similar effect. Because the lip radius was very small for these nose inlets having large values of d/D, an increase in lip radius was presumed to be desirable. The NACA C cowling was therefore tested with the lip radius increased to approximately twice the original value; the NACA 1–70–030 nose inlet was tested with a similar increase in lip radius and with an added internal fairing (fig. 6). The value of d/D for these nose inlets was decreased from 0.70 to 0.69 by these modifications.

Figures 54 and 55 present pressure distributions for the two nose inlets with increased lip radii. Comparison of these figures with figures 26 and 34 shows that the sharp local-pressure peak measured at the lip at low values of inlet-velocity ratio has been removed. The knees of the critical-speed curves (figs. 56 and 57) are consequently shifted to lower values of V_1/V_0, with the result that the critical speeds of these nose inlets are increased in this range. The internal losses measured for the original and modified lip radii were insignificant throughout the test ranges of inlet-velocity ratio and angle of attack. A lip radius somewhat in excess of $0.025Y$ therefore seems to be desirable for nose inlets of large values of d/D. References 11 and 12 and other investigations indicate, however, that inordinate increases in lip radius can adversely affect the external-pressure distribution.

Effects of variations in basic profile.—Three nose inlets having $\frac{d}{D}=0.60$ and $\frac{X}{D}=1.50$ and having profiles that differ from the NACA 1-series profile were tested to show the effect of such differences (fig. 7). The first of these three profiles was derived directly from an ellipse. The second and third profiles were obtained by proportional distortion of the NACA 1-series profile according to the arbitrary equation

$$\frac{y'}{Y}=\frac{y}{Y}\left(\frac{1+K}{1+K\frac{y}{Y}}\right)$$

where

y'/Y nondimensional ordinate of modified profile
y/Y nondimensional ordinate of basic profile (NACA 1-series)
K arbitrary factor

The two nose inlets tested are designated by the particular value of the K-factor used in their derivation.

Pressure distributions over the three nose inlets at $\alpha=0°$ are presented in figure 58 along with the pressure distribution for the NACA 1–60–150 nose inlet. The characteristic flat pressure distribution of the NACA 1–60–150 nose inlet at high values of inlet-velocity ratio is not found for the modified nose inlets. Instead, a pressure peak over the forward portion of the nose occurs at all values of inlet-velocity ratio; the height of the peak is greatest for the nose inlet having the greatest thickness near the lip.

Figure 59 shows the critical Mach number characteristics for the modified nose inlets. An inlet-velocity-ratio range for constant critical speed, which is characteristic of the NACA 1-series nose inlet, does not exist for the modified nose inlets. The critical speed decreases with decrease in inlet-velocity ratio through the entire range. The critical Mach number curves are compared (at $\alpha=0°$) with those for the NACA 1–60–150, 1–60–100, and 1–60–075 nose inlets in figure 60. The comparison shows that the rate of decrease of critical Mach number for the modified noses is lower than the rate of decrease which occurs below the knee of the curves for the NACA 1-series nose inlets. The critical speeds for the modified nose inlets, however, are lower than those of the NACA 1-series nose inlets of comparable maximum critical speed, except at very low values of inlet-velocity ratio beyond the range wherein the comparable NACA 1-series nose inlets are designed to operate.

These tests show that deviations from the NACA 1-series profile that cause appreciable departure from the characteristic flat pressure distribution can cause important reductions in critical speeds. The NACA 1-series ordinates, which have been shown to approach closely the optimum from the standpoint of critical speed, should be accurately applied in order to realize the optimum characteristics.

Effect of variations in fineness ratio.—In order to investigate the effect of varying the fineness ratio of the test body, the NACA 1–60–100 and 1–60–050 nose inlets were tested with and without cylindrical skirts. (The test body, however, as shown in fig. 8, still retained a cylindrical length of 2 diameters.) The fineness ratio of the body was decreased by 9 and 18 percent for the NACA 1–60–100 and 1–60–050 nose inlets, respectively. The effect of these changes on critical-speed characteristics was found to be negligible. Comparison of the critical speed of the NACA C cowling as measured on the test body of the present report and on a nacelle in reference 1 substantiates this finding. The over-all fineness ratios of the test body and nacelle were 5.5 and 2.4, respectively. The critical speeds measured for the NACA C cowling agree closely with the critical speeds measured in the tests of reference 1. The critical speed of the nose inlet therefore appears to be essentially independent of the over-all fineness ratio of the body. It should be noted, however, that this conclusion is based on tests of nose inlets which employed an appreciable length of cylindrical afterbody; other types of afterbody may appreciably affect the critical-speed characteristics.

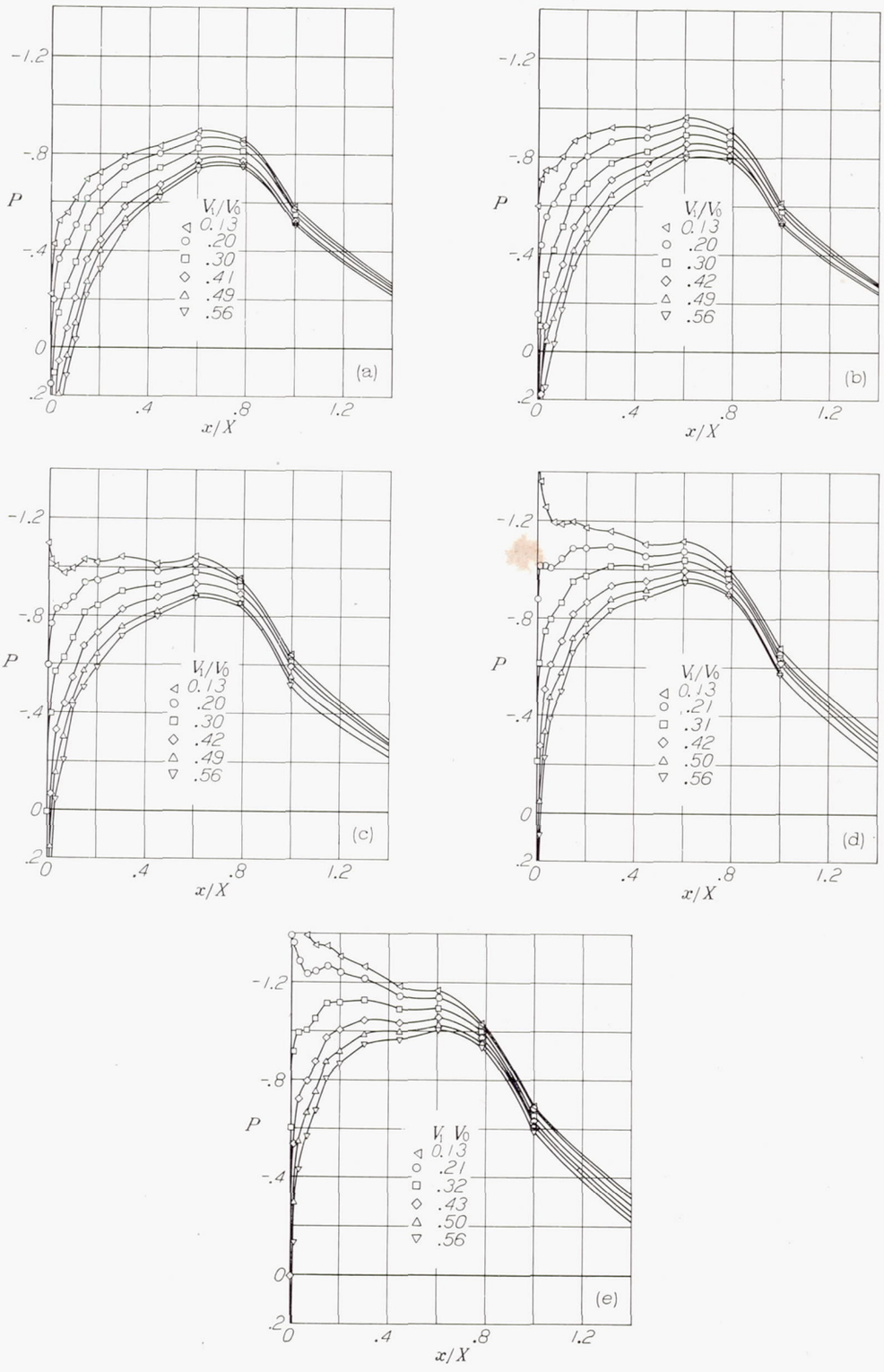

(a) $\alpha = -0.1°$. (b) $\alpha = 1.8°$.
(c) $\alpha = 3.8°$. (d) $\alpha = 5.8°$.
(e) $\alpha = 7.9°$.

FIGURE 54.—Pressure distributions over the NACA 1-70-030 nose inlet with increased lip radius. $M_0 = 0.40$

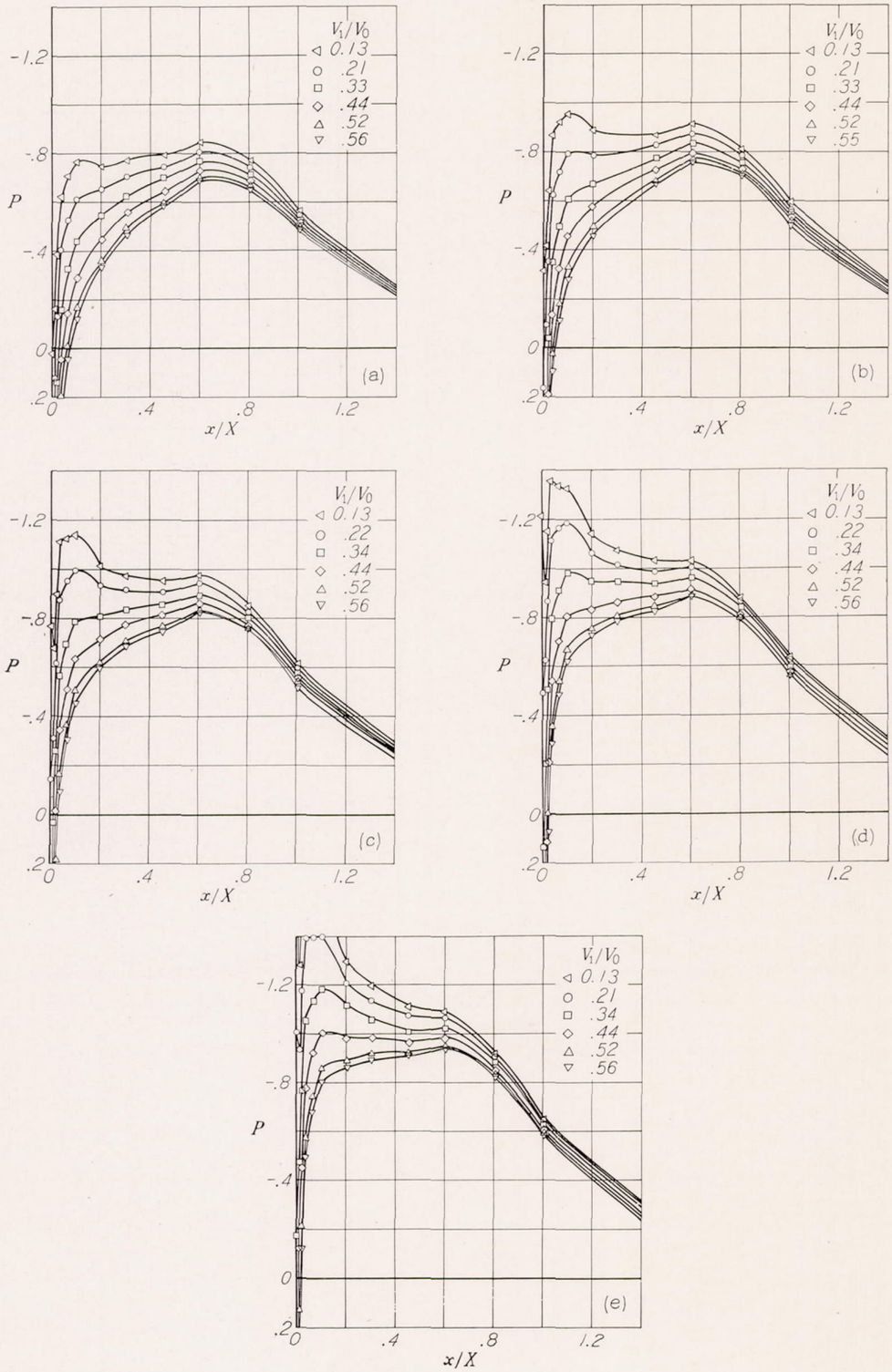

(a) $\alpha=-0.1°$. (b) $\alpha=1.8°$.
(c) $\alpha=3.8°$. (d) $\alpha=5.8°$.
(e) $\alpha=7.8°$.

FIGURE 55.—Pressure distributions over the NACA C cowling with increased lip radius. $M_0=0.40$.

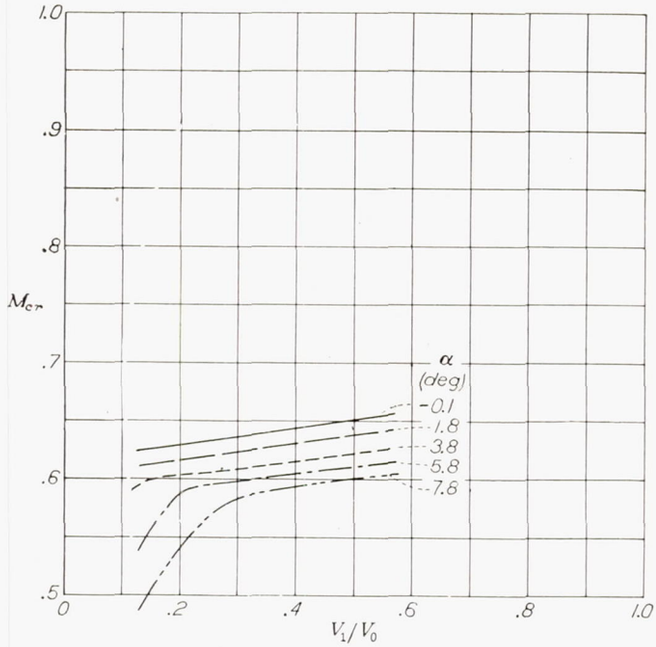

FIGURE 56.—Critical Mach numbers for the NACA 1-70-030 nose inlet with modified lip radius.

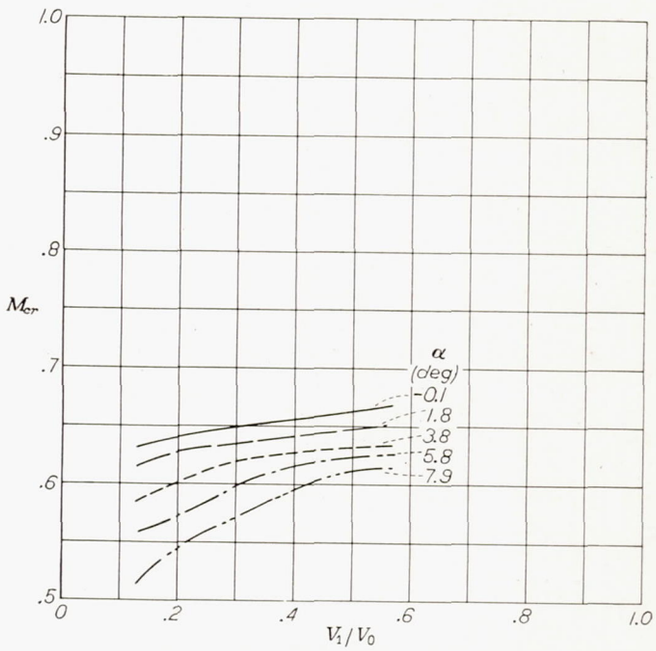

FIGURE 57.—Critical Mach numbers for the NACA C cowling with modified lip radius.

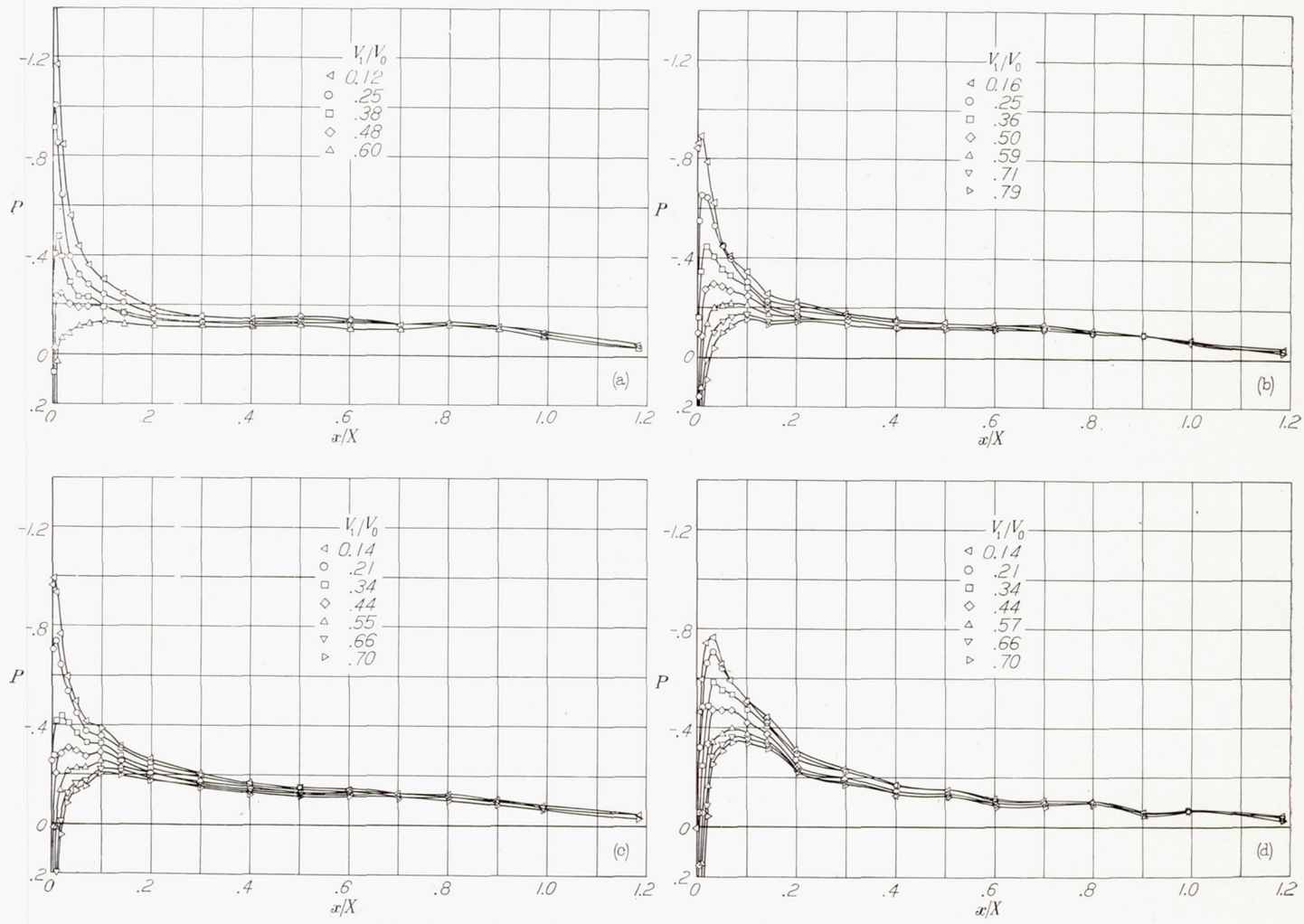

(a) NACA 1-60-150 nose inlet; $M_0=0.30$. (b) Elliptical; $M_0=0.30$.
(c) $K=0.5$; $M_0=0.40$. (d) $K=1.5$; $M_0=0.40$.

FIGURE 58.—Pressure distributions over the modified nose inlets tested. NACA 1-60-150 nose inlet included for comparison; $\alpha=0°$.

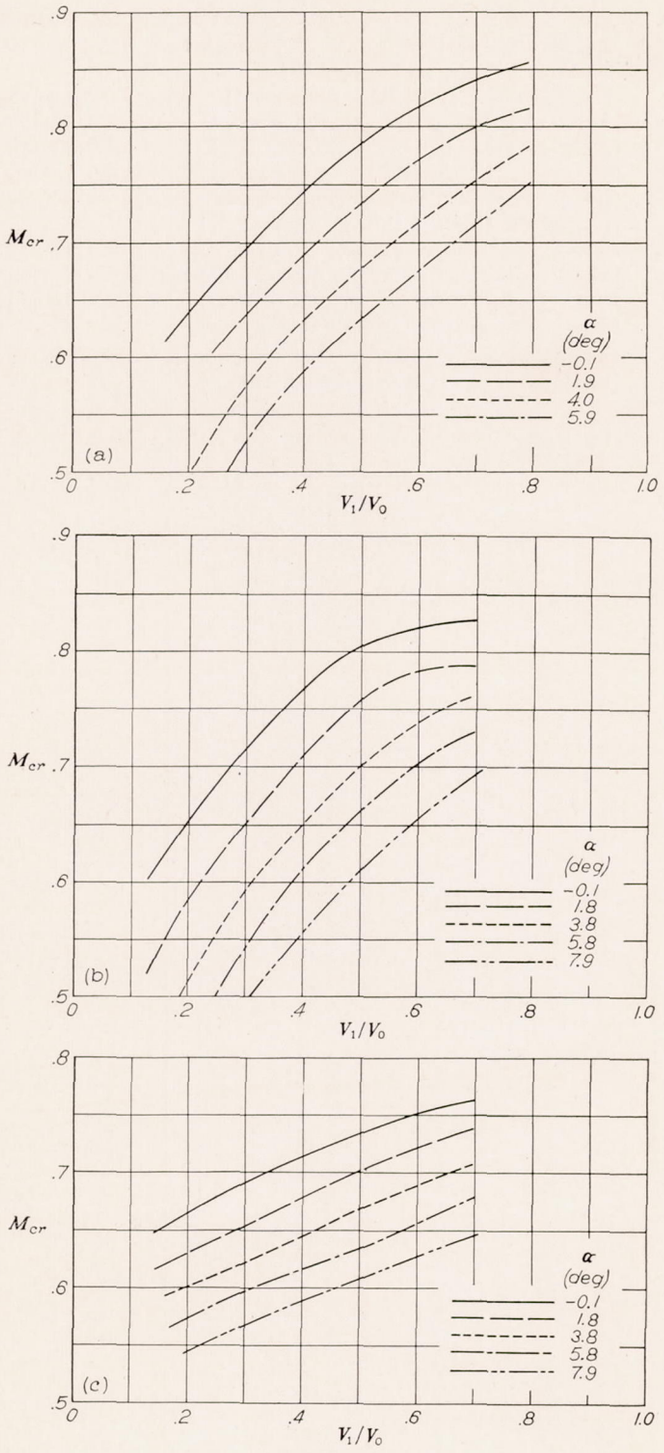

(a) Elliptical.
(b) K=0.5.
(c) K=1.5.

FIGURE 59.—Critical Mach numbers of the modified nose inlets tested.

SUMMARY OF RESULTS

An analysis of the nose-inlet shapes developed in previous investigations to represent the optimum from the standpoint of critical speed has shown that similarity exists between the nondimensional profiles of inlets which have widely different proportions and critical speeds. With the nondimensional similarity of such profiles established, the large differences in critical speeds of these nose inlets must be a function of their proportions.

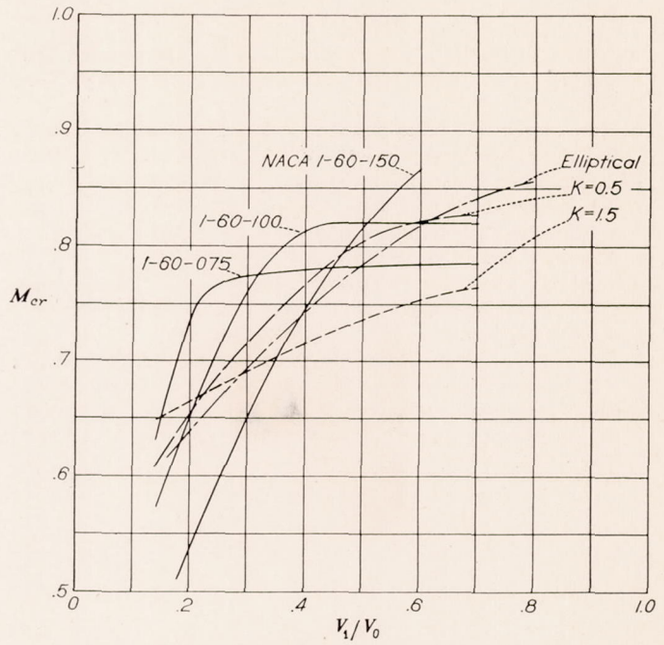

FIGURE 60.—Comparison of the critical Mach numbers of the modified and NACA 1-series nose inlets. α=0°.

The nondimensional ordinates of the B nose inlet, which were developed in a previous investigation to be optimum from the standpoint of critical speed, were extended and modified slightly to improve the fairing. These ordinates, now designated the NACA 1-series, were then applied to a group of nose inlets involving a systematic variation of proportions. Wind-tunnel tests of these nose inlets were made through wide ranges of inlet-velocity ratio and angle of attack at Mach numbers of 0.3 and 0.4. Tests of representative nose inlets were carried to high speed (a maximum Mach number of 0.7). Pressure distributions and critical Mach number characteristics are presented for each of the nose inlets tested. The results of these tests show that the length ratio (ratio of length to maximum diameter) of the nose inlet is the primary factor governing the maximum critical speed. The effect of inlet-diameter ratio (ratio of inlet diameter to maximum diameter) on critical speed is, in general, secondary; but this ratio has an important function in governing the extent of the inlet-velocity-ratio range for maximum critical speed. The highest critical Mach number attained for any of the nose inlets tested was 0.89.

The data have been arranged in the form of design charts from which NACA 1-series nose-inlet proportions can be selected for given values of critical Mach number and air-flow quantity. Examples of nose-inlet selections are presented for a typical jet-propulsion installation (critical Mach number of 0.83) and for two conventional radial-engine installations (critical Mach number of 0.76).

The selection charts and NACA 1-series ordinates have been shown to be applicable to the design of cowlings with spinners and to the design of high-critical-speed fuselage scoops. The possibility of application of the NACA 1-series ordinates to the experimental development of wing inlets is also indicated.

LANGLEY MEMORIAL AERONAUTICAL LABORATORY,
NATIONAL ADVISORY COMMITTEE FOR AERONAUTICS,
LANGLEY FIELD, VA., *June 8, 1945.*

REFERENCES

1. Robinson, Russell G., and Becker, John V.: High-Speed Tests of Conventional Radial-Engine Cowlings. NACA Rep. No. 745, 1942.
2. Becker, John V.: Wind-Tunnel Tests of Air Inlet and Outlet Openings on a Streamline Body. NACA ACR, Nov. 1940.
3. Becker, John V., and Baals, Donald D.: Wind-Tunnel Tests of a Submerged-Engine Fuselage Design. NACA ACR, Oct. 1940.
4. Von Kármán, Th.: Compressibility Effects in Aerodynamics. Jour. Aero. Sci., vol. 8, no. 9, July 1941, pp. 337–356.
5. Silverstein, Abe, and Guryansky, Eugene R.: Development of Cowling for Long-Nose Air-Cooled Engine in the NACA Full-Scale Wind Tunnel. NACA ARR, Oct. 1941.
6. Valentine, E. Floyd: Preliminary Investigation Directed toward Improvement of the NACA Cowling. NACA ARR, April 1942.
7. Molloy, Richard C., and Brewster, James H., III: New Research on the Cowling and Cooling of Radial Engines. NACA ARR, May 1942.
8. McHugh, James G.: Progress Report on Cowlings for Air-Cooled Engines Investigated in the NACA 19-Foot Pressure Wind Tunnel. NACA ARR, July 1941.
9. Smith, Norman F., and Baals, Donald D.: Wind-Tunnel Investigation of a High-Critical-Speed Fuselage Scoop Including the Effects of Boundary Layer. NACA ACR No. L5B01a, 1945.
10. Wright, Ray H.: Estimation of Pressures on Cockpit Canopies, Gun Turrets, Blisters, and Similar Protuberances. NACA ACR No. L4E10, 1944.
11. Von Doenhoff, Albert E., and Horton, Elmer A.: Preliminary Investigation in the NACA Low-Turbulence Tunnel of Low-Drag Airfoil Sections Suitable for Admitting Air at the Leading Edge. NACA ACR, July 1942.
12. Smith, Norman F.: High-Speed Investigation of Low-Drag Wing Inlets. NACA ACR No. L4I18, 1944.
13. Fedziuk, Henry A.: High-Speed Wind-Tunnel Tests of Gun Openings in the Nose of the Fuselage of a ¼-Scale Model. NACA ACR, July 1942.

U. S. GOVERNMENT PRINTING OFFICE: 1950

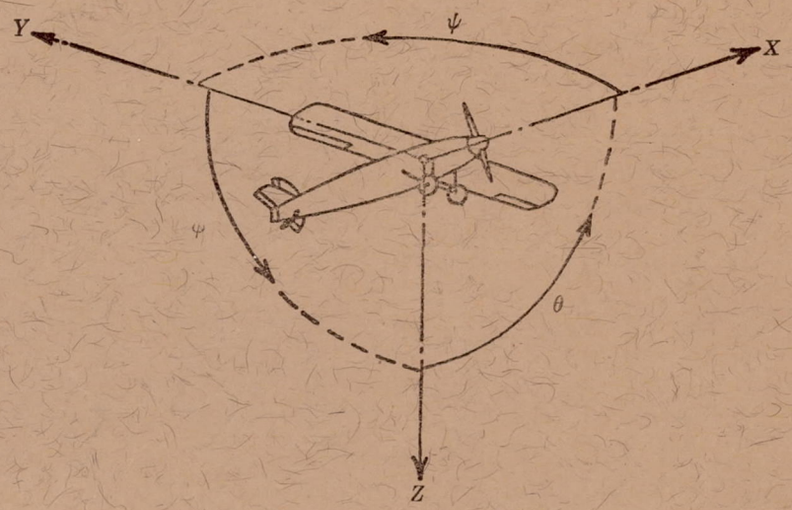

Positive directions of axes and angles (forces and moments) are shown by arrows

Axis		Force (parallel to axis) symbol	Moment about axis			Angle		Velocities	
Designation	Symbol		Designation	Symbol	Positive direction	Designation	Symbol	Linear (component along axis)	Angular
Longitudinal	X	X	Rolling	L	$Y \longrightarrow Z$	Roll	ϕ	u	p
Lateral	Y	Y	Pitching	M	$Z \longrightarrow X$	Pitch	θ	v	q
Normal	Z	Z	Yawing	N	$X \longrightarrow Y$	Yaw	ψ	w	r

Absolute coefficients of moment

$C_l = \frac{L}{qbS}$ (rolling) $\quad C_m = \frac{M}{qcS}$ (pitching) $\quad C_n = \frac{N}{qbS}$ (yawing)

Angle of set of control surface (relative to neutral position), δ. (Indicate surface by proper subscript.)

4. PROPELLER SYMBOLS

D Diameter

p Geometric pitch

p/D Pitch ratio

V' Inflow velocity

V_s Slipstream velocity

T Thrust, absolute coefficient $C_T = \frac{T}{\rho n^2 D^4}$

Q Torque, absolute coefficient $C_Q = \frac{Q}{\rho n^2 D^5}$

P Power, absolute coefficient $C_P = \frac{P}{\rho n^3 D^5}$

C_s Speed-power coefficient $= \sqrt[5]{\frac{\rho V^5}{P n^2}}$

η Efficiency

n Revolutions per second, rps

Φ Effective helix angle $= \tan^{-1}\left(\frac{V}{2\pi r n}\right)$

5. NUMERICAL RELATIONS

1 hp=76.04 kg-m/s=550 ft-lb/sec

1 metric horsepower=0.9863 hp

1 mph=0.4470 mps

1 mps=2.2369 mph

1 lb=0.4536 kg

1 kg=2.2046 lb

1 mi=1,609.35 m=5,280 ft

1 m=3.2808 ft